ABSTRACT

GUADERRAMA, LUCAS RIVAS. Strengthening of Steel Web Plates Using CFRP. (Under the direction of Sami H. Rizkalla, Ph.D.)

With an increasing demand to strengthen steel structures, alternative strengthening techniques are being investigated. Carbon Fiber Reinforced Polymer (CFRP) materials provide a possible strengthening alterative due to their high material performance, light weight, and resistance to corrosion. The behavior of CFRP materials has recently been investigated by studying their effect in compression resistance, relating to the principle compression stresses arising from pure shear stress conditions. This thesis presents an experimental program that consists of two phases of research. The first phase was conducted to study the effects that geometry of a steel plate have on the effectiveness on the CFRP strengthening system. To complete the first phase of research, fourteen specimens were tested in uniaxial compression. The specimens tested had varying slenderness and aspect ratios ranging from 48 to 154 and 1.2 to 2.4, respectively. Eight of the specimens tested were strengthened with high modulus small diameter CFRP strands on both faces of the steel plate. In order to determine the effectiveness of the strengthening system, six un-strengthened control specimens were tested. The second phase of the experimental program was conducted to examine the effect that different types of small diameter CFRP strands have on the behavior of a strengthened specimen. Eighteen specimens were tested in the same manner as the first phase. Two slenderness and aspect ratios were selected to be investigated. Twelve of the specimens tested were strengthened with three different types of small diameter CFRP strands varying in mechanical properties. Furthermore, the effect of multiple layers of CFRP strengthening was investigated. The results of the experimental

program were used to determine whether the small diameter CFRP strands being investigated would be effective in increasing the shear capacity of a steel girder.

Strengthening of Steel Web Plates Using CFRP

by
Lucas Rivas Guaderrama

A thesis submitted to the Graduate Faculty of
North Carolina State University
in partial fulfillment of the
requirements for the degree of
Master of Science

Civil Engineering

Raleigh, North Carolina

2015

APPROVED BY:

_____	_____
Rudolf Seracino, Ph.D.	Gregory W. Lucier, Ph.D.

_____
Sami H. Rizkalla, Ph.D.
Committee Chair

DEDICATION

I dedicate this thesis to my parents, James and Lydia Guaderrama, for their unwavering love and support.

BIOGRAPHY

Lucas Rivas Guaderrama was born and raised in Las Cruces, NM. He enrolled in the Civil Engineering Department at New Mexico State University in August 2009. While completing his Bachelor's degree, he gained experience in the construction and engineering industries through summer internships with various organizations. In May 2013, Lucas completed his Bachelor of Science degree and graduated with honors. In August 2013, he began his Master of Science degree program at North Carolina State University majoring in Civil Engineering with an emphasis in structural engineering and mechanics. Lucas plans to begin his career as a structural engineer upon the completion of his graduate degree.

ACKNOWLEDGMENTS

I would like to thank my advisor and committee chair Dr. Sami Rizkalla for the extensive guidance, expertise, and advice he has given me throughout my graduate program. I would like to extend special thanks to Dr. Rudolf Seracino for kindly accepting to be a member of my advisory committee. Thank you to Dr. Gregory Lucier for his guidance and expertise in many facets of this research program.

Thank you to Nippon Steel and Sumikin Materials Company for their continued financial support of this research endeavor. Thank you to Jonathon McEntire and Jerry Atkinson for their technical expertise and willingness to impart that expertise on all of us performing experimental research. I also give special thanks to Dr. Hatem Seliem for his efforts and advice throughout the first phase of this research program.

I am grateful to all of the students and staff at the Constructed Facilities Laboratory for their help as well as the friendship they have extended. I would also like to extend special thanks to Hamid Kazem for the joint effort put forth in this research.

Thank you to my family and friends for giving me support and encouragement in all that I do. Finally, I extend my heartfelt gratitude to my parents for all that they have done for me. Without you, this would not have been possible.

TABLE OF CONTENTS

LIST OF TABLES

LIST OF FIGURES

LIST OF EQUATIONS

CHAPTER 1 : Introduction

1.1 Background

Many of the aging steel bridges in the United States are in need of retrofit or repair. Degradation of steel structural members due to environmental conditions and increase of vehicular weight from initial design specifications create the need for strengthening of these steel bridges. The new bridge design codes also require designing for higher vehicular live loads in comparison to those used in the initial design of the bridges. Thus, certain steps must be taken to safely rehabilitate existing steel bridges. Existing bridges without any signs of distress, may require flexural and shear strengthening to meet the current design standards. Flexural strengthening of steel bridges has been investigated and documented by Tabrizi et al (2013).

The research documented in this thesis explores shear strengthening of steel bridges. Fundamentally, if a stress element is subjected to pure shear forces, principle tension and principle compression stresses are induced as shown in Figure 1.1. Combination of these principle stresses can lead to buckling failure in the direction of the compression stresses.

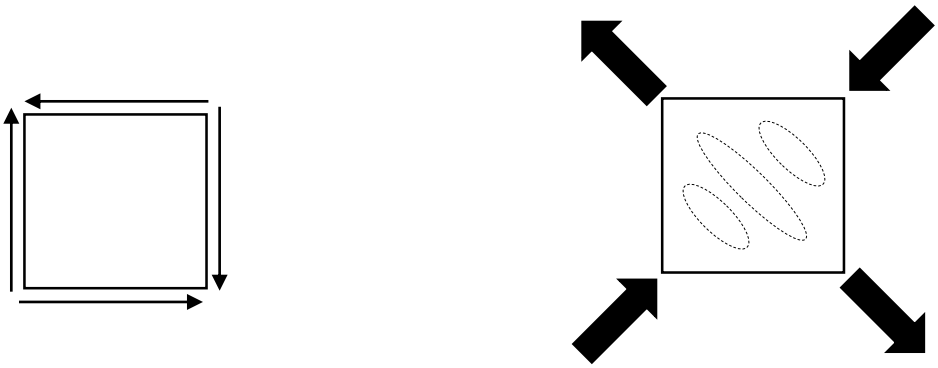

Figure 1.1: Shear Buckling Phenomenon

The shear strength of the web plate is controlled by either elastic buckling (in case of a slender web) or yielding of the material (in case of a non-slender web). The capacity of the web plate and the shear strength of the steel girder can be increased by reducing the state of stress in the web plate due to the applied load. The elastic buckling of web plates is directly related to level of the principal compressive stresses induced at the high shear zone(s) of the girder.

This research investigates the use of Carbon Fiber-Reinforced Polymer (CFRP) materials for the purposes of shear strengthening of the web of typical plate girders. Bonding of CFRP materials reduce the stress level in the web, and could potentially increase the shear and buckling capacity of the web. Furthermore, CFRP strengthening systems have many well documented properties including corrosion resistance, high strength-to-weight ratios, and ease of construction in comparison to the use of steel plates; which are commonly used in practice to increase the shear capacity of a steel girder.

The use of CFRP materials to increase compression resistance has recently been undertaken by few researchers to understand this behavior including Fam et al (2006) and Zhao et al (2009). The research reported in this thesis investigates the efficiency of CFRP materials to enhance shear strength of steel girders, and in particular their compressive strength. The ability to undergo large deformations associated with buckling is also investigated.

1.2 Objectives

The objective of this research is to explore the potential use of small diameter CFRP strands for shear strengthening of steel bridge girders. The initial objective is to determine the effectiveness of these strands to increase the buckling capacity, and consequently, the compressive capacity of steel web plates. The research program considered several parameters that are believed to have an influence on the behavior and effectiveness of the proposed CFRP strengthening system. The research program consisted of two phases: Phase I and Phase II.

Phase I focused on determining the effect of the slenderness ratios and aspect ratios on the proposed strengthening system using small diameter CFRP strands for strengthening steel web plates. High modulus small diameter CFRP strands were used in the first phase to examine the effect of geometry of the steel plates on the proposed strengthening system.

Phase II focuses on examining the effectiveness of three different types of small diameter CFRP strands. Two slenderness ratios and aspect ratios of steel plates were used in this phase in order to determine the effects of the different material properties on the behavior.

1.3 Scope

The first phase of the experimental program comprised of fourteen specimens. Eight steel plates were strengthened with high modulus (HM) small diameter CFRP strands and six un-strengthened steel plates were used as control specimens. The plates varied in height-to-thickness ratios (h/t), to investigate various slenderness ratios. The plates also varied in height-to-width ratios (h/b), to study different aspect ratios. A limited number of specimens did not contain polyurea putty in order to determine its effect on the uniaxial compressive behavior of the strengthened plates. The second phase included testing of steel plates with two slenderness and two aspect ratios in each category. The specimens were strengthened using three different types of CFRP strands: high modulus (HM), intermediate modulus (IM), and high tensile strength/low modulus (LM). The objective of the second phase is to identify the most effective type of CFRP strands which can be used to enhance to buckling capacity of the steel web plates.

The second chapter in this thesis provides background information on the preparation and strengthening of steel compression members using FRP strengthening systems. The chapter will highlight the related research that has been performed in this field.

The third chapter describes the experimental program including the fabrication of the test specimens, the test setup, and instrumentation used. The material properties of the steel and CFRP strands used in this experimental program are reported based on the tested material coupons. Chapter three describes the strengthening techniques used in the experimental program.

The fourth chapter presents test results that were recorded through the experimental program including the behavior of the specimens. The effects of the different variables considered in the experimental program are discussed and analyzed.

The fifth chapter will summarize findings of the research program and recommends future work to complete the research on shear strengthening of webs in steel bridge girders.

CHAPTER 2 : Literature Review

2.1 Introduction

Many of the aging bridges in the United States are in need of strengthening or repair and need to be updated to current design loads. Previous research indicates that it is effective to use Fiber Reinforced Polymers (FRP) to increase the flexural capacity of steel girders. The research reported in this thesis investigates the potential use of FRP strengthening systems to increase the shear capacity to match the increase of flexural capacity. As previously discussed, shear failure occurs primarily due to the principle compression forces induced by the high shear forces, typically located near supports. The current conventional strengthening techniques used in industry include welding steel plates to the web of girders in the high shear zone areas and/or the corroded sections. The downside to this technique is the increase of dead load, the labor intensity, cost of construction, and interruption of traffic flow. Carbon Fiber Reinforced Polymer (CFRP) strengthening systems provide an excellent alternative for increasing the shear capacity of steel girders due to their mechanical and physical properties such as its high corrosion resistance and high strength to weight ratio. The performance of CFRP materials in tension is clear and their benefits are well known; however, their behavior in compression is still relatively uncertain. This chapter discusses a summary of significant research that has been reported for preparation, bond behavior, and strengthening of steel members that are subjected to compressive forces using FRP strengthening systems.

2.2 Surface Preparation

The effectiveness of FRP strengthening systems is highly dependent on the bond between the FRP and the surface to be strengthened. Debonding of the FRP material can be avoided by proper preparation of the strengthened surface, as well as selecting appropriate strengthening materials for the given application (Schnerch, 2006 and Linghoff, 2009).

Steel substrates must be properly prepared prior to application of the FRP strengthening system in order to ensure proper bond between the FRP material and the steel. Proper preparation of the surface includes removing all weak and undesirable materials on the untreated surface in order to expose the steel. Common surface treatments involve mechanical abrasion techniques including wire brushing, sand paper, and grit blasting. The most effective process in removing unwanted materials such as oil, mill scale, and rust is by grit blasting (Holloway & Cadei, 2002). Research has also shown that the size of the grit used can have an effect on the bond behavior. After grit blasting has been performed it is necessary to remove the excess grit that is still present on the blasted surface. Removal of excess grit can be performed by dry wiping, vacuuming, or removal by solvents. If chemical solvents are used, excess solvents should be used in order to elude the recontamination of the steel surface (Schnerch, 2006).

2.3 Bond Behavior

In order to have a better understanding of the strengthening limitations of FRP strengthening systems, the bond between a treated surface and the strengthening material must be well understood. Significant research has been performed investigating the bond between a treated steel surface and FRP strengthening systems.

Research has been done on the properties of the adhesive/epoxy of an FRP strengthening system. Xia and Teng (2005) investigated the behavior of FRP to steel bonded joints. Test results from this research program showed that using adhesives with higher strain capacities will result in better bond performance when compared to adhesives with high tensile strength. This sort of behavior was also exhibited by test results reported from Wu et al (2012). Test results from this experimental program indicated that ductile adhesives have a greater ability to distribute forces across the bonded area. This in-turn results in higher debonding resistances.

Hidekuma et al (2012) investigated the bond between steel and CFRP materials. An experimental program was performed by applying CFRP materials to the surface of a steel plate and subjecting the specimen to an axial tension force. Two types of CFRP materials were used for strengthening, one was CFRP strand sheets, and the other was a conventional carbon fiber material. The two CFRP materials had similar elastic modulus and tensile strength properties.

Other parameters within the experimental program included the number of layers of CFRP material, width of CFRP, length of step, and type of step. Test results indicated that as the number of layers of CFRP increased, the risk of debonding also increased. Furthermore, the strand sheets achieved higher debonding strengths when compared to the conventional carbon fiber material. The tests results also indicated that a small bonding surface may induce debonding; thus, the bonding area should be as large as possible.

Jiao and Zhao (2004) researched the use of CFRP materials to strengthen heat affected areas of butt-welded high strength steel tubes. Test were conducted on un-welded tubes spliced together by CFRP materials on the outside of the tubes. The spliced steel tubes were subjected to axial tension. The test results exhibited bond behavior similar to that of double-lap shear type specimens. Similar tests were performed on specimens butt-welded together, and wrapped with CFRP material near the welded area. Test results indicated that the addition of the CFRP material could be used to regain the lost yield strength in the heat affected zone of the steel tubes. The testing also revealed a critical bond length for the CFRP materials in this application. Additional bonded length from the critical bond length did not exhibit improved bond characteristics.

2.4 Strengthening to Increase the Axial Compression Resistance

A fair amount of research has recently been reported on the implementation of FRP systems to increase the axial compression resistance of steel members. Several research programs are investigating the strengthening of steel columns, both long and short, by using FRP strengthening systems. A significant amount of research has also been performed on the strengthening of plate and thin walled structures using FRP strengthening. Other researchers are investigating shear strengthening of steel girders by applying FRP strengthening systems to the webs of the beams. The following sections will give an overview of the significant findings for selected topics pertaining to members subjected to compression stresses.

2.4.1 Column Strengthening

Buckling of columns can be divided into two separate categories: elastic buckling and inelastic buckling. The mode of buckling is determined by the slenderness of the column. If a column is long or slender, it will experience elastic, global buckling. If a column is very short or stocky, it will experience inelastic buckling. Shaat and Fam (2006) performed experimental tests on both long and short hollow columns that were strengthened with an FRP strengthening system. The specimens were placed under uniaxial compression loads until a reduction in load carrying capacity was reached. Un-strengthened short and long columns were used as control specimens. Different strengthening configurations were used for short and long columns to delay their anticipated failure modes. Figure 2.1 depicts the different configurations of the strengthening systems used.

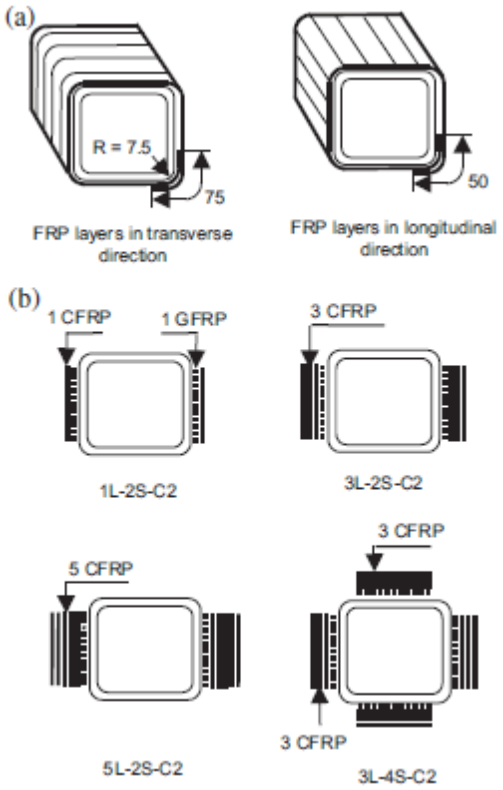

Figure 2.1: Orientations and Configurations of Applied Strengthening System (Shaat & Fam, 2006)

Tests showed an increase in axial load capacity of 18% and up to 23% for transversely wrapped short columns and longitudinally wrapped long columns, respectively. These tests also indicated that imperfections of the long columns, such as out-of-straightness, had a great effect on the results and efficiency of the CFRP strengthening system. In another experimental program reported by Shaat and Fam (2009), slender steel columns were strengthened with CFRP plates. Hollow columns were placed under uniaxial compression loads until a reduction in load carrying capacity was reached.

Tests showed that the buckling loads of the strengthened specimens were higher than the un-strengthened control specimens. Furthermore, the effect of the strengthening system increased with an increase of the slenderness ratio of the steel column. For example, the buckling loads were increased by 6%, 35%, and 71% for columns with slenderness ratios of 46, 70, and 93, respectively. Finally, the axial stiffness of the steel columns was increased with the addition of the CFRP strengthening system. The increase in axial strength and axial stiffness with an increase in slenderness ratio is shown in Figure 2.2.

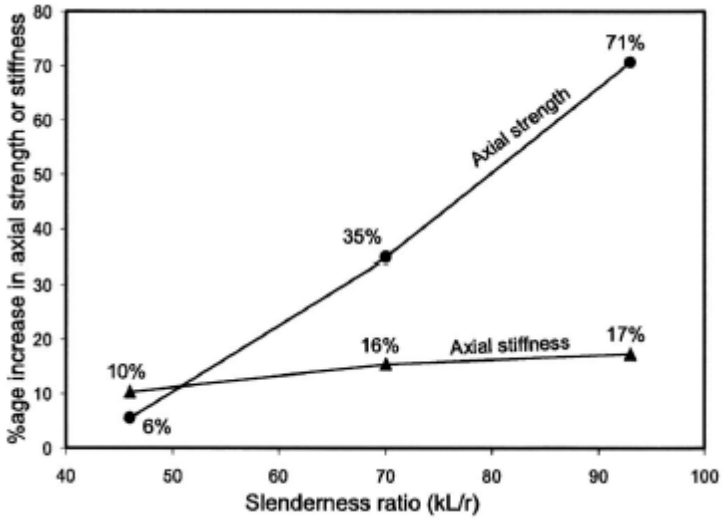

Figure 2.2: Effect of Slenderness Ratio (Shaat & Fam, 2009)

Harries et al (2009) performed an experimental program to study the effect of FRP strengthening systems on global and local buckling for long and short steel columns. The experimental program included strengthening of WT sections with various slenderness ratios and strengthening techniques applied to the stem of the WT section. The research findings

indicate that the elastic global buckling behavior of long sections is not greatly influenced by the FRP strengthening system. However, the FRP strengthening improves the local buckling behavior of the WT sections. The test results show that increasing the effective radius of gyration in the weak axis proportionally increases the load carrying capacity of the section and prevents the formations of plastic "kinks" along the stem of the WT.

The plastic behavior of short square hollow steel columns strengthened with CFRP materials was investigated by Bambach and Elchalakani (2007). Strengthened specimens and un-strengthened control specimens were subjected to axial compression forces and subsequently underwent large axial deformations. Test results showed that the CFRP materials increased the ultimate strength of the columns. Furthermore, the effect of the CFRP strengthening system proved to be greater with higher slenderness ratios as shown in Figure 2.3.

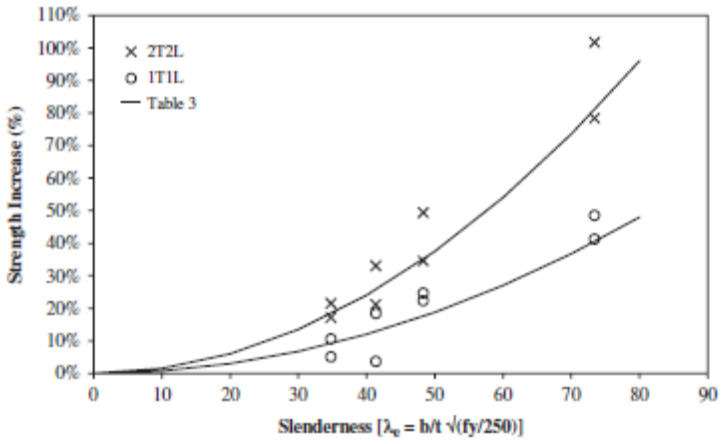

Figure 2.3: Strength Increase Relationship (Bambach & Elchalakani, 2007)

Further analysis of the results indicated that the applied CFRP materials increased the energy dissipation of the columns, when compared to the un-strengthened control specimens. Unlike the ultimate strength, the energy dissipation of the columns increased with a decrease in slenderness ratio.

Haedir and Zhao (2011) studied short steel tubular columns reinforced with high-strength CFRP sheets. Parameters within the experimental program consisted of varying slenderness ratios, number of layers of CFRP sheets, and orientation of the CFRP sheets. The CFRP sheets were oriented either transversely, longitudinally, or a combination of the two with respect to the direction of the applied load. Strengthened and un-strengthened control specimens were subjected to axial compression forces and loaded until a failure was reached.

Test results indicated that applying the CFRP sheets in both the transverse and longitudinal direction was the most effective in increasing the compressive strength of the column. The axial shortening of the columns was also decreased by 10% with the addition of the CFRP sheets. Furthermore, wrapping the column with longitudinal sheets first, followed by transverse sheets, showed the most increase in axial rigidity.

2.4.2 Thin Walled Section Strengthening

Aguilera and Fam (2013) conducted research on strengthening hollow steel section T-Joints using FRP plates. Figure 2.4 shows how transverse compression forces were applied to hollow steel sections through a steel joint member. Parameters within the experimental program included web height to thickness ratio (h/t), type of FRP plate, thickness of FRP plate, and width of FRP plate. FRP plates were applied to the out-facing webs of the hollow steel sections in order to determine their effect on delaying buckling of the member.

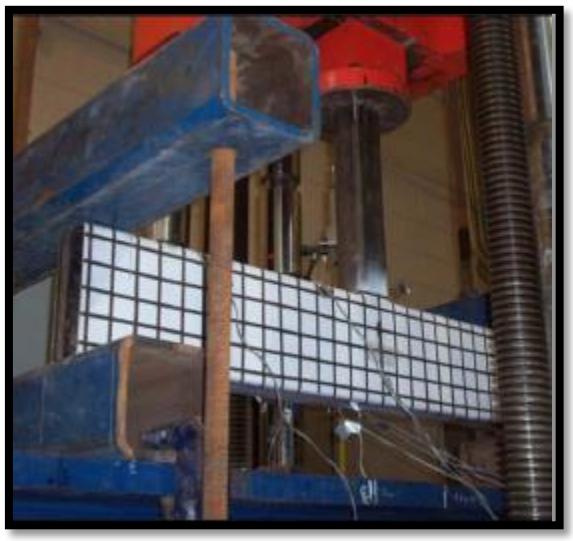

Figure 2.4: Application of Compressive Load on Hollow Member (Aguilera & Fam, 2013)

Test results showed that the strengthening effectiveness increased as the (h/t) ratio of the member increased, but did not necessarily increase the member's ductility. For example, as the (h/t) ratio increased from 34 to 65, the strength of the section increased from 9% to 38%.

On the other hand, for thick walled members, FRP retrofitting did increase the ductility and thus the energy dissipation of the member. The total width of the FRP plates was shown to have a significant effect on the strengthening system as well. When the FRP plate covered approximately 40% of the total span, the failure mode of the beam changed from local buckling to shear failure near the supports for (h/t = 65) members and plate delamination for (h/t = 34) members.

Kabir and Nazari (2011) studied the use of FRP patches to repair damaged thin walled steel cylinders. In this investigation, the thin walled cylinders were subjected to uniaxial compressive loading. The specimens tested in the experimental program varied in diameter-to-thickness ratios and the results were compared with an intact un-strengthened cylinder. Notches were made in the steel cylinders using a spark technique in order to control the amount of intentional damage imparted on the specimen, as shown in Figure 2.5. Subsequently, FRP patches were wrapped around the damaged specimen.

Figure 2.5: Intentionally Damaged Specimen (Kabir & Naziri, 2011)

Test results indicated that by applying FRP patches to the damaged area of the cylinders, adequate buckling strength can be reached as compared to the undamaged cylinder. Furthermore, by adding more layers of FRP strengthening, the effect of the repair system becomes greater by reducing the damage to the FRP patches caused by the onset of buckling.

The web-crippling behavior of rectangular hollow sections (RHS) strengthened with CFRP sheets and plates was investigated by Zhao et al (2006). Different strengthening configurations were used for the RHS near the application of the bearing force. Testing showed that CFRP strengthening significantly increased the web-crippling capacity of the RHS sections. The main reason for this was determined to be a change in failure mode from web buckling to web yielding. Figure 2.6 shows a typical failure mode of a strengthened specimen in this study.

Figure 2.6: Typical Failure of Strengthened Specimen (Zhao et al, 2006)

The CFRP strengthening was found to be the most effective for sections with large web depth-to-thickness ratios. This research was continued by Fernando et al (2009) by focusing on only one CFRP configuration, but using various adhesives for the CFRP strengthening system. Furthermore, preliminary finite element modeling was performed to verify the experimental results and gain a better understanding of the bond between the CFRP and the steel substrate.

Zhao and Al-Mahaidi (2009) explored the web-crippling behavior of light-steel beams strengthened with CFRP plates subjected to end bearing forces. The researchers varied the sides of the web where the CFRP plates were applied on: CFRP on the outer side, CFRP on the inner side, and CFRP on both sides as shown in Figure 2.7.

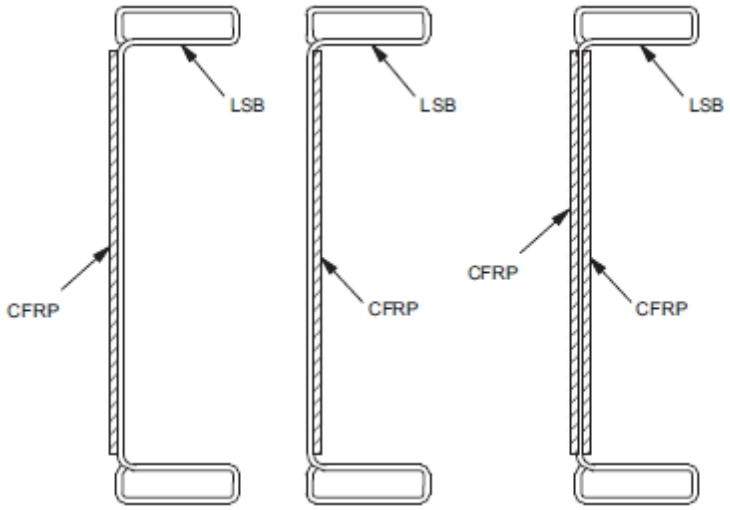

Figure 2.7: Applications of Strengthening System (Zhao & Al-Mahaidi, 2009)

Un-strengthened light-steel beams were used as control specimens. Tests indicated that applying CFRP plates to both sides of the web were the most effective in increasing the web-crippling capacity of the light-steel beams, followed by applying plates to the inner side, and outer side. When the CFRP plates were applied to both sides of the web, the increase in bearing capacity ranged from three to five times the strength of the un-strengthened light-steel beam. The increase in the capacity of the section was attributed to the CFRP plates providing restraint against rotation of the web.

2.4.3 Shear Strengthening

In addition to increasing a bridge girder's flexural capacity, the girder's shear capacity should also be increased to match the girder's increased flexural capacity. Along with research done

on thin walled sections, some research has been reported on increasing the shear capacity of an existing steel girder.

A research program by Patnaik et al (2008) studied the application of CFRP strips to high shear zone areas in built-up steel girders. Beam specimens were strengthened by applying one layer of CFRP strips on both sides of the web. The CFRP strips ran continuously from the supports to the point of load application. Figure 2.8 shows a typical elevation of a CFRP shear strengthened beam (top) and an un-strengthened control specimen (bottom).

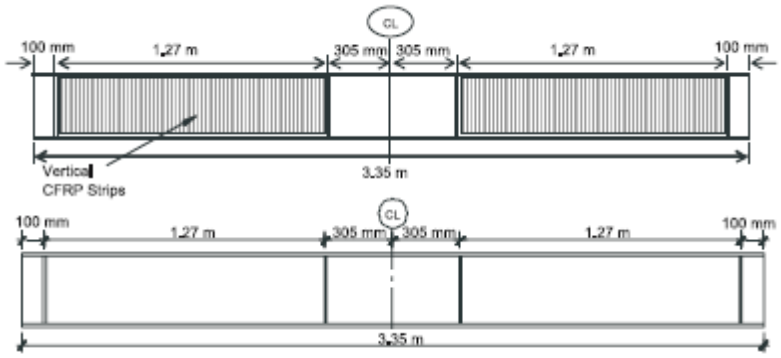

Figure 2.8: Elevation of a Shear Strengthened Beam (Patnaik et al, 2008)

The beam specimens were subjected to four point bending in order to produce a shear failure of the specimen. Three tests were performed: Two strengthened beams and one un-strengthened control specimen. The load at which the control specimen failed at indicated that the specimen failed by elastic web buckling.

One of the strengthened test specimens failed at a load which suggested that the web yielded, thus failed by inelastic web buckling. By adding the CFRP strips along the high shear zone, the shear strength of the beam was increased by 26%. The results from the other strengthened specimen were inconclusive due to a failure of the weld between the web and the flange. Figure 2.9 displays a typical failure of the shear test beams.

Figure 2.9: Typical Shear Failure (Patnaik et al, 2008)

Similar to Panaik, Narmashiri et al (2010) investigated the application of CFRP strips near high shear zones on the web of I-beams to increase the shear capacity of the section. The experimental program included the number of CFRP strips placed within the high shear zones as well as the use of CFRP strips to either one or both sides of the web. I-beams without any CFRP strips were tested as control specimens.

Test results showed that applying CFRP strips to both sides of the web was more effective in increasing the shear capacity as compared to only applying the strips to one side of the web. Testing also indicated that there was very little increase in the amount of shear capacity when three strips of CFRP were used instead of two strips of CFRP on both sides of the web.

The study also showed that the vertical deflection of the specimen, as displayed in Figure 2.10, was reduced with the addition of the CFRP strips.

Figure 2.10: Vertical Deflection of Specimen (Narmashiri et al, 2010)

The experimental test results were verified by numerical simulations and thus indicated the effectiveness of the CFRP strips for shear strengthening applications.

CHAPTER 3 : Experimental Program

This chapter describes an experimental program undertaken to investigate the effectiveness of small diameter carbon fiber reinforced polymer (CFRP) strands for shear strengthening of steel bridges by increasing the compressive strength and buckling capacity of steel web plates of bridge girders. Mechanical properties of the steel and strengthening materials, the fabrication of test specimens, the test setup, and instrumentation used in the experimental program are presented in this chapter. The process of applying the CFRP strengthening system to the steel plates is also presented.

3.1 Material Properties

3.1.1 Steel Properties

The tested specimens consisted of high-strength low-alloy Grade 50, designated by ASTM A572, steel plates that were supplied by a nearby steel manufacturing plant. Tension coupons were prepared and tested in accordance with ASTM A370 using a universal MTS testing machine. The deformations of the coupons were measured using a two inch extensometer and the load applied to the specimen was measured directly by the MTS testing machine. Figure 3.1 shows a typical test setup used for the steel coupons. Nominal dimensions of the tension coupons are shown in Figure 3.2. The actual dimensions of the coupons, however, were measured with a caliper and a digital micrometer to ensure accuracy of the measurements and test results. Three coupons were tested for each plate thickness used in the experimental program. The plates and tension coupons were from the same batch

in order to ensure that the material characteristics of the tension coupons would match those of the steel plates being used in the experimental program.

Figure 3.1: Typical Tension Test Setup

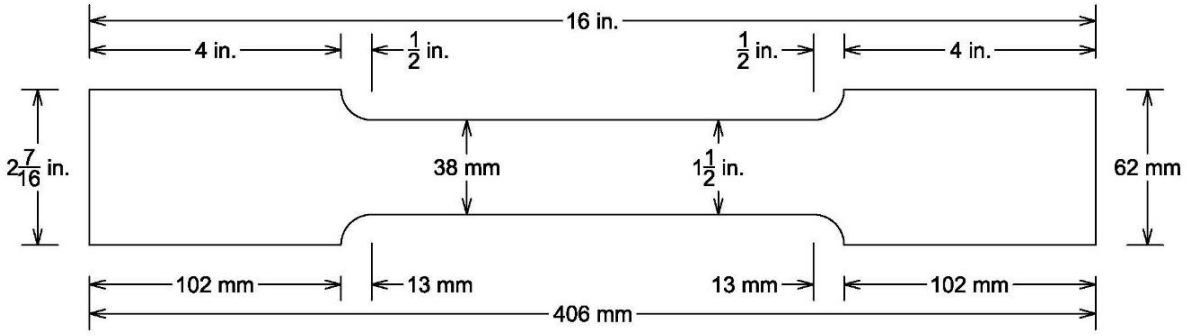

Figure 3.2: Typical Tension Coupon

Typical stress-strain curves for the three different thicknesses used in the experimental program are shown in Figure 3.3. Furthermore, yield strength, yield strain, and modulus of elasticity values are given in Table 3.1. The plot displays the varying stress-strain behaviors for varying thicknesses of steel. The five-sixteenths inch thick specimens exhibited a well-defined yield point and yield plateau. On the contrary, the three-eighths inch and half inch thick specimens did not have well defined yield strength or yield plateaus. Therefore, the yield strength for these two thicknesses was determined using the 0.2 percent offset method, per ASTM A370. From the material testing results, it was determined that the five-sixteenths inch plates were Grade 50 steel while the three-eighths inch and half inch plates were Grade 65. Grade 50 steel was ordered for all of the plates; however, it is very common for Grade 65 steel to be commercialized as dual grade steel.

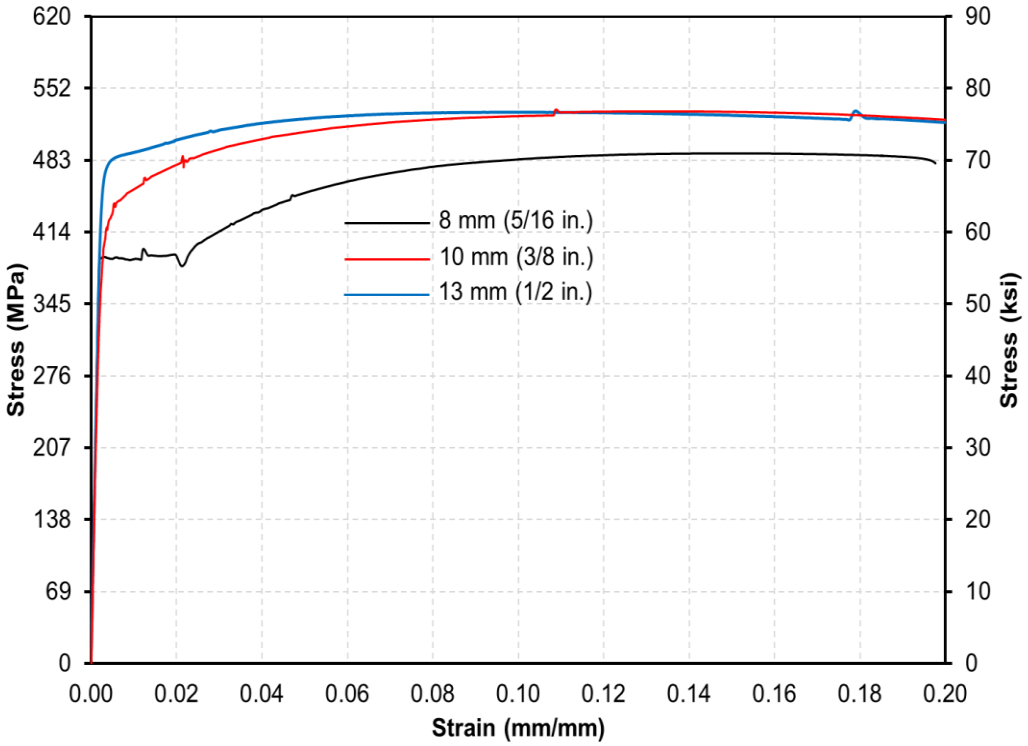

Figure 3.3: Typical Stress-Strain Behavior of Steel Tension Coupons

Table 3.1: Typical Mechanical Properties of Steel

Steel Thickness	Yield Strain	Yield Strength		Elastic Modulus	
	(%)	ksi	Mpa	ksi	MPa
5/16" (8 mm)	0.20	64	443	28,800	199,000
3/8" (10 mm)	0.23	66	454	29,000	200,000
1/2" (13 mm)	0.23	57	392	28,000	198,000

3.1.2 CFRP Properties

The average cross-sectional area of the three types of CFRP strands were determined by using volume displacement. 15 individual strands, for each type of CFRP strand, were selected at random and were cut to an approximate length of twelve inches. The exact length of each strand was measured using a digital caliper accurate to 0.0004 inches. After measurement of the strands was complete, the strands were placed inside a calibrated burette and the amount of displaced water was recorded. Figure 3.4 displays the burette and strands as described. This procedure was followed for all of the strand types used in this investigation.

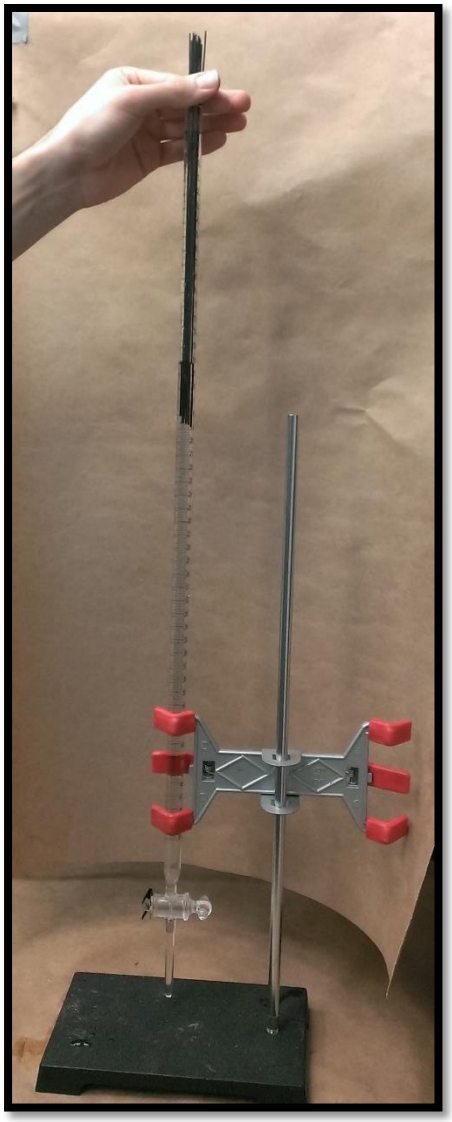

Figure 3.4: Burette and CFRP Strands

The tensile properties of high modulus (HM), intermediate modulus (IM) and low modulus (LM) strands were determined. Several specimens were prepared for each strand type and were tested in uniaxial tension.

The total length of each specimen was 12 inches long, with a gauge length of 5 inches long. In order to capture strain values during testing, two motion capturing sensors were attached on the single strand within the gauge length using a silicon-based epoxy that would allow the sensors to bond to the strand. Figure 3.5 displays the test set-up used for the testing of the CFRP strands.

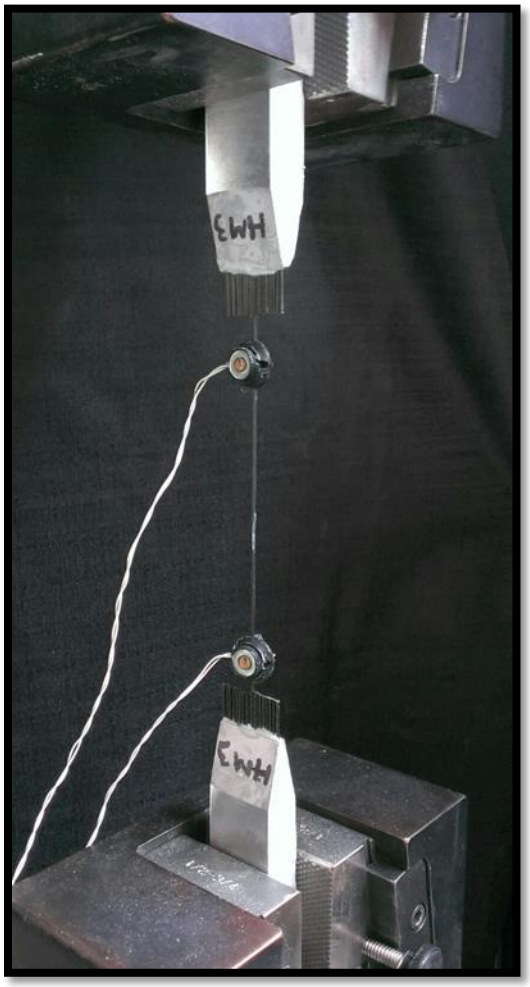

Figure 3.5: CFRP Strand Test Setup

The measured tensile strength, ultimate strain, and elastic modulus for the three types of CFRP strands are given in Table 3.2. The measured stress-strain behavior for the three types of CFRP strands are shown in Figure 3.6. Test results indicate that the high modulus strands were the stiffest strands, followed by the intermediate modulus and low modulus/high tensile strands. Furthermore, the ultimate stress and ultimate strain values were lower for the high modulus in comparison to the intermediate modulus and low modulus strands.

Table 3.2: Typical Mechanical Properties of CFRP Strands

CFRP Type	Ultimate Strain	Ultimate Strength		Elastic Modulus	
	(%)	ksi	MPa	ksi	MPa
Low Modulus (LM)	1.68	340	2350	20,000	140,000
Intermediate Modulus (IM)	1.04	320	2200	31,000	214,000
High Modulus (HM)	0.32	120	827	35,500	245,000

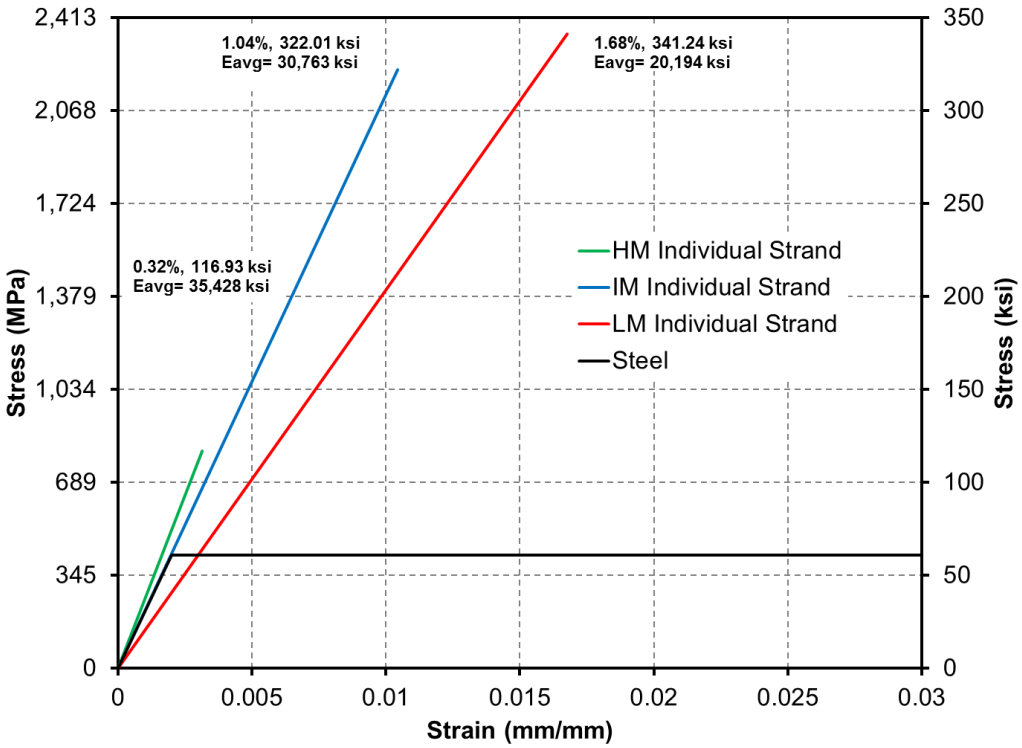

Figure 3.6: Typical Stress-Strain Behavior of CFRP Strands

At the time of strengthening, witness panels were fabricated to determine the properties of the strengthening system that is being applied to the steel plates. After a week of curing, the witness panels were cut using a wet saw into 12 inch long, 1 inch wide specimens. Similar to the individual strands, the witness panel coupons were tested in tension. Similar to the individual strands, strain was determined by using data obtained from two motion capturing sensors that were attached on the coupon within the gauge length using a silicon-based epoxy. Figure 3.7 displays the test setup for the testing of the witness panel coupons.

From the tension tests, the elastic modulus, ultimate stress, and ultimate strain for the witness panel coupons were determined for each strand type. These values are given in Table 3.3. The stress-strain relationship of the materials in relation to steel is shown in Figure 3.8. Test results clearly indicate that the elastic modulus values are proportionally reduced in comparison to the single strand tests. This can be attributed to the increase of the epoxy matrix.

Due to the proprietary nature and recent production of the epoxy adhesive material, the material properties of the epoxy adhesive alone are not currently available through published works. It should be noted that the material properties for the epoxy adhesive were not determined in this research program.

Figure 3.7: CFRP Witness Panel Test Setup

Table 3.3: Typical Mechanical Properties of CFRP Witness Panel Coupons

CFRP Type	Ultimate Strain	Ultimate Strength		Elastic Modulus	
	(%)	ksi	MPa	ksi	MPa
Low Modulus (LM)	1.58	64.6	445	5,753	31,247
Intermediate Modulus (IM)	0.76	64.4	444	8,619	59,426
High Modulus (HM)	0.32	30.6	211	9,830	67,775

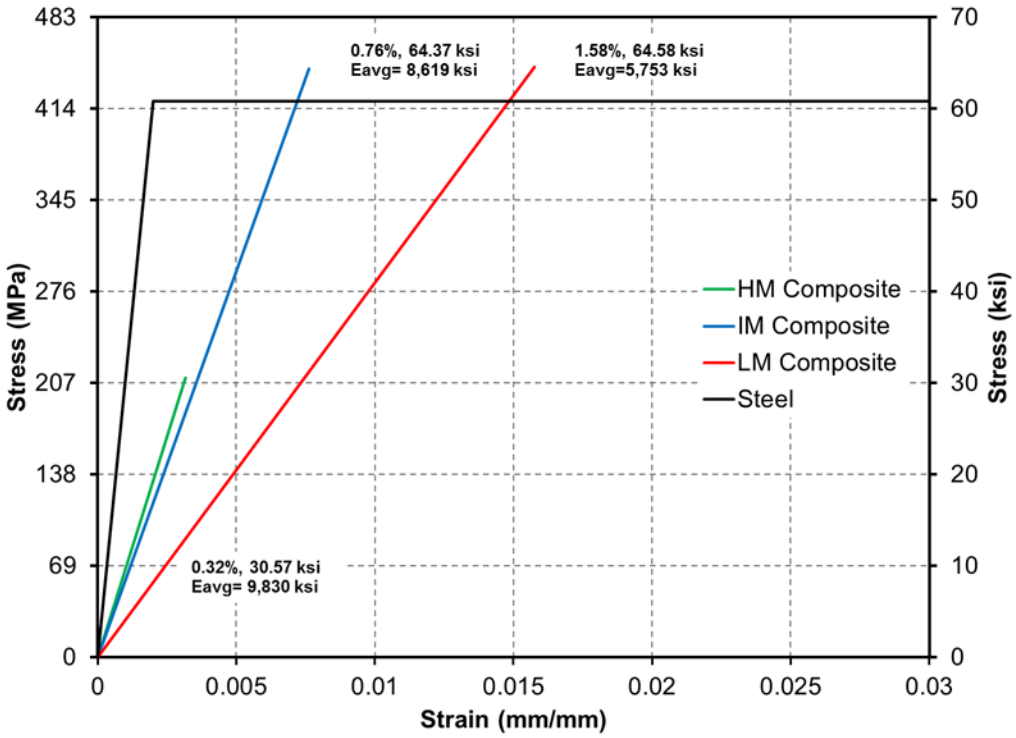

Figure 3.8: Typical Stress-Strain Behavior of CFRP Coupons

3.2 Test Specimens

For each test specimen, a steel plate was welded to high-strength steel sleeves using metal inert gas (MIG) welding. The welding process was performed in stich configured welds on opposite sides of the plate to distribute the stresses induced by the heat created by the welding process. Figure 3.9 depicts the welding process that was followed during the experimental program.

Figure 3.9: Welding of Test Specimens

3.2.1 Application of the Strengthening System

To ensure proper adherence of the strands to the steel surface, the steel plates were sandblasted prior to the commencement of the application process. After sandblasting, the plates were sealed in plastic shrink wrap to minimize any possible corrosion. When the plastic wrap was removed, compressed air and acetone were used to clean the surface of any sand residue that may have been present from the sandblasting process. Strain gauges were then applied to the steel surface on the same day of strengthening before the application of

the primer resin. Figure 3.10 displays a sandblasted plate with strain gauges attached to the clean surface.

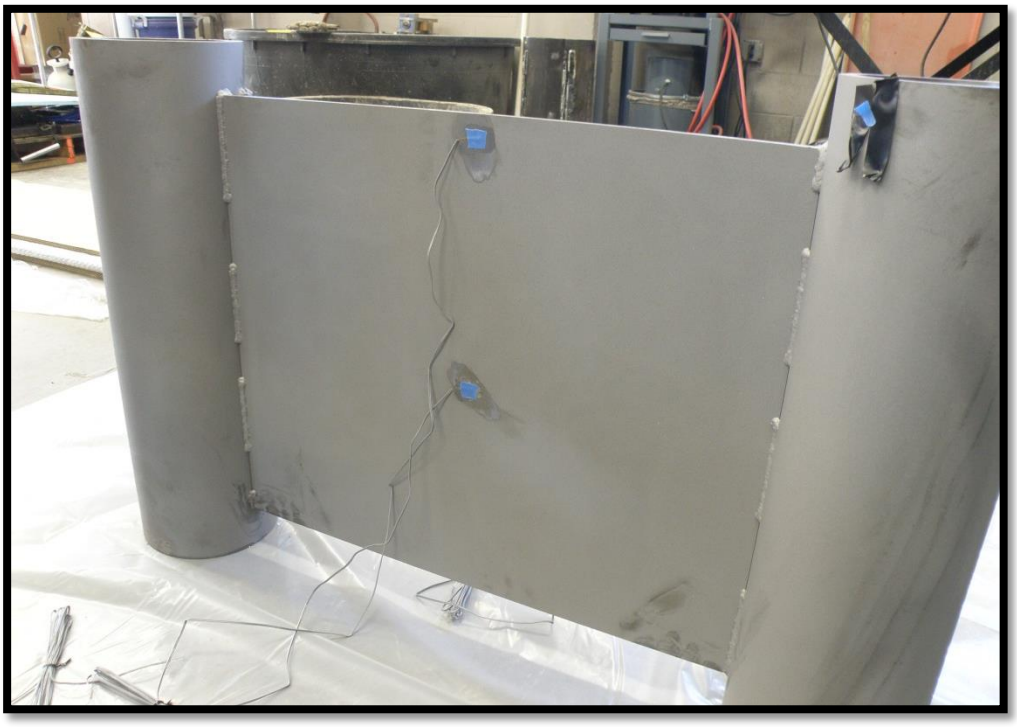

Figure 3.10: Sandblasted Plate with Strain Gauges

The primer resin was applied to the steel plates after the application of strain gauges. The primer resin was a mixture of resin and hardener with a ratio of 1:1. The components of the mixture were weighed using a digital scale and mixed using an electric mixer for two minutes. The primer resin was then applied to the clean steel surface using a paint roller as shown in Figure 3.11. Once the entire specimen was coated with the primer resin, a minimum of two hours elapsed prior to the application of any other strengthening material.

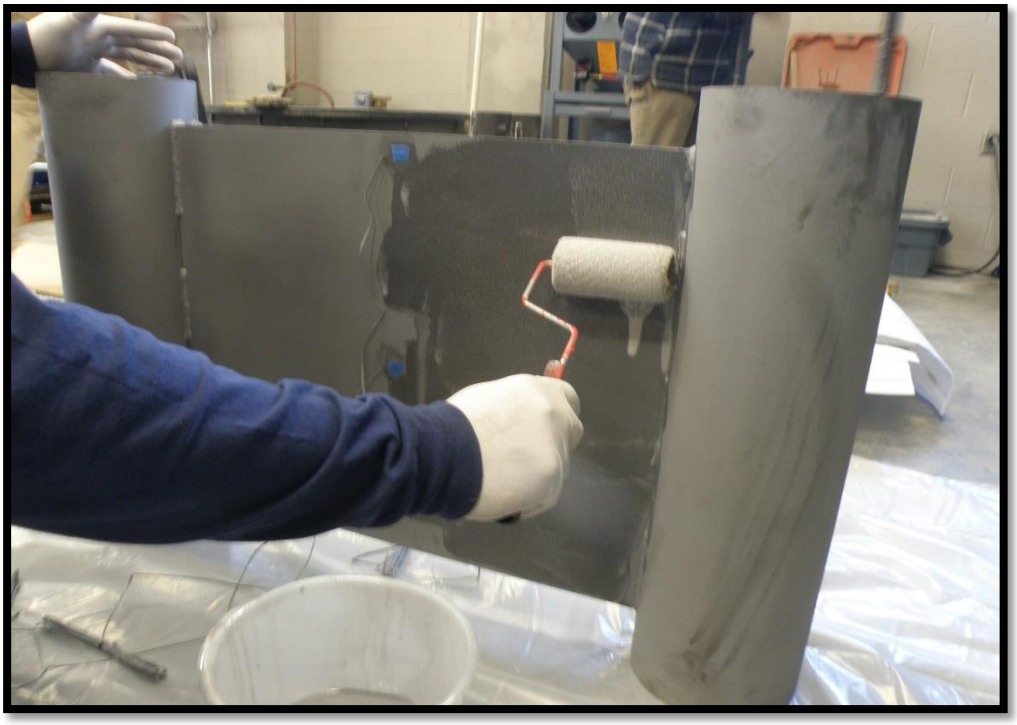

Figure 3.11: Application of Primer Layer

The polyurea putty layer, if any was to be applied to the steel, was applied after an appropriate amount of time had elapsed after the application of the primer resin. The polyurea putty consisted of a 3:1 ratio of resin and hardener, respectively. The components of the mixture were weighed using a digital scale and mixed using an electric mixer for two minutes, similar to the primer resin. The polurea putty was then applied to the primed steel surface using putty knives in order to ensure a smooth layer of the material would be achieved. Figure 3.12 displays the polyurea putty coated steel plate. The polyurea putty was to cure a minimum of six hours prior to application of the CFRP strands.

Figure 3.12: Polyurea Putty Coated Test Specimen

The CFRP strands were carefully cut to required lengths using shears. Two different types of epoxy adhesives were used depending on whether or not the plate was strengthened with polyurea putty. Regardless of the type of epoxy, the mixing ratios were to be the same. A mixing ratio of 4:1 for the resin and hardener was used. The components were weighed using a digital scale and mixed using an electric mixer for a minimum of two minutes. Once a consistent mixture was attained, a thick layer of the epoxy was applied to the steel surface using putty knives. Once the initial layer of epoxy was applied, the wires from the strain gauges were passed through the gaps between the CFRP strands. Figure 3.13 displays the process of passing strain gauge wires through the gaps of the strands. Subsequently, the

CFRP strands were applied to the steel surface. Putty knives were used to press down on the strands, allowing excess epoxy to squeeze through the gaps between the strands. A second thin layer of epoxy was then applied on the strands and smoothed using putty knives. Figure 3.14 presents the process of applying the second layer of epoxy. The strengthened specimens were left to cure for at least seven days before any testing.

Figure 3.13: Passing Strain Gauge Wires through Gaps of CFRP Strands

Figure 3.14: Application of Second Layer of Epoxy

If a second layer of the CFRP strengthening system was to be applied, it was applied after the specimens with one layer of CFRP were tested. Prior to application of the second layer of CFRP strands, the surface of the strengthened specimens were sanded using 150 grit sanding sponges until a proper bonding surface was achieved. Once the sanding was completed, the plates were blown with compressed air to remove excess epoxy material, and were thoroughly cleaned with acetone to ensure a clean surface. Figure 3.15 shows the described sanding process.

Figure 3.15: Sanding Process of First Layer of CFRP

A base layer of epoxy was applied to the surface of the existing CFRP layer. Next, the wires from the strain gauges were passed through the gaps between the CFRP strands that needed to be applied. Finally, the CFRP strands were applied to the strengthened surface. Just as before, putty knives were used to press down upon the strands allowing excess epoxy from the base layer to squeeze through the gaps of the CFRP strands. A second and final thin layer of epoxy was applied to the surface and smoothed with putty knives. The strengthened specimens were left to cure for at least seven days prior to any further testing. Upon completion of testing, the test specimens were cut from the sleeves using a plasma cutter.

New test specimens were subsequently welded to the clean, unused portion of the sleeves. The same process would follow until the sleeves no longer provided available welding space.

3.3 Test Setup

The test setup utilized for this experimental program consisted of HSS 4x4x1/2 members throughout. The frame was tied down to the strong floor at four points to ensure stability of the setup during testing. To place the prepared test specimens into the test setup, two six inch diameter chrome painted, high-strength steel pins (referred to as pins henceforth) were inserted inside the sleeves of the test specimen. It should be noted that after the pins were manufactured, holes were drilled through them at a specified distance from their ends in order to allow high-strength pre-stressing bars to pass through them. Both the inside of the sleeves and the pins were greased in order to reduce the friction between the two materials. Subsequently, high strength pre-stressing bars (referred to as HS bars) were passed through the pins. Nuts were threaded onto the top and bottom of each HS bar in order to ensure the bar stayed in proper position prior to lifting into the test setup. Finally, the entire apparatus of the HS bars, pins, sleeves, and test specimen were inserted in an upright position within the test frame. Figure 3.16 depicts both the computer rendering of the test setup (on the left) and the actual setup (on the right) for both the elevation and side views of the setup.

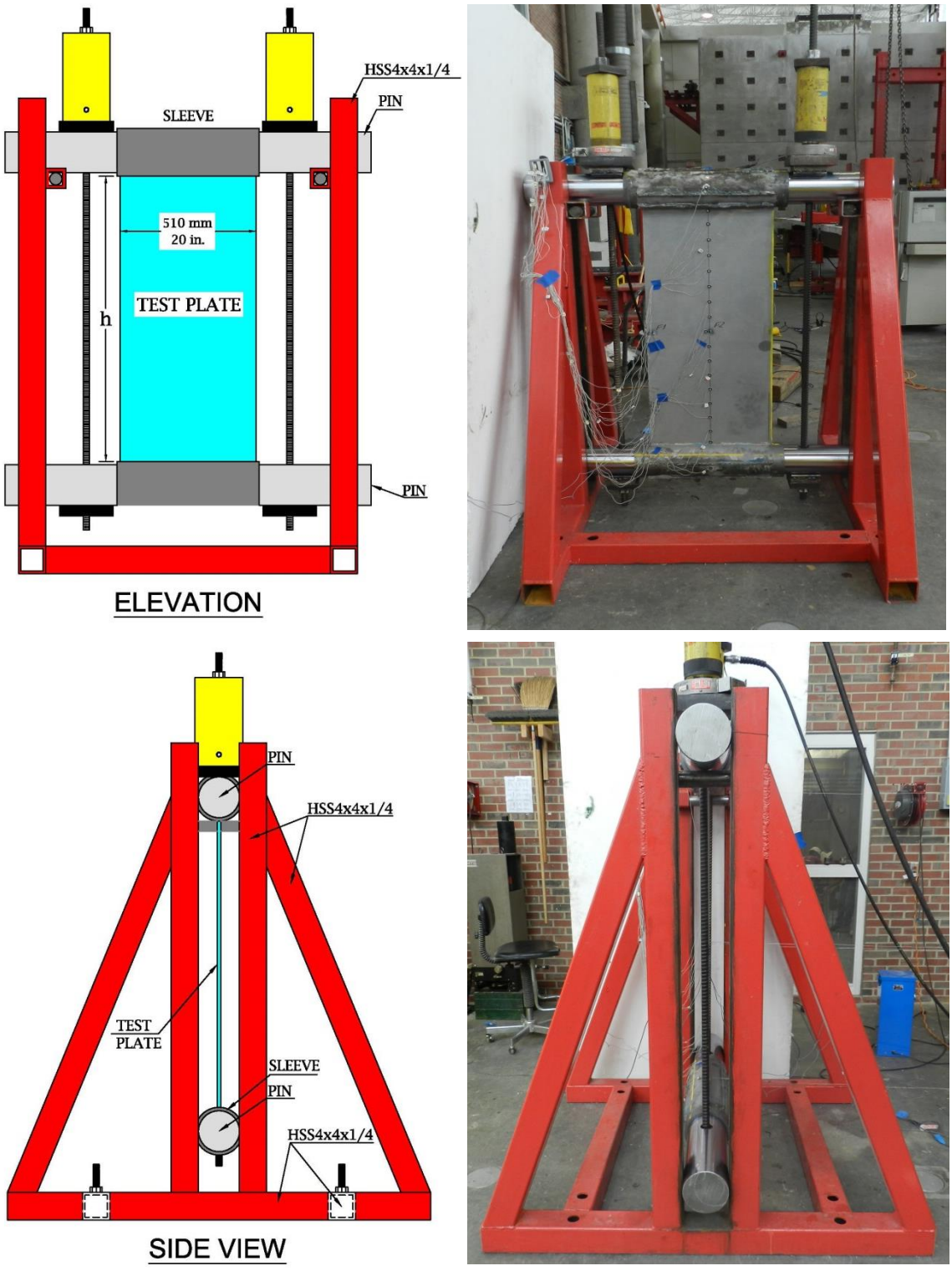

Figure 3.16: Test Setup

3.4 Load Application

In order to apply a compressive load to the test specimens, load was applied to the pins via the HS bars. "Bearing Plates" were fabricated to apply the load to the pins. The bearing plates consisted of two steel cylindrical rods welded to a steel plate. As for the top pin, bearing plates were passed through the HS bars, with the bearing plate directly contacting the top of the pin. Figure 3.17 displays a bearing plate and its orientation to the pin. Following the bearing plates, loading plates were placed through the HS bars. The loading plates were 2 inch thick steel plates. The loading plates served as a platform for the load cell to directly rest on, and thus directly applying the load to the bearing plate. Figure 3.18 depicts the usage of the bearing and loading plates used in the test setup.

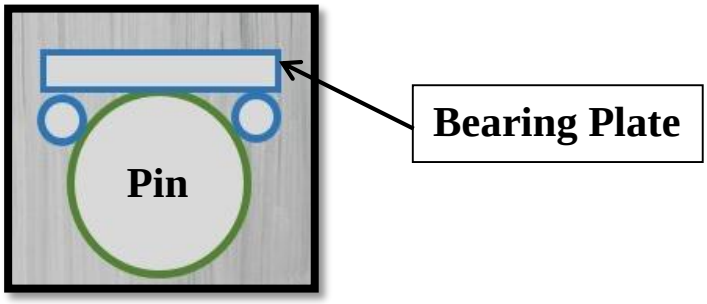

Figure 3.17: Bearing Plate and Pin

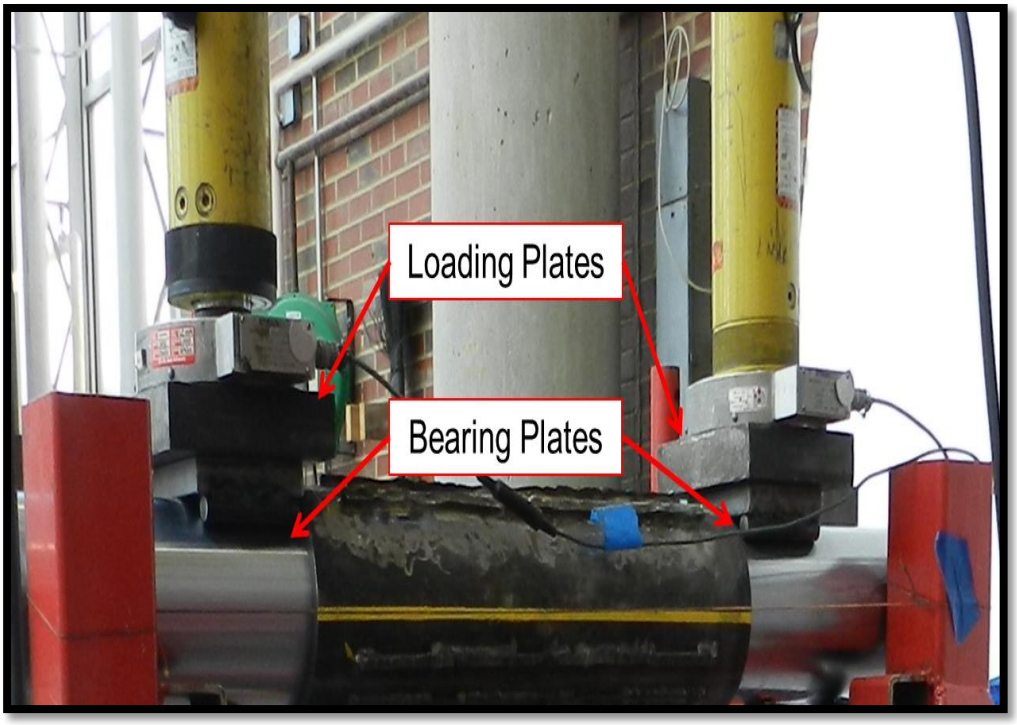

Figure 3.18: Loading Plates and Bearing Plates

Hydraulic jacks passed through the HS bars and were placed on top of the load cells. A plate and nut were placed on top of the hydraulic jacks in order to lock the HS bars in place from the top. Different capacities of hydraulic jacks were used for varying plate slenderness ratios. From the bottom pin, bearing plates were passed through each HS bar, and were locked in place by a plate and nut; thus, locking the HS bars in place from the top and the bottom. Figure 3.19 displays how the HS bars are locked in place at the bottom pin. Once the HS bars were locked in place, hydraulic hoses were connected to the hydraulic jacks. The two hydraulic hoses were connected to a splitter that was connected to a hand hydraulic pump.

The splitter ensured that each of the hydraulic jacks received an equal amount of hydraulic fluid from the hand pump; thus, applying equal load to each side of the pins. The load was applied by the hand pump at a constant pace throughout the experimental procedure in order to achieve consistent results. Furthermore, when load was applied to the test specimen, the sleeves were able to rotate about the two pins; thus attempting to replicate a pin-pin connection.

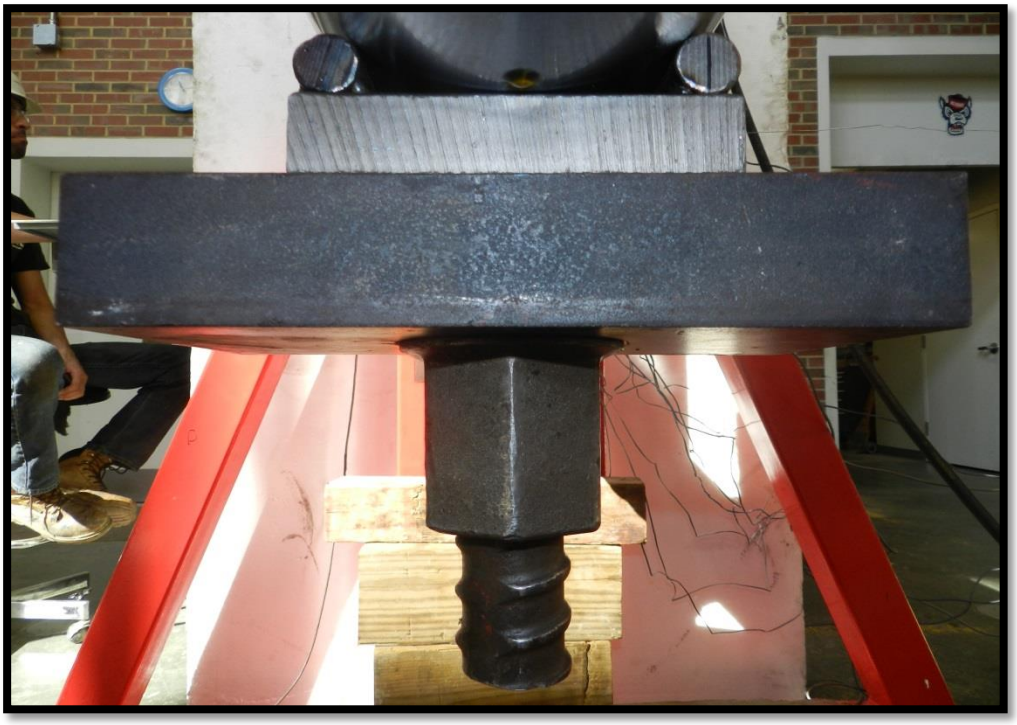

Figure 3.19: Loading Plates and Bearing Plates

3.5 Instrumentation

Load cells were utilized to capture the exact loads that were being applied to the specimen by each hydraulic jack. In order to ensure proper contact between the load cell and the hydraulic jack, washers were placed on top of the loading surface of the load cell prior to placing the hydraulic jack on the load cell. Thus, the hydraulic jack transferred the load to the washer, which directly transferred the load to the load cell. Similar to the hydraulic jacks, different load cells were used depending on the size of specimen that was to be tested.

Electrical resistance strain gauges were used to measure the local longitudinal (in the direction of the load) strain. All of the strain gauges used in the experimental program were 5mm in length. The strain gauges were applied at the mid-height of the specimen; one being one inch away from the unloaded edge of the specimen, another being one half inch away from the center of the specimen. This pattern was used for both faces of the specimen. For an un-strengthened specimen, four strain gauges were used. For a strengthened specimen, eight strain gauges were used; four were applied to the steel surface, and the other four were on the surface of the CFRP layer. Figure 3.20 and Figure 3.21 display strain gauges applied to an un-strengthened specimen as well as a strengthened specimen, respectively. The strain output from the testing process allows the determination of whether elastic or inelastic buckling is occurring.

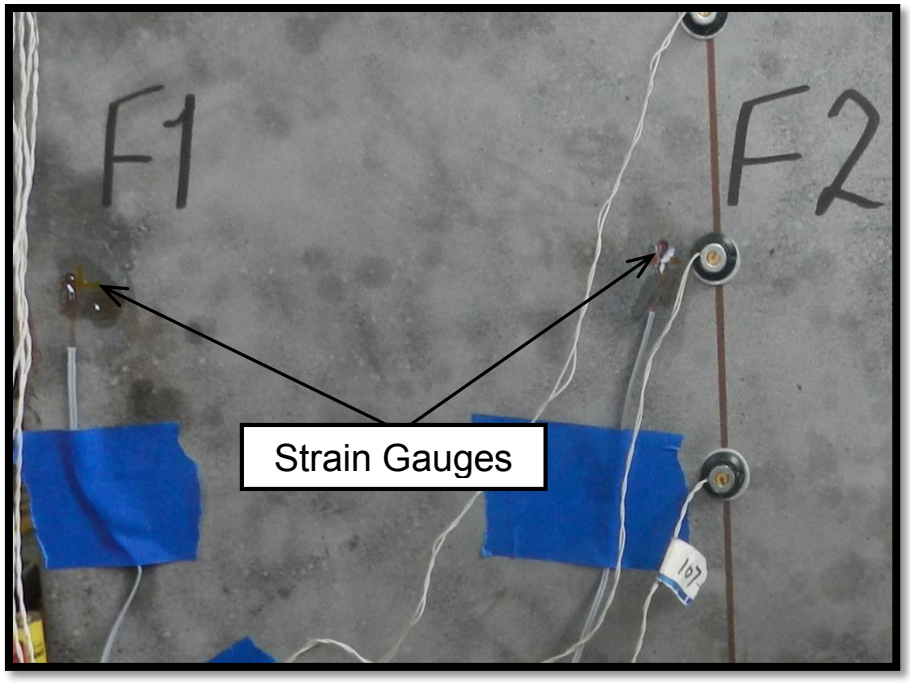

Figure 3.20: Strain Gauges on Un-Strengthened Test Specimen

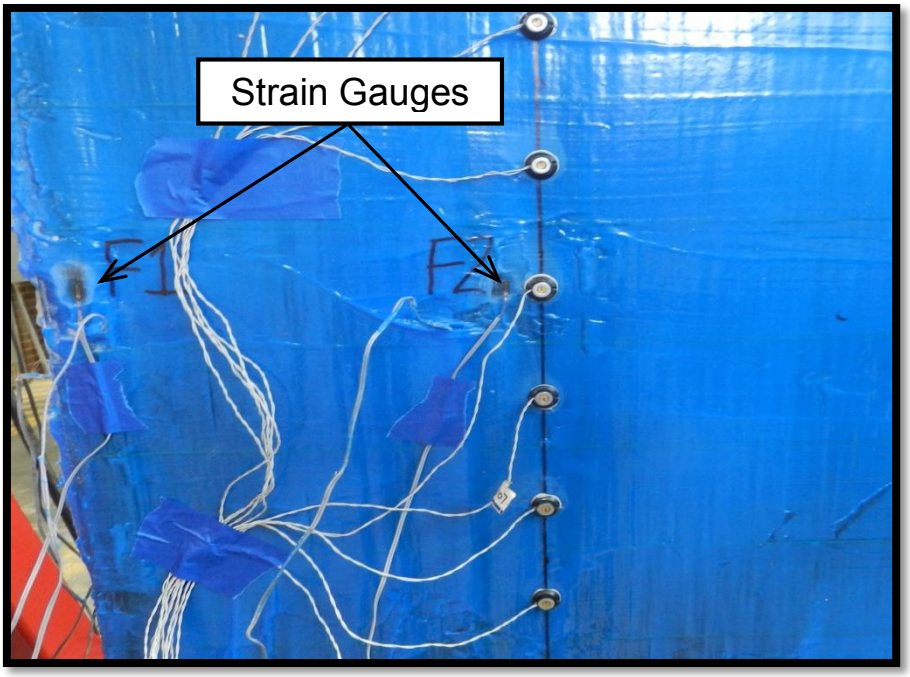

Figure 3.21: Strain Gauges on Strengthened Test Specimen

String potentiometers were used to measure lateral deflections of the specimen due to the compressive load. The string potentiometers were attached along the vertical centerline of the specimen at the top and bottom ends, as well as at the mid-height. A total of four string potentiometers were used for each test; one at the top end, one at the bottom end, and two at the mid-height of the specimen. Figure 3.22 shows the arrangement of string potentiometers utilized for the experimental program. The string potentiometers provided load-deflection behavior in order to determine the lateral deflections at any given load.

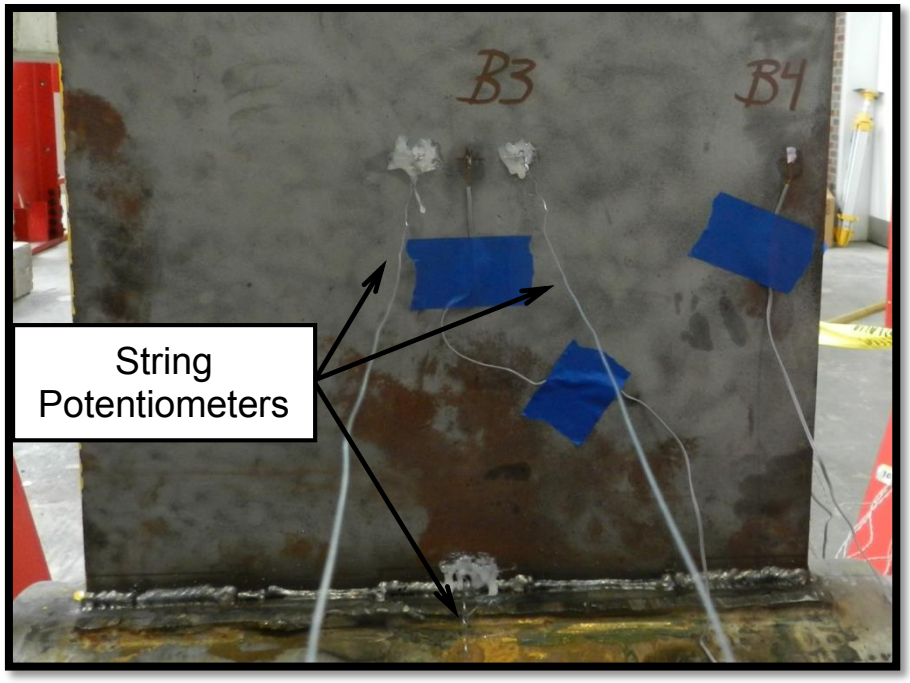

Figure 3.22: String Potentiometers on Backside of Test Specimen

For a truly pin-pin connection, there would be zero deflection at the top and bottom of a specimen when load is applied to it due to the center of rotation being directly underneath the point of load application. Figure 3.23 shows how the center of rotation of the specimen is located at the center of the pin, rather than at the top of the specimen. Thus, the deflections at the top and bottom of the specimens are not equal to zero. The net deflection was calculated by subtracting the average deflection at the top and bottom of the specimens from the deflection at the center of the specimens. The net deflection serves as a more accurate representation of lateral deflection values as compared to the measured deflection at the mid-height of the specimen.

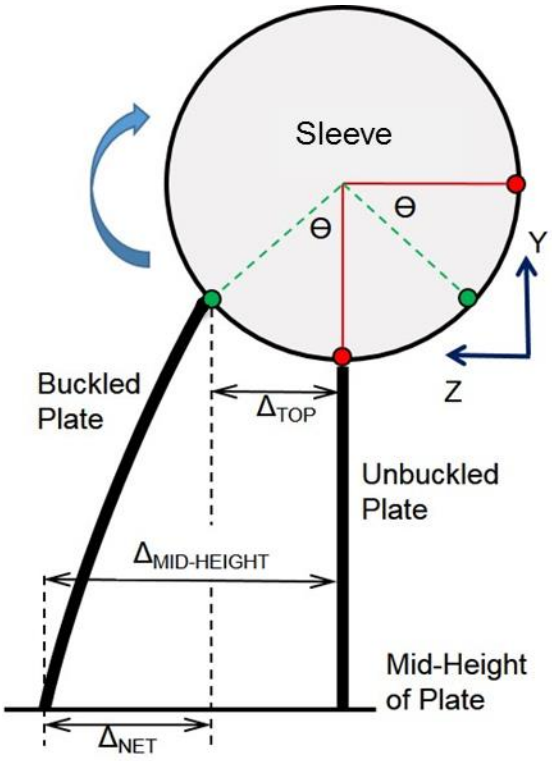

Figure 3.23: Net Deflection of Specimen and Rotation of Sleeve

A motion capturing system was used to measure the overall deflected shape of the specimens, longitudinal strains, and lateral deflections. The motion capturing system creates a three-dimensional coordinate system by the use of Infrared Emitting Diodes (IRED) attached to the plate at given points of interest. The arbitrary coordinate system is established about a point specified by the user. Any subsequent movement of the IREDs will then be captured by the camera system, in reference to the established coordinate system. The motion capturing system has an accuracy of 0.004 inches and a resolution of 0.0004 inches. The IREDs were attached to the front faces of the test specimens over their entire heights along

their centerlines and had three inch spacing. Figure 3.24 shows the arrangement of the IREDs attached to the test specimens.

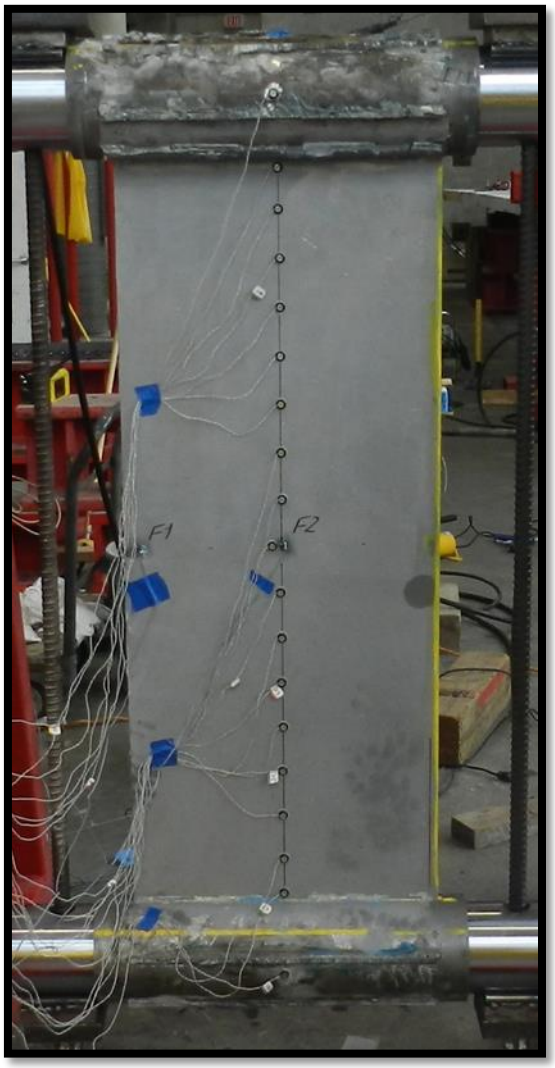

Figure 3.24: Arrangement of IRED Sensors on Test Specimen

One IRED was also attached to each sleeve as shown in Figure 3.24 to monitor the sleeve's movement, and thus, the sleeve's rotation. The purpose of this was to determine whether or not the sleeves were rotating uniformly when load was applied to the specimen. This rotation is shown in Figure 3.23. The motion capturing system would capture the vertical displacement (Y) and the out-of-plane displacement (Z) of the IRED attached to the sleeve. From these values the angle of rotation of each sleeve (θ) was calculated as shown in Equation 3.1:

$$\boldsymbol{\theta}\,(\boldsymbol{deg}) = \frac{\mathbf{180}\sqrt{(\Delta \boldsymbol{Z})^{\mathbf{2}} + (\Delta \boldsymbol{Y})^{\mathbf{2}}}}{\boldsymbol{\pi r}} \qquad \text{Equation 3.1}$$

Where r is the outer radius of the sleeve, which is equal to 3.5 inches. ΔZ and ΔY are the measured deformations in the Z and Y directions, respectively.

3.6 Test Matrices

For Phase I, there were a total of fourteen specimens tested. Eight of the specimens had a single layer of HM small diameter CFRP strands on each face of the specimen. The remaining six specimens were un-strengthened and used as control specimens. Table 3.4 is the test matrix for Phase I containing all of the specimens that were tested. The specimen designation is self-descriptive. For example, specimen I-24-3/8-S-P means that the specimen is from Phase I, is 24 inches tall, 3/8 inches thick, and is strengthened with putty.

Table 3.4: Test Matrix of Phase I

Matrix of Phase I							
Plate Designation	h		t		h/t	Strengthening	Polyurea Putty
	mm	in.	mm	in.			
I-24-1/2-U	610	24	13	1/2	48	NO	NO
I-24-1/2-S-P						YES	YES
I-24-3/8-U			10	3/8	64	NO	NO
I-24-3/8-S-P						YES	YES
I-24-5/16-U			8	5/16	77	NO	NO
I-24-5/16-S-P						YES	YES
I-24-5/16-S						YES	NO
I-48-1/2-U	1220	48	13	1/2	96	NO	NO
I-48-1/2-S-P						YES	YES
I-48-3/8-U			10	3/8	128	NO	NO
I-48-3/8-S-P						YES	YES
I-48-5/16-U			8	5/16	154	NO	NO
I-48-5/16-S-P						YES	YES
I-48-5/16-S						YES	NO

For Phase II, a total of eighteen specimens were tested. Six of the specimens were strengthened with one layer of either HM, IM, or LM small diameter CFRP strands on each face of the specimen. Another six of the specimens were strengthened with two layers of either HM, IM, or LM small diameter CFRP strands on each face of the specimen. The last six of the specimens were un-strengthened control specimens. Table 3.5 presents the test matrix for Phase II. The specimen designation is self-descriptive. For example, specimen II-48-5/16-2IM means that the specimen is from Phase II, is 48 inches tall, 5/16 inches thick, and is strengthened with two layers of intermediate modulus strands.

Table 3.5: Test Matrix of Phase II

Matrix of Phase II						
Plate Designation	h		t		h/t	Strand Type
	mm	in.	mm	in.		
II-24-5/16-LM-U	610	24	8	5/16	77	NO (CONTROL)
II-24-5/16-IM-U						NO (CONTROL)
II-24-5/16-HM-U						NO (CONTROL)
II-24-5/16-1LM						LM
II-24-5/16-1IM						IM
II-24-5/16-1HM						HM
II-24-5/16-2LM						LM
II-24-5/16-2IM						IM
II-24-5/16-2HM						HM
II-48-5/16-LM-U	1220	48	8	5/16	154	NO (CONTROL)
II-48-5/16-IM-U						NO (CONTROL)
II-48-5/16-HM-U						NO (CONTROL)
II-48-5/16-1LM						LM
II-48-5/16-1IM						IM
II-48-5/16-1HM						HM
II-48-5/16-2LM						LM
II-48-5/16-2IM						IM
II-48-5/16-2HM						HM

CHAPTER 4 : Experimental Results, Analysis, and Discussion

This chapter presents the analysis used to determine the effectiveness of the proposed CFRP materials for strengthening steel plates subjected to uniaxial compression forces. The assumptions used to predict the behavior of the test specimens, comparison of the behavior of the different strengthening systems, the parameters that were considered, and the criteria used to evaluate the effectiveness of the strengthening systems are described in this chapter. A thorough discussion of the test results and decision making steps for selecting the most effective strengthening system is also presented for each of the two phases completed in the experimental program.

4.1 First Phase

The following sections present typical behavior of the specimens tested in Phase I of the experimental program. These selected specimens are representative of typical results that were observed in Phase I. It should be mentioned that the control specimens used in this phase were tested independently from the strengthened specimens. Test results of the remaining specimens tested in Phase I are provided in the Appendices section. Table 4.1 presents the specimens that are discussed in the following sections.

Table 4.1: Phase I Test Specimens Discussed

Selected Specimens from Phase I			
Mark	**h/t**	**h/b**	**Strengthening**
I-24-(1/2)	48	1.2	U
			S-P
I-24-(5/16)	77		U
			S-P
			S (w/out Putty)
I-48-(1/2)	96	2.4	U
			S-P

4.1.1 Specimens: I-24-(1/2)

The specimens in this category were 24 inches tall, 20 inches wide, and half of an inch thick. Thus, the specimens have a slenderness ratio and aspect ratio of 48 and 1.2, respectively. Specimen I-24-(1/2)-U was used as an un-strengthened control specimen; the "U" indicating the specimen is un-strengthened. Specimen I-24-(1/2)-S-P was strengthened with one layer of HM small diameter CFRP strands on each face of the specimen. Furthermore, a layer of polyurea putty was applied between the steel surface and the CFRP strands. Thus, the "S" and the "P" in the specimen mark indicate that the specimen is strengthened (S) with a layer of polyurea putty (P).

4.1.1.1 Specimen I-24-(1/2)-U

The strain gauges that were placed at the mid-height of the specimen were used to measure the localized longitudinal strain in the direction of the applied compressive load. Test results indicate that the measured strains were virtually equal across the mid-height; therefore, the average measured strains are presented in Figure 4.1 for the compression and tension face of the specimen.

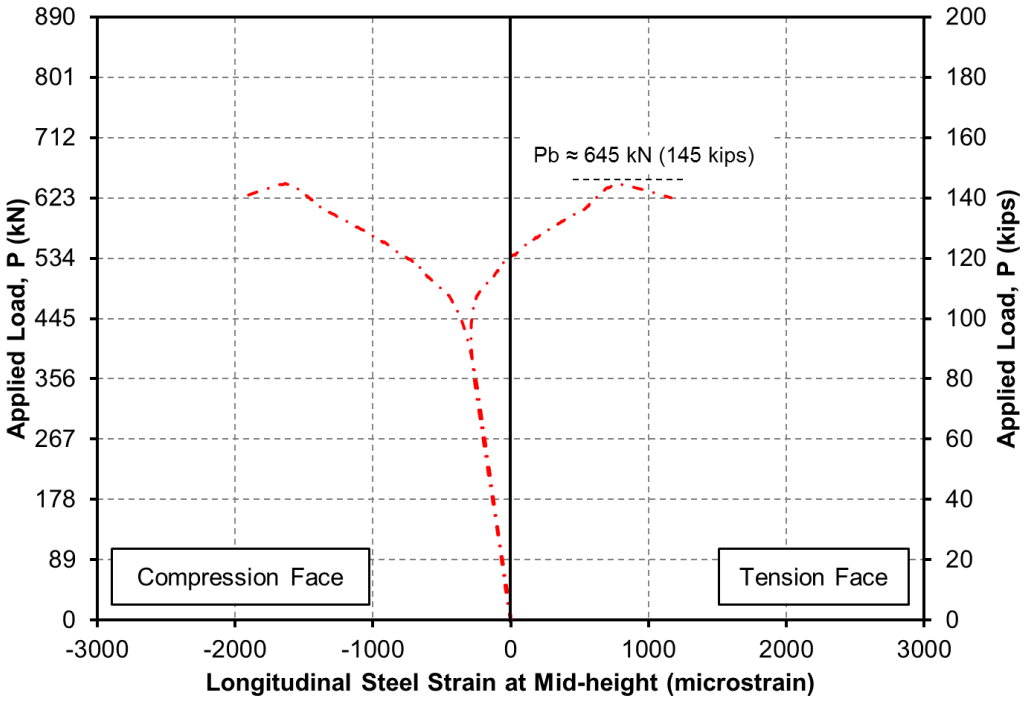

Figure 4.1: Longitudinal Strain-Load Relationship at Mid-height of Specimen I-24-(1/2)-U

It is evident from Figure 4.1 that the measured strains on both sides of the specimen were in compression until bending becomes more predominant. The measured strains on the compression face were higher than those measured on the tension face due to the combination of axial compression and the second order effects induced by the lateral deflection of the specimen. The buckling load of the specimen is 145 kips; evident by the clear reduction of loading carrying capacity of the specimen after this load level. Since the corresponding measured strain was less than the yield strain at the buckling load, it was concluded that the behavior was elastic buckling. Therefore, the failure of the system was due to loss of stability rather than a material failure.

The string potentiometers placed along the vertical centerline of the plate were used to measure the lateral deflection of the specimen due to the applied load. The net lateral deflection was calculated by subtracting the average measured deflections at the top and bottom of the specimen from the average measured deflection at the mid-height of the specimen. Figure 4.2 depicts the net lateral deflection of specimen I-24-(1/2)-U.

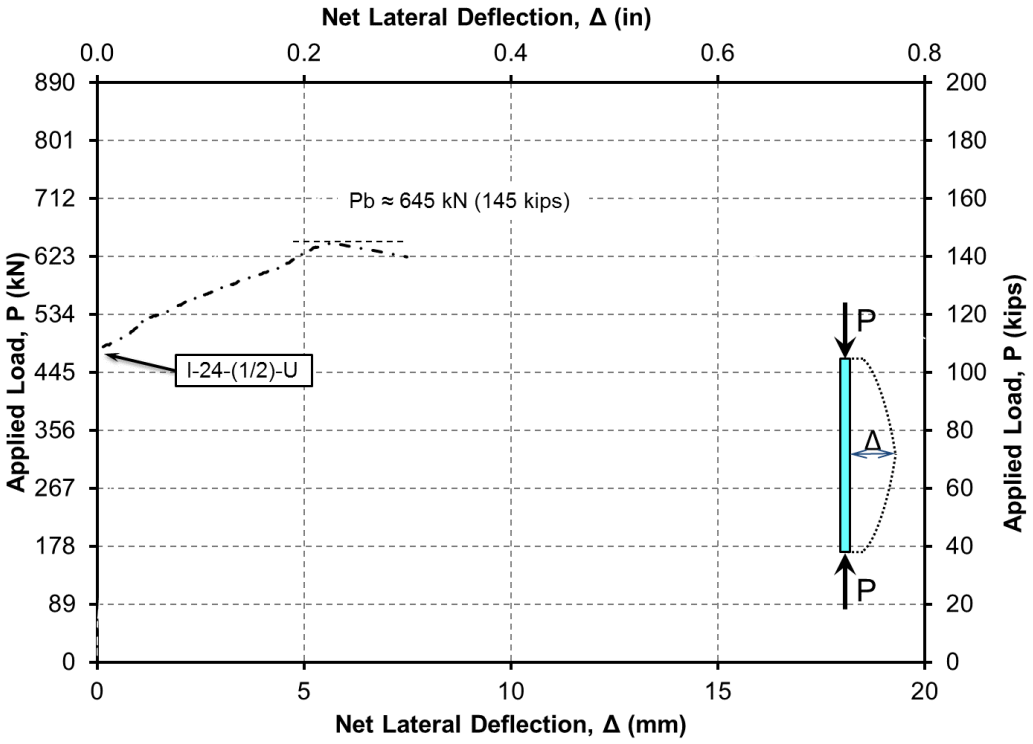

Figure 4.2: Net Lateral Deflection-Load Relationship at Mid-height of Specimen I-24-(1/2)-U

The results shown in Figure 4.2 confirm the behavior and the results shown in Figure 4.1. There is virtually zero lateral deflection at the mid-height of the specimen until the applied load approached the buckling load. Once the specimen began to bend, the lateral deflection began to increase along with the increase in applied load until buckling occurred, followed by loss of the load carrying capacity. Figure 4.3 shows the side view of specimen I-24-(1/2)-U after it has buckled. The tension and compression faces are identified on the figure. The buckled shape shown in Figure 4.3 was the typical buckled profile for all of the specimens tested in the experimental program.

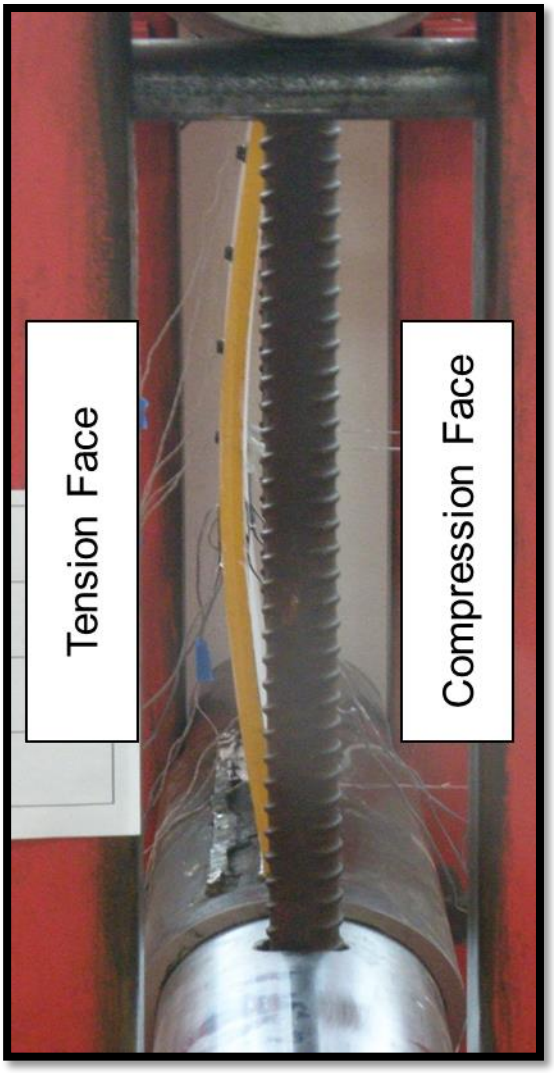

Figure 4.3: Side View of Specimen I-24-(1/2)-U after Buckling

4.1.1.2 Specimen I-24-(1/2)-S-P

Figure 4.4 exhibits the average longitudinal strain for the steel and CFRP at the mid-height of the specimen. The two diagrams in the plot are the measured average strains for the strain in the steel and CFRP material for the same specimen. The behavior clearly indicates that the buckling load of the specimen is 177 kips. Furthermore, the measured strain on the compression face of the specimen indicates that the specimen was very close to yielding at the buckling load, but still experienced elastic buckling. Figure 4.5 compares the un-strengthened specimen with the strengthened specimen. Test results indicate that adding one layer of HM CFRP strands increased the buckling capacity by 22%. When comparing the load-strain behaviors of the strengthened and un-strengthened specimens, it is clear imperfection of the strengthened specimen induced bending due to the applied compression load in comparison to the un-strengthened specimen.

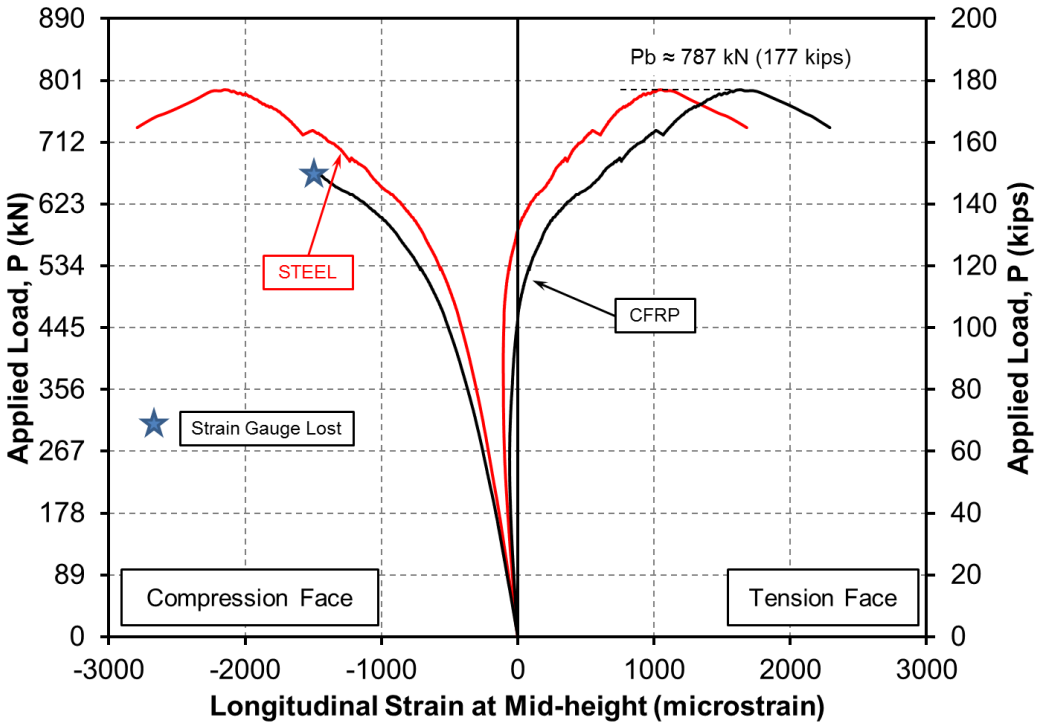

Figure 4.4: Longitudinal Strain-Load Relationship at Mid-height of Specimen I-24-(1/2)-S-P

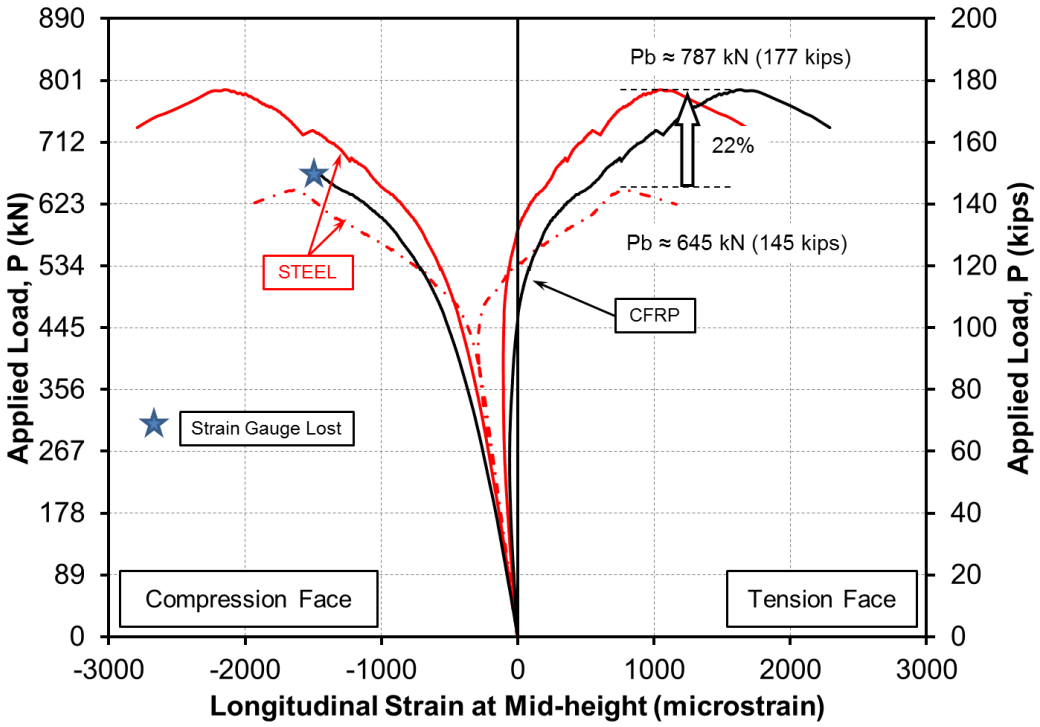

Figure 4.5: Longitudinal Strain-Load Relationship Comparison of I-24-(1/2) Specimens

Figure 4.6 shows the net lateral deflection of specimen I-24-(1/2)-S-P. Figure 4.7 combines the lateral deflections of specimens I-24-(1/2)-U and I-24-(1/2)-S-P. The increase in the buckling load of 22% is also shown in Figure 4.7.

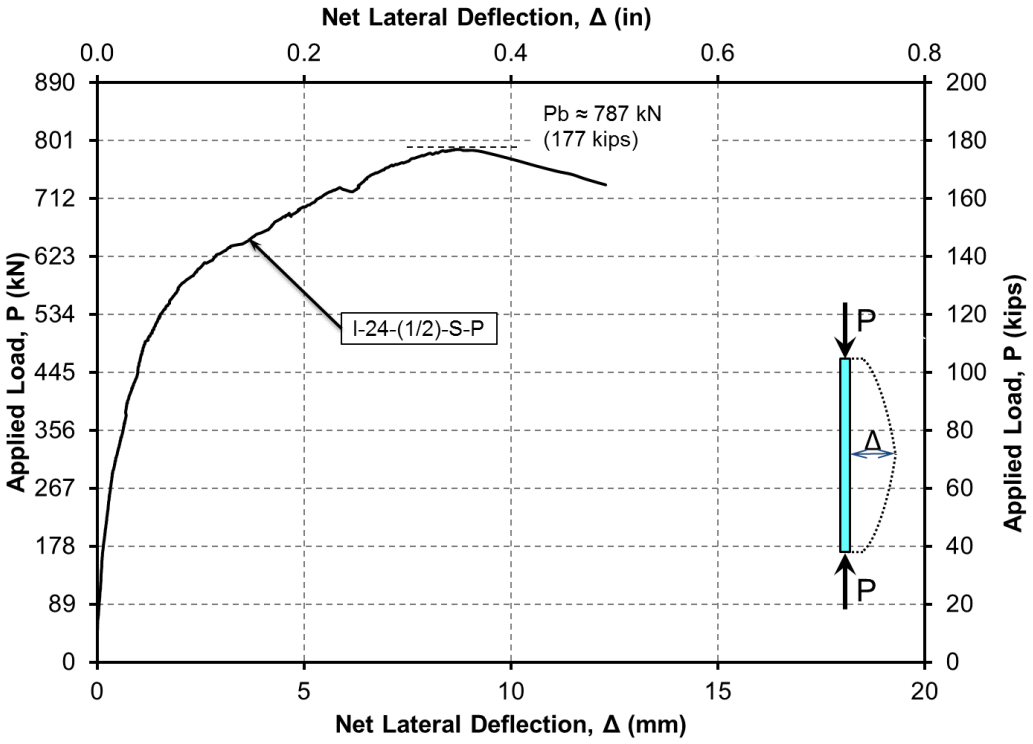

Figure 4.6: Net Lateral Deflection-Load Relationship at Mid-height of Specimen I-24-(1/2)-S-P

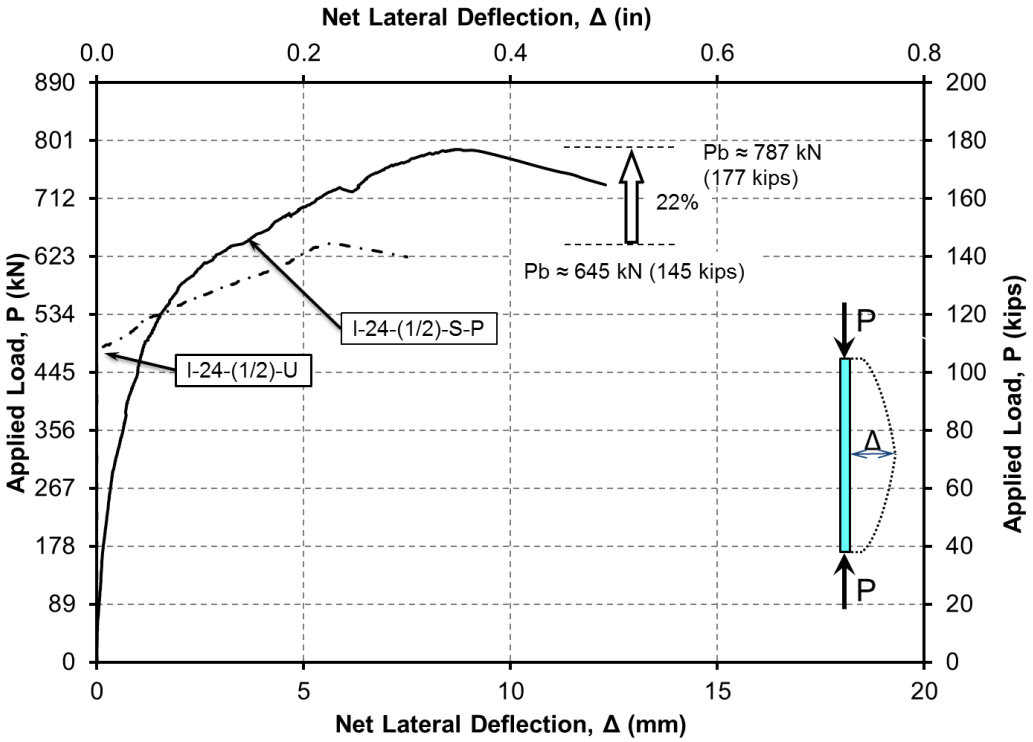

Figure 4.7: Net Lateral Deflection-Load Relationship Comparison of I-24-(1/2) Specimens

The addition of an FRP strengthening system is not normally expected to reduce the initial lateral stiffness of the specimen. Variation of the thickness of the applied strengthening system on either side of the specimen may lead to possible eccentricity of the applied compression load and induce secondary moment which can alter the behavior of the specimen. Moreover, using two different steel plates for the control and strengthen specimen could also have different residual stresses which can also affect the behavior.

4.1.2 Three Dimensional Measurements

A motion capturing system was used for all of the specimens tested in the experimental program. The system is capable of measuring the deformation of a specimen in three dimensions. The system provided lateral deflection measurements, strain measurements, as well as sleeve rotation angles. Figure 4.8 shows the deflected shape for specimen I-24-(1/2)-S-P at three different applied loads levels. Similar plots were generated for other test specimens tested in Phase I and Phase II.

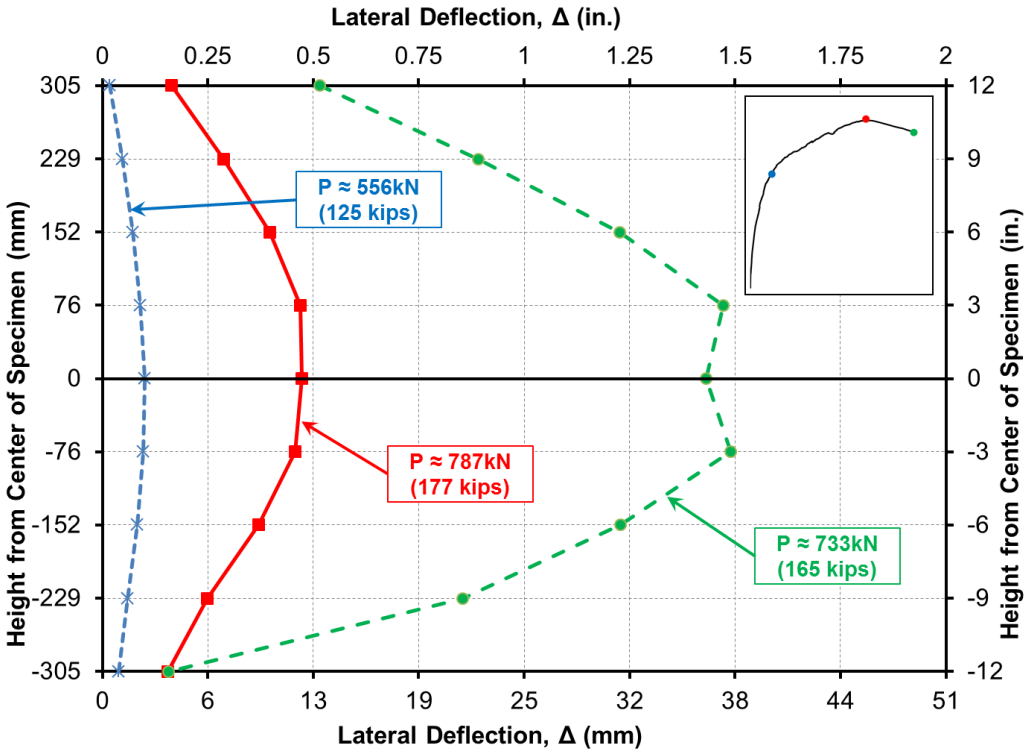

Figure 4.8: Incremented Measured Loads vs. Lateral Deformation of Specimen I-24-(1/2)-S-P

The angle of rotation for the top and bottom sleeves as load is applied to specimen I-24-(1/2)-S-P is shown in Figure 4.9. It is clear that as load is gradually applied to the specimen, the angle of rotation is increased. Thus, proving that the designed test set-up performed as it was intended to. Similar plots were developed for all of the test specimens in Phase I and Phase II.

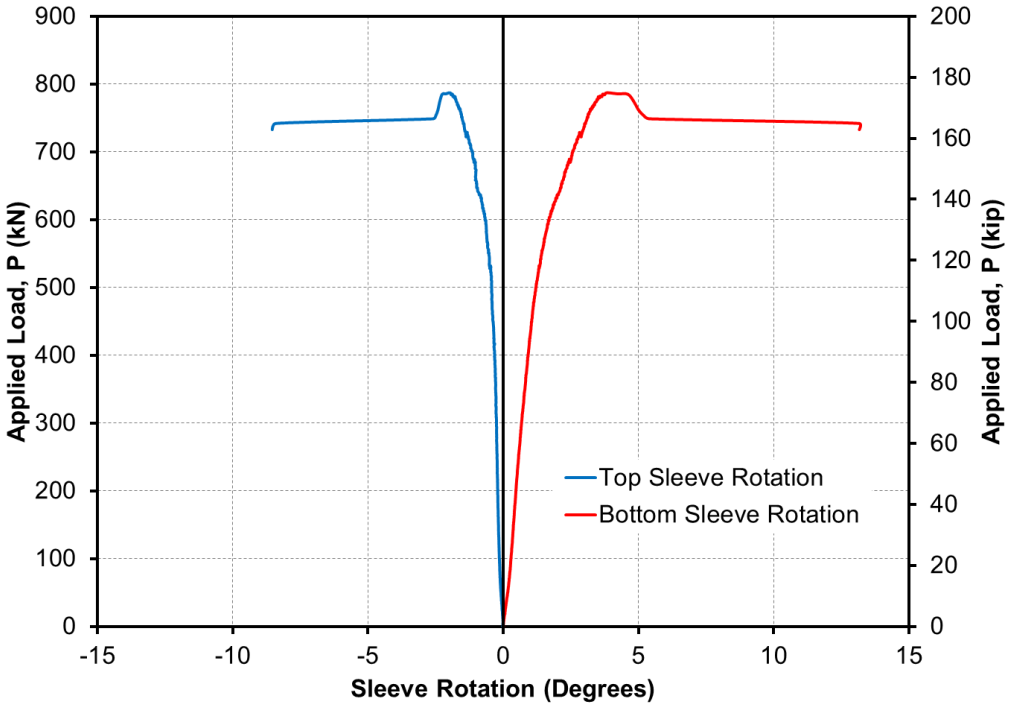

Figure 4.9: Measured Sleeve Rotation-Load Relationship of Specimen I-24-(1/2)-S-P

4.1.3 Specimens: I-24-(5/16)

The specimens in this category are 24 inches tall, 20 inches wide and five-sixteenths of an inch thick. Thus, the specimens have a slenderness ratio and aspect ratio of 77 and 1.2, respectively.

4.1.3.1 Specimen I-24-(5/16)-U

This specimen was used as an un-strengthened control specimen. The measured average strains are shown in Figure 4.10 for the compression and tension face of the specimen.

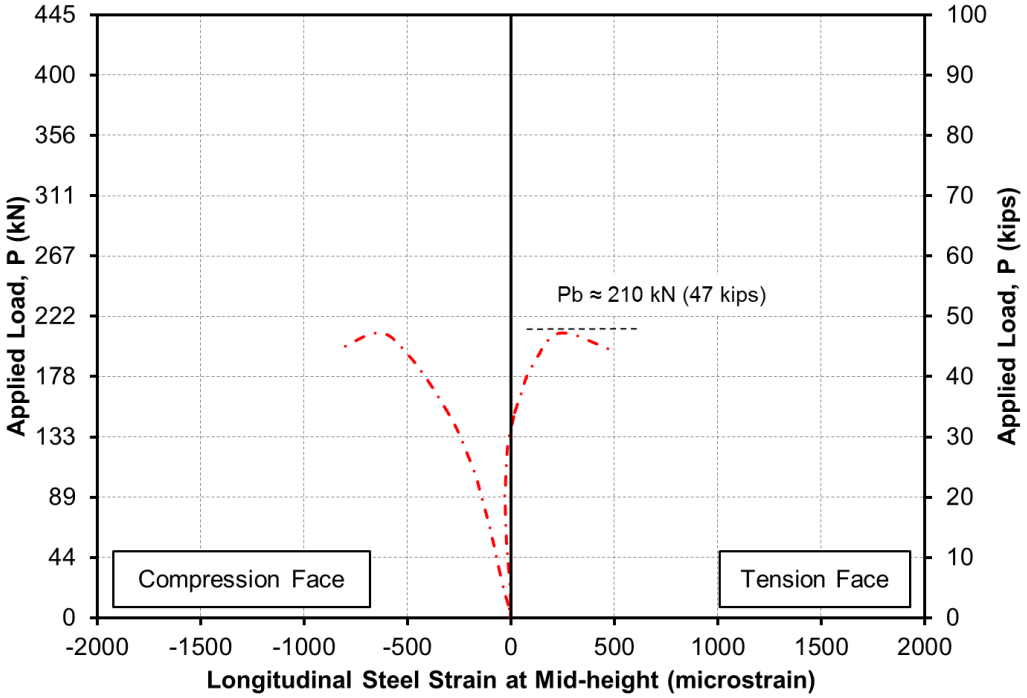

Figure 4.10: Longitudinal Strain-Load Relationship at Mid-height of Specimen I-24-(5/16)-U

Figure 4.10 shows that the buckling load of the specimen was 47 kips; evident by the clear reduction of loading carrying capacity of the specimen beyond this load level. Since the corresponding measured strain was less than the yield strain, it was evident that the exhibited behavior was elastic buckling.

The measured net lateral deflection of specimen I-24-(5/16)-U is shown in Figure 4.11. The presence of lateral deflection becomes noticeable at approximately half of the buckling load.

After this load level, the lateral deflection increases with an increase in load until buckling is reached.

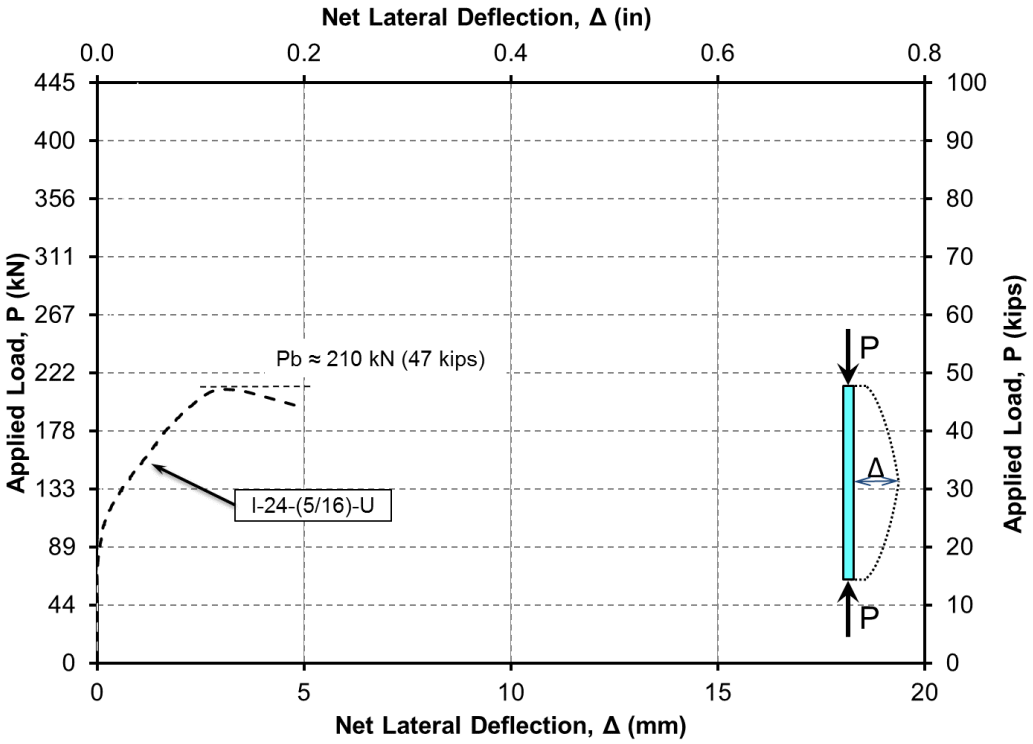

Figure 4.11: Net Lateral Deflection-Load Relationship at Mid-height of Specimen I-24-(5/16)-U

4.1.3.2 Specimen I-24-(5/16)-S-P

This specimen was strengthened with one layer of HM small diameter CFRP strands on both faces of the specimen. A layer of polyurea putty was used to separate the CFRP strands from the face of the steel. Figure 4.12 shows the measured longitudinal steel and CFRP strains at the mid-height of the specimen. The buckling load of the specimen was 66 kips. Figure 4.13

compares the un-strengthened specimen with the strengthened specimen. Test results indicate that using one layer of HM CFRP strands, there is a 40% increase in the buckling load. It was observed that the steel strain values of the strengthened specimen were less than the steel strain values of the un-strengthened specimen at any given load level.

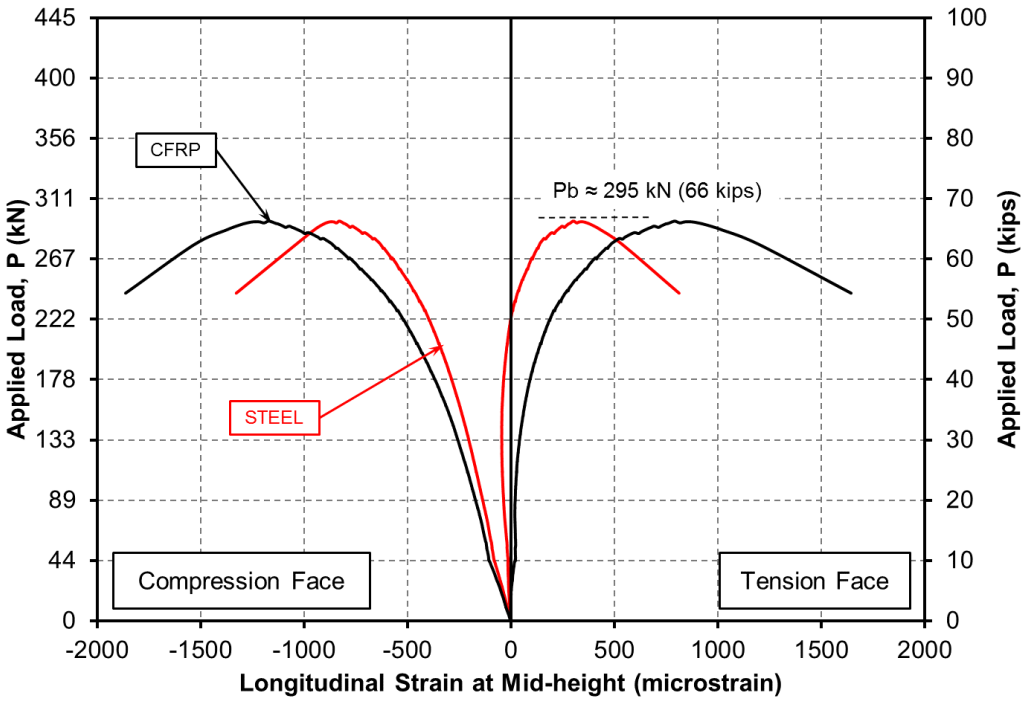

Figure 4.12: Longitudinal Strain-Load Relationship at Mid-height of Specimen I-24-(5/16)-S-P

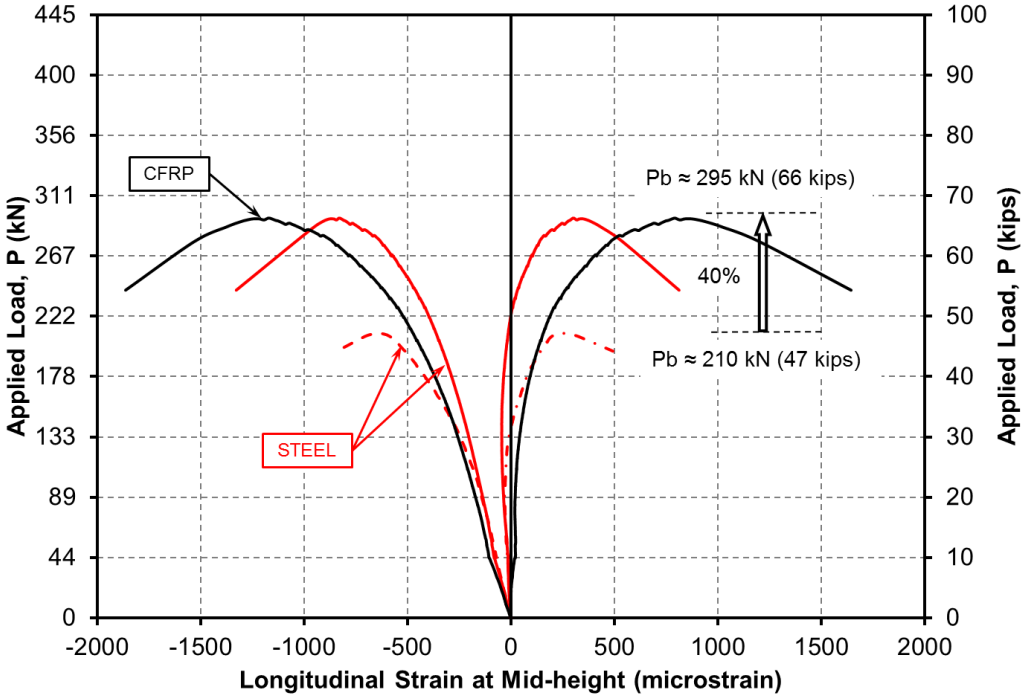

Figure 4.13: Longitudinal Strain-Load Relationship Comparison of I-24-(5/16) Specimens with Putty

Figure 4.14 displays the lateral deflection of specimen I-24-(5/16)-S-P. Figure 4.15 compares the lateral deflections of control specimen I-24-(5/16)-U and strengthened specimen I-24-(5/16)-S-P. It is clear that the initial lateral stiffness of the strengthened specimen is higher than that of the un-strengthened specimen, evident by the delayed on-set of secondary bending for the strengthened specimen.

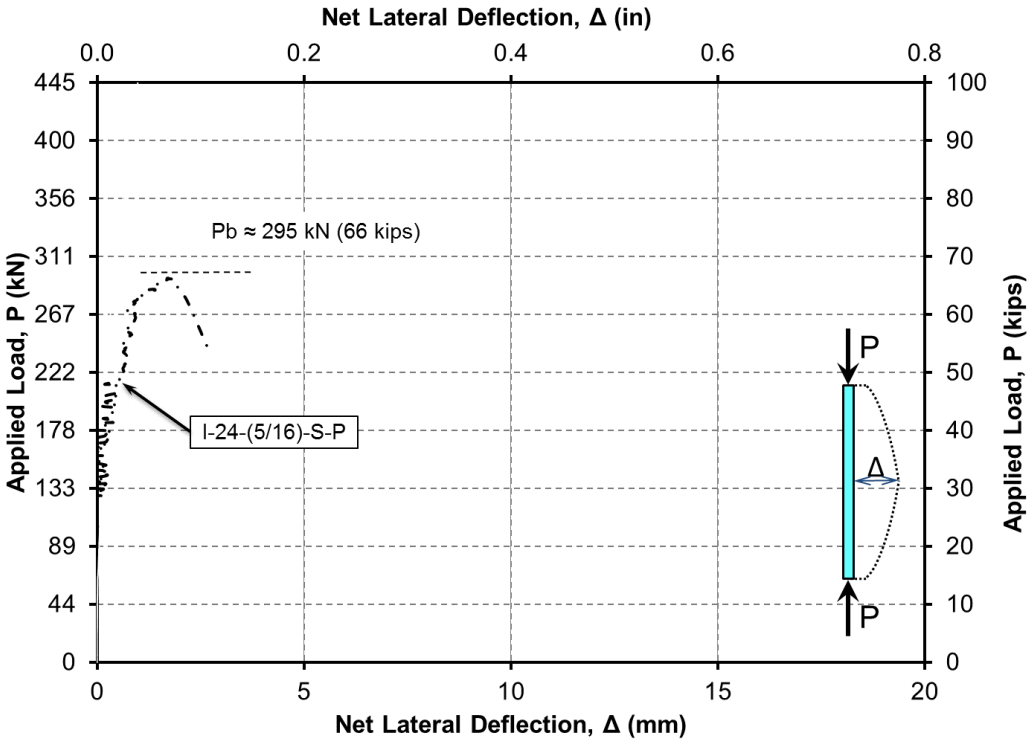

Figure 4.14: Net Lateral Deflection-Load Relationship at Mid-height of Specimen I-24-(5/16)-S-P

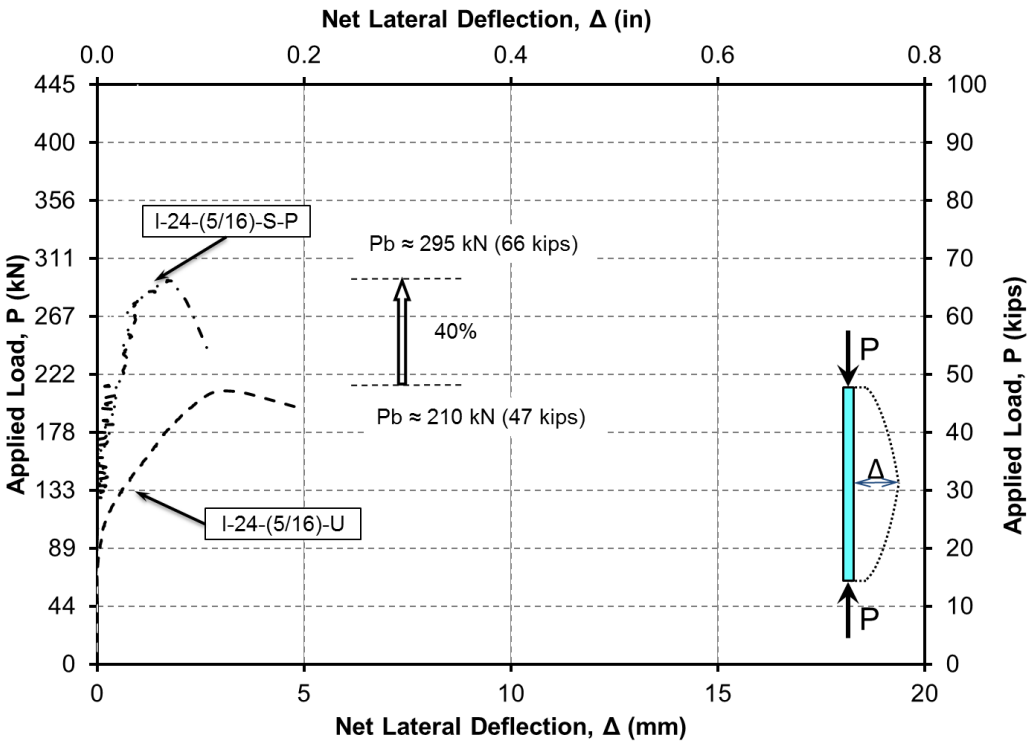

Figure 4.15: Net Lateral Deflection-Load Relationship Comparison of I-24-(5/16) Specimens with Putty

4.1.3.3 Specimen I-24-(5/16)-S

This specimen was strengthened with one layer of HM small diameter CFRP strands on both sides of the specimen. No polyurea putty was used, however, to separate the CFRP strands from the face of the primed steel. Figure 4.16 shows the measured longitudinal steel and CFRP strains at the mid-height of the specimen. The measured buckling load of the specimen was 73 kips. Figure 4.17 compares the un-strengthened specimen with the strengthened specimen.

Test results indicate that using one layer of HM CFRP strands, an increase in the buckling load capacity of 55% can be achieved. Similar to specimen I-24-(5/16)-S-P, it is observed that there is a reduction in measured strain values at the level of the steel for the strengthened specimen when compared to the measured steel strain values for the un-strengthened specimen.

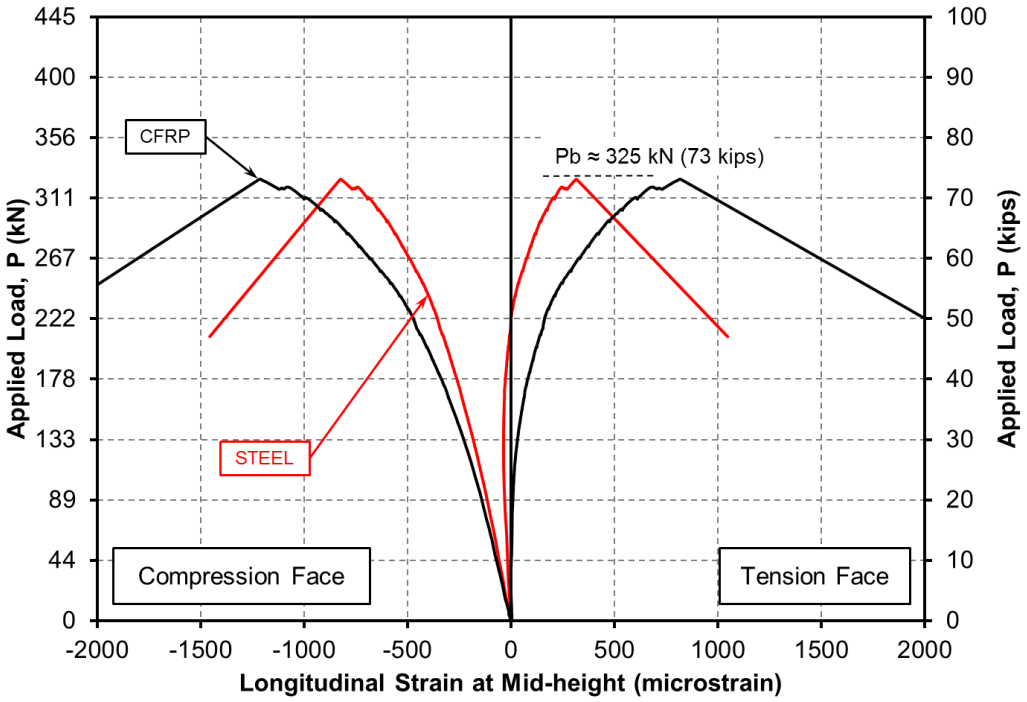

Figure 4.16: Longitudinal Strain-Load Relationship at Mid-height of Specimen I-24-(5/16)-S

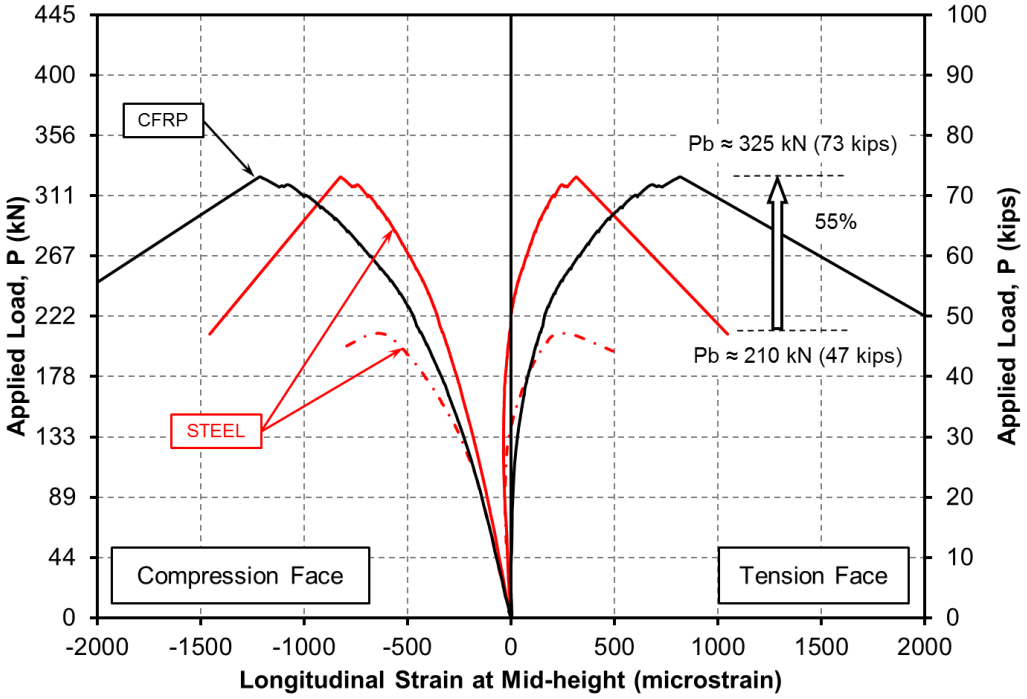

Figure 4.17: Longitudinal Strain-Load Relationship Comparison of I-24-(5/16) Specimens without Putty

Figure 4.18 displays the lateral deflection behavior of specimen I-24-(5/16)-S. Figure 4.19 compares the lateral deflections of control specimen I-24-(5/16)-U and strengthened specimen I-24-(5/16)-S. The apparent reduction in initial lateral stiffness of the strengthened specimen can be attributed to the factors previously discussed including variable CFRP thicknesses and imperfections of the steel plate.

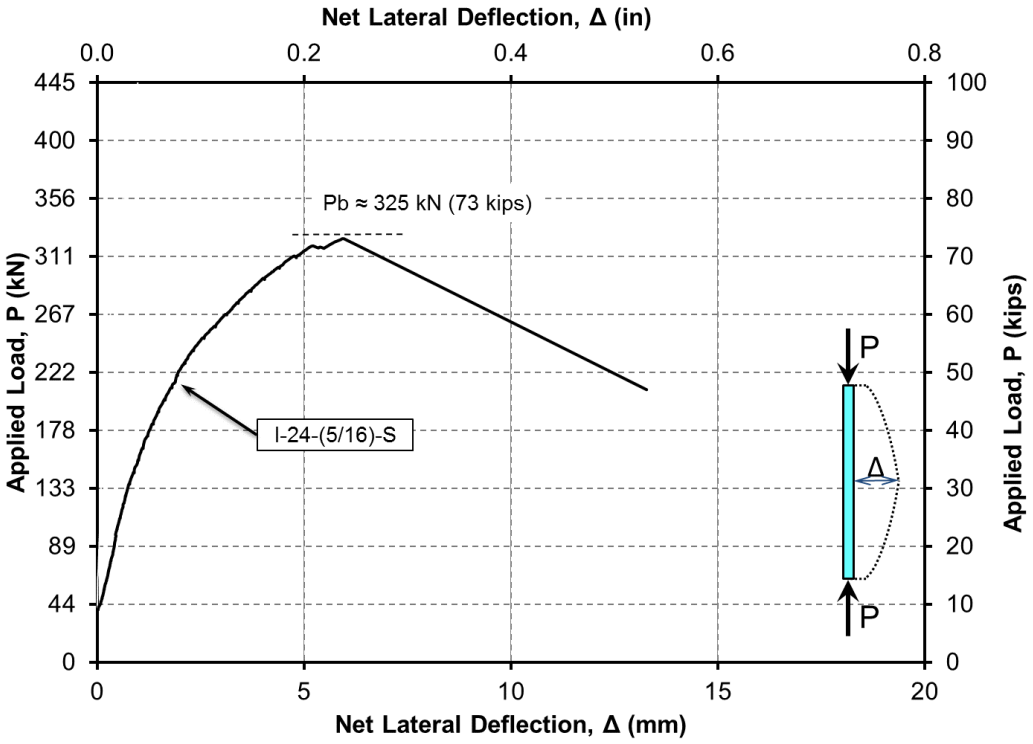

Figure 4.18: Net Lateral Deflection-Load Relationship at Mid-height of Specimen I-24-(5/16)-S

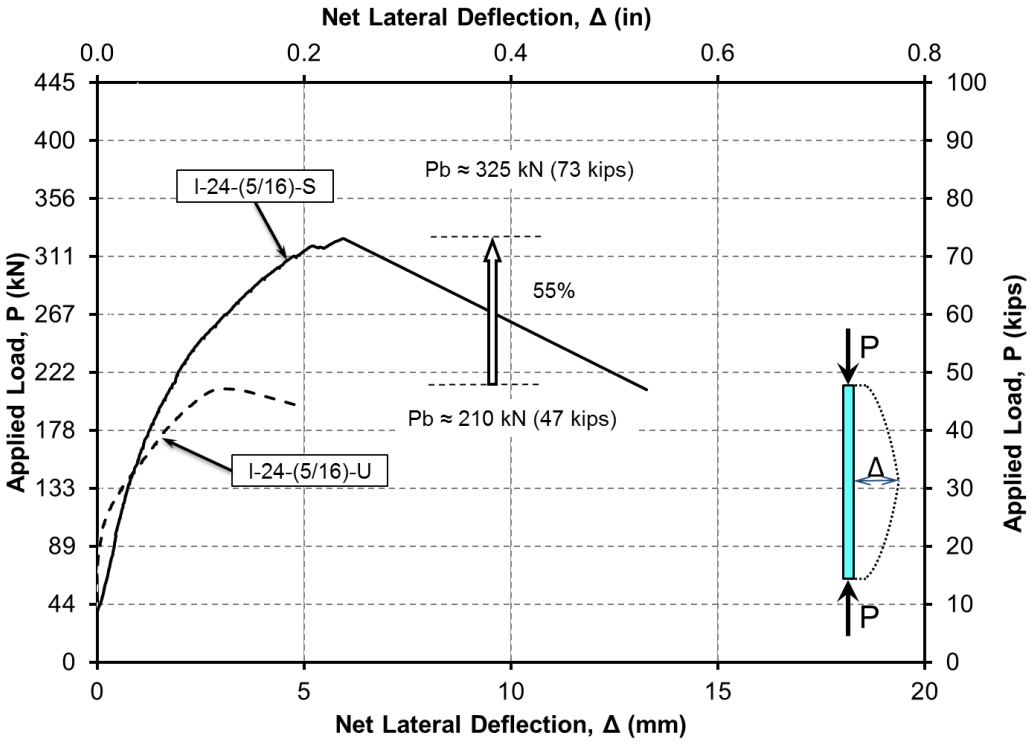

Figure 4.19: Net Lateral Deflection-Load Relationship Comparison of I-24-(5/16) Specimens without Putty

4.1.4 Specimens: I-48-(1/2)

The specimens in this category were 48 inches tall, 20 inches wide and half an inch thick. Thus, the specimens have a slenderness ratio and aspect ratio of 96 and 2.4, respectively.

4.1.4.1 Specimen I-48-(1/2)-U

Specimen I-48-(1/2)-U was used as an un-strengthened control specimen. The measured average load-strain relationship is shown in Figure 4.20 for the compression and tension face of the specimen.

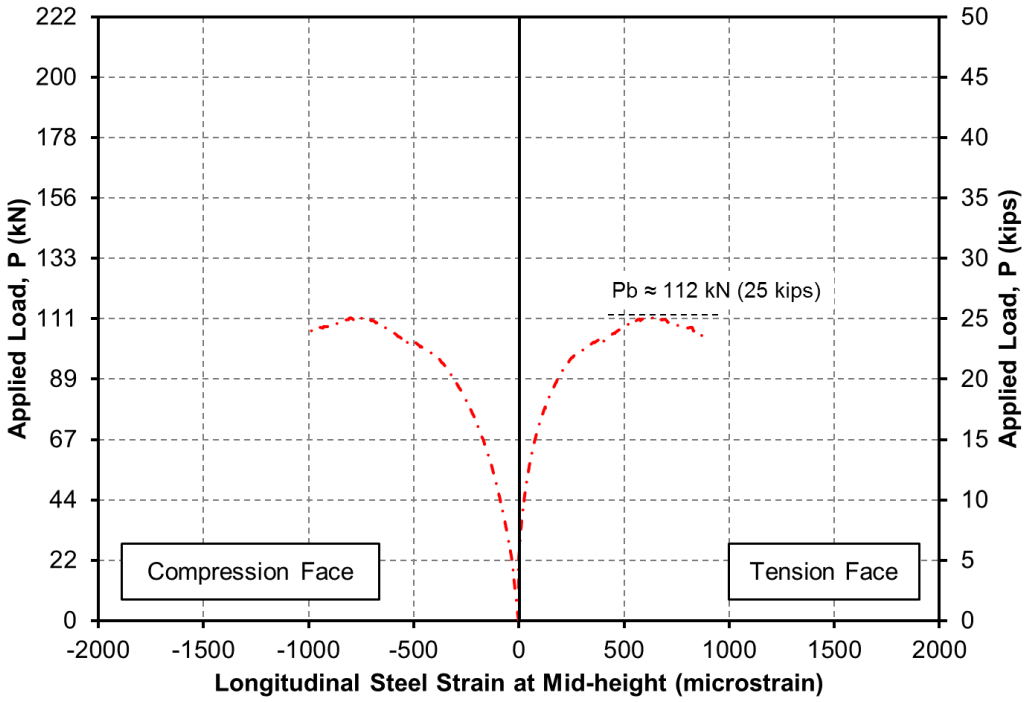

Figure 4.20: Longitudinal Strain-Load Relationship Comparison of I-48-(1/2)-U

Figure 4.20 indicates that the buckling load of the specimen was 25 kips; evident by the clear reduction of loading bearing capacity of the specimen beyond this load level. Since the corresponding measured strain was less than the yield strain, it was evident that the behavior was elastic buckling. It is also clear that secondary bending of the specimen is prevalent in

this case since the measured strains on one side of the plate was in tension at a small applied load. This sort of behavior can be attributed to initial out-of-straightness of the plate before testing which became more dominate for longer, more slender specimens.

Net lateral deflection of specimen I-48-(1/2)-U is shown in Figure 4.21. It is clear that the lateral deflection occurs at a very low applied load due to the presence of out-of-straightness in the specimen, confirming the measured load-strain behavior.

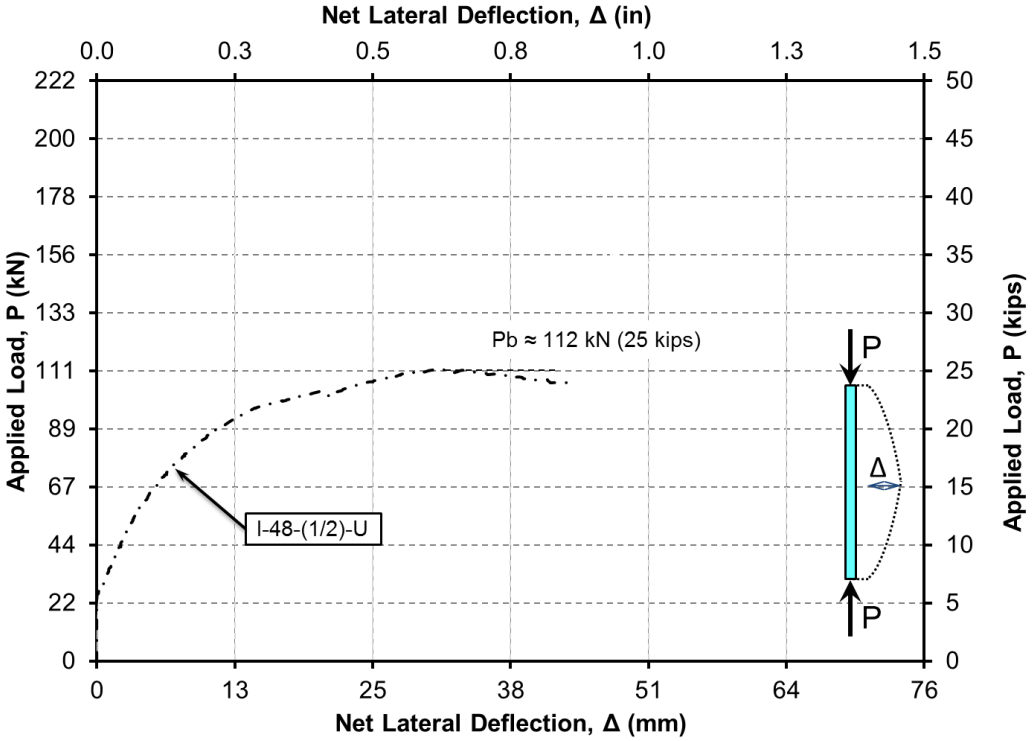

Figure 4.21: Net Lateral Deflection-Load Relationship at Mid-height of Specimen I-48-(1/2)-U

4.1.4.2 Specimen I-48-1/2-S-P

Figure 4.22 shows the measured average strains across the mid-height of the specimens for the compression and tension face for the strengthened specimen I-48-(1/2)-S-P. Figure 4.23 combines the load-strain behaviors for the control specimen I-48-(1/2)-U and strengthened specimen I-48-(1/2)-S-P.

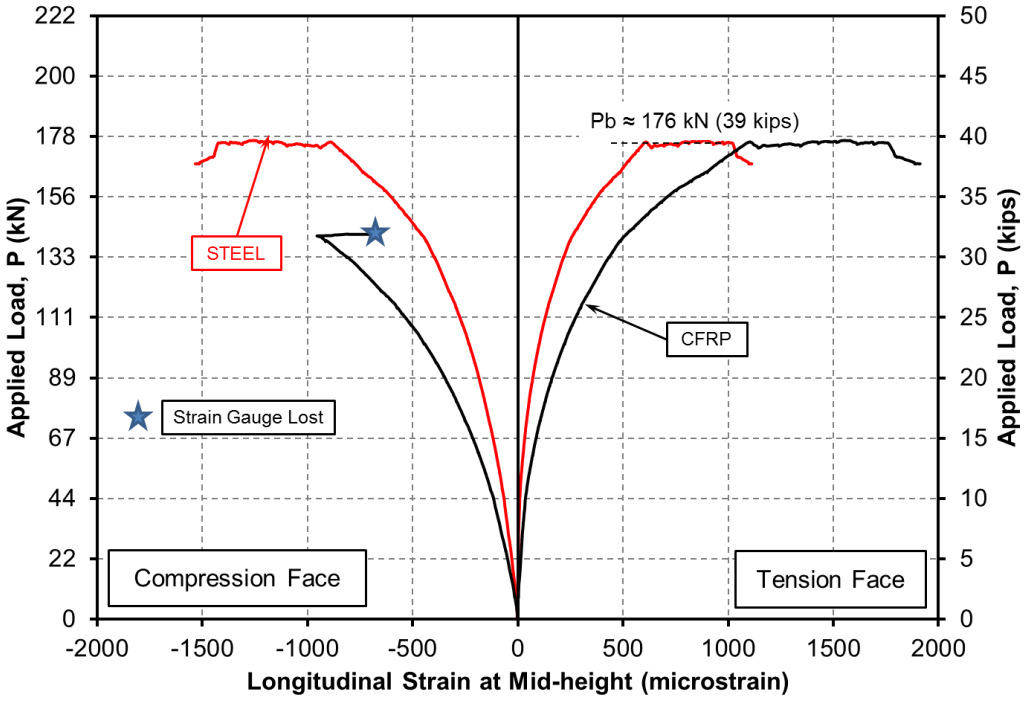

Figure 4.22: Longitudinal Strain-Load Relationship at Mid-height of Specimen I-48-(1/2)-S-P

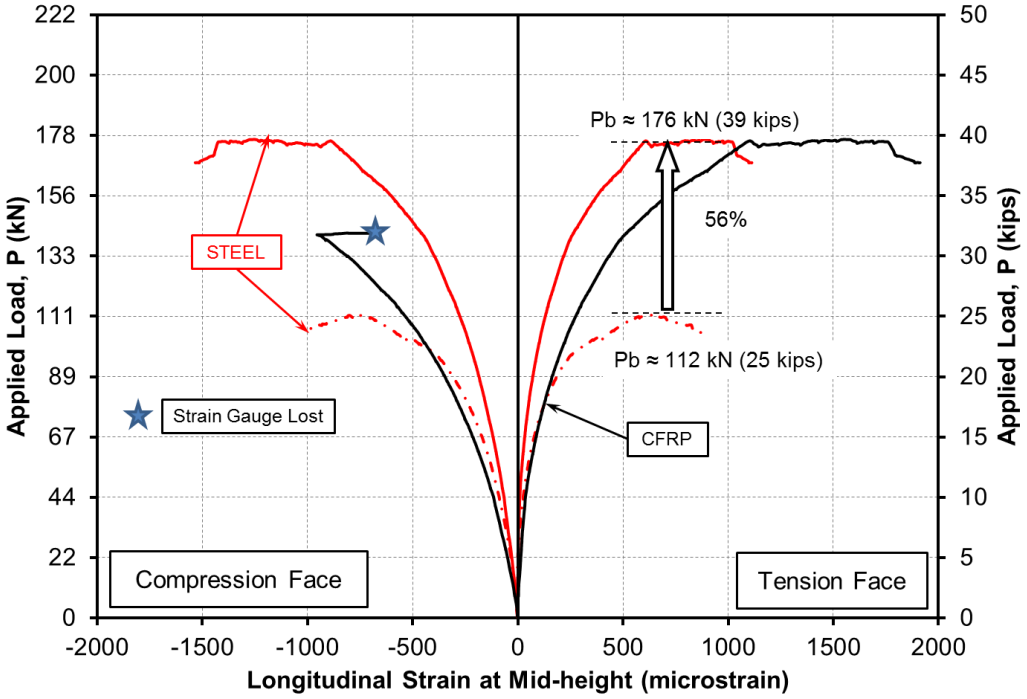

Figure 4.23: Longitudinal Strain-Load Relationship Comparison of I-48-(1/2) Specimens

Test results indicate that with the addition of a single layer of HM small diameter CFRP strands on both faces of the specimen, the buckling load was increased by 56%. Results also showed that the measured steel strain for the strengthened specimen is lower than the measured steel strain in the un-strengthened specimen at any given applied load level. This behavior clearly emphasizes that the CFRP strands are effective in sharing the load in conjunction with the steel and thus justifying the measured increase of the buckling load.

Figure 4.24 displays the lateral deflection behavior of specimen I-48-(1/2)-S-P. Figure 4.25 compares the lateral deflections of specimens I-48-(1/2)-U and I-48-(1/2)-S-P.

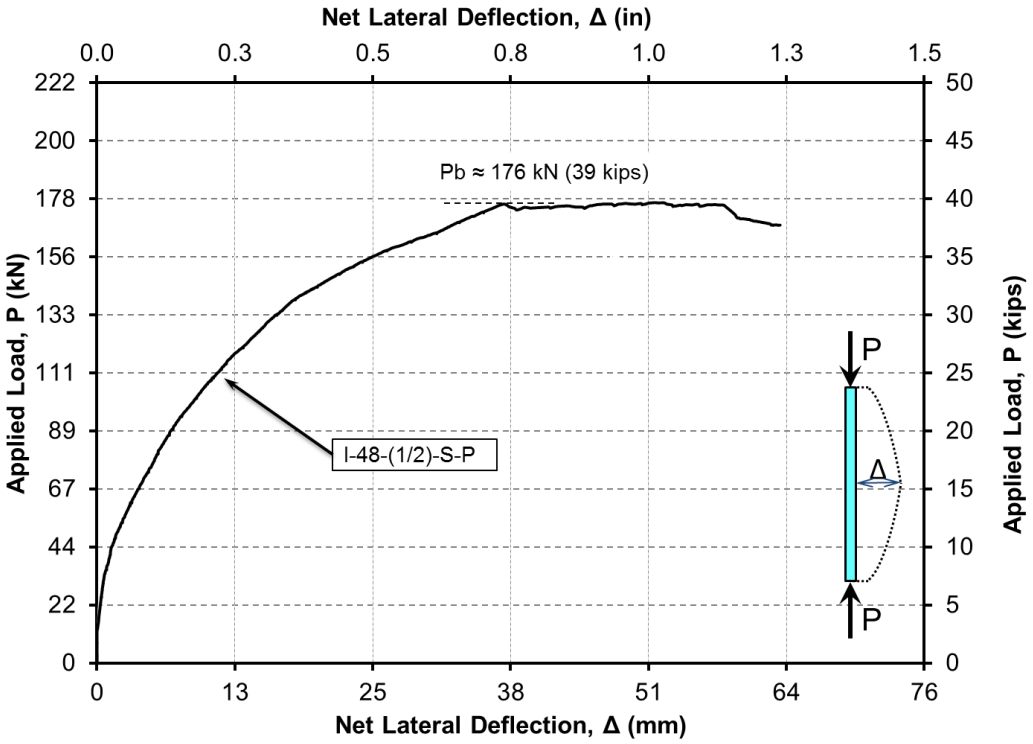

Figure 4.24: Net Lateral Deflection-Load Relationship at Mid-height of Specimen I-48-(1/2)-S-P

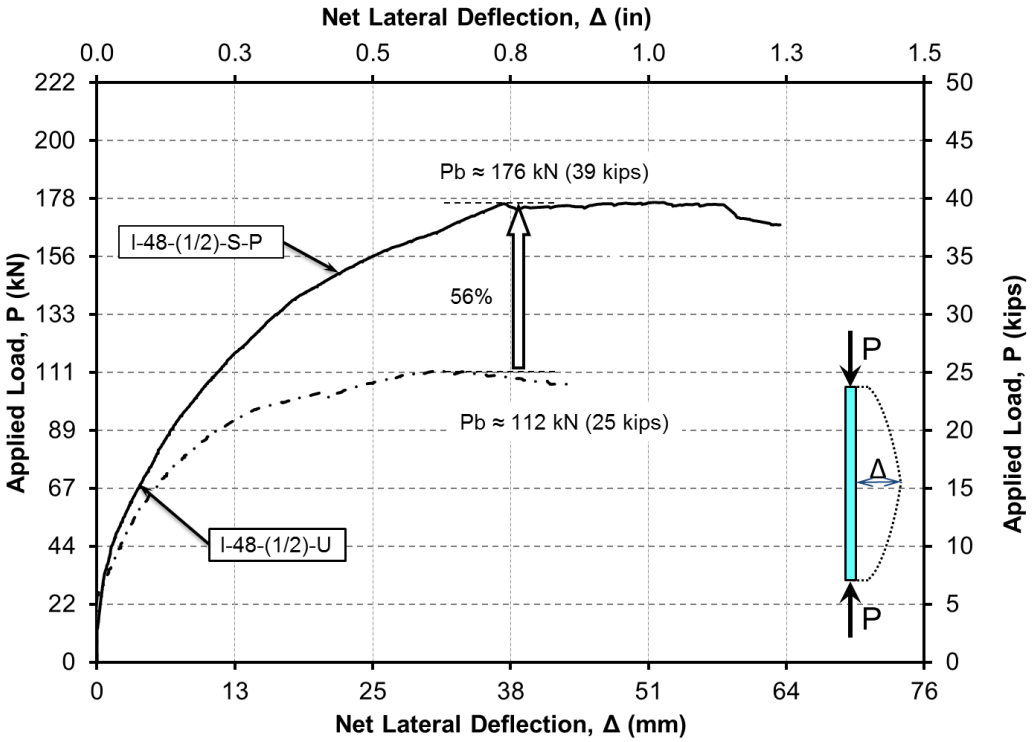

Figure 4.25: Net Lateral Deflection-Load Relationship Comparison of I-48-(1/2) Specimens

It is clear that the initial lateral stiffness of the strengthened specimen is slightly higher than that of the un-strengthened specimen. This behavior is expected of specimen with similar initial characteristics. The increase of the overall stiffness is due to the addition of the strengthening system consisting of HM small diameter CFRP strands applied.

4.1.5 Research Findings of Phase I

Several observations were made from the measured behavior of the specimens tested in Phase I. Test results indicated that the application of HM small diameter strands to both faces of the specimen was effective in increased the buckling load for all of the tested specimens. Furthermore, results indicated that all of the tested specimens experienced elastic buckling.

It was observed that there were excellent bond characteristics between the steel and the small diameter CFRP strands. There were no signs of debonding observed during the testing up to buckling on either the compression or tension faces of the specimens. The presence and absence of the polyurea putty did not seem to have any obvious contributions to the bond characteristics.

Test results revealed that initial out-of-straightness and imperfections can vary significantly for each steel plate. These initial imperfections of the specimens can have a great effect on the behavior of the specimen and thus the results of the test. Based on this observation, it was decided for Phase II, to test the same steel plates as control specimens prior to applying the CFRP strengthening system in order to compare the same plate before and after strengthening.

4.2 Second Phase

The following sections present test results of the specimens tested in Phase II of the experimental program. Based on the test results measured in Phase I, two slenderness ratios and two aspect ratios were selected that would ensure elastic buckling would be achieved. The selected slenderness ratios were 77 and 154. The two selected aspect ratios were 1.2 and 2.4. Three different types of small diameter CFRP strands were used to determine their effectiveness on the buckling behavior of the specimens. It should be mentioned that the control specimens used in this phase were strengthened and tested as strengthened specimens. Polyurea putty was used for all of the strengthened specimens tested in Phase II. A summary of the specimens discussed in the following sections are given in Table 4.2.

Table 4.2: Phase II Test Specimens Discussed

Mark	h/t	h/b	Strand Type	Number of Layers
II-24-(5/16)	77	1.2	LM	0
				1
				2
			IM	0
				1
				2
			HM	0
				1
				2
II-48-(5/16)	154	2.4	LM	0
				1
				2
			IM	0
				1
				2
			HM	0
				1
				2

4.2.1 Specimens: II-24-(5/16)-LM

The specimens in this category were 24 inches tall, 20 inches wide and five-sixteenths inches thick. Thus, the specimens have a slenderness ratio and aspect ratio of 77 and 1.2, respectively. Specimen II-24-(5/16)-LM-U was used as an un-strengthened control specimen. Specimen II-24-(5/16)-1LM was strengthened with one layer of low modulus (LM) small diameter CFRP strands on each face of the specimen. Specimen II-24-(5/16)-2LM was strengthened with two layers of LM small diameter CFRP strands on each face of the specimen.

The strain gauges that were placed at the mid-height of the specimen were used to measure the local longitudinal strains at the surface of the steel plate due to the applied compressive load. The measured strains were virtually equal across the mid-height; therefore, the average measured strains are presented in Figure 4.26 for the compression and tension faces of the specimens.

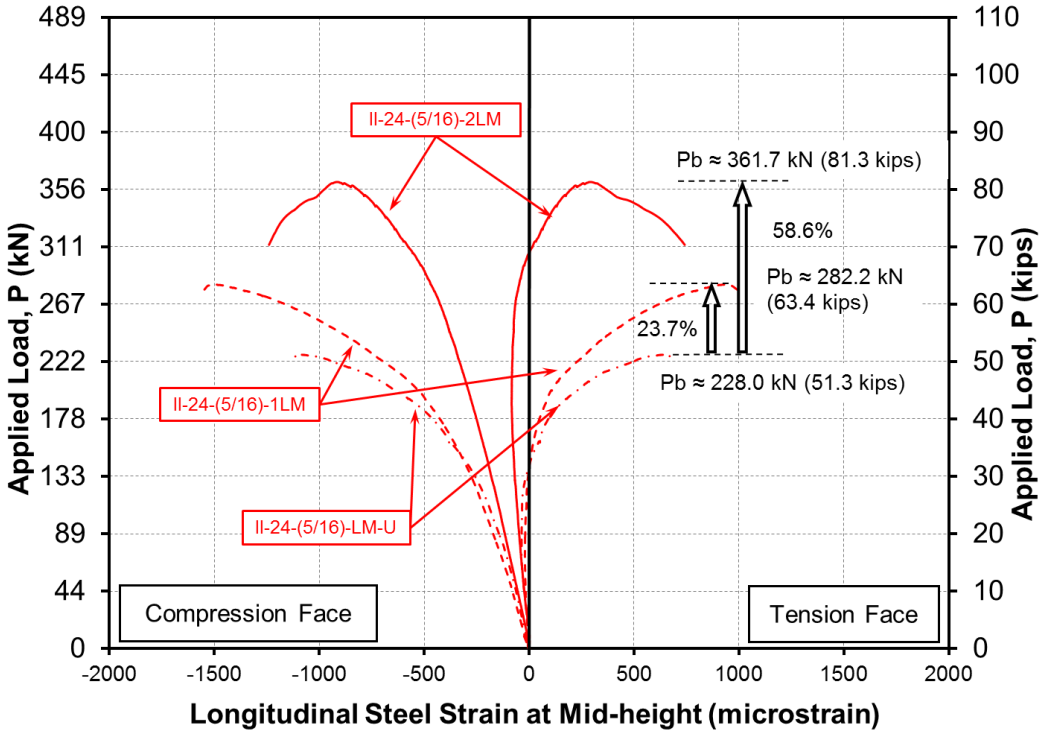

Figure 4.26: Longitudinal Strain-Load Relationship at Mid-height of II-24-(5/16)-LM Specimens

Figure 4.26 indicates that the buckling load of the un-strengthened specimen, II-24-(5/16)-LM-U, was 51.3 kips. With the addition of a single layer of LM CFRP strands, the buckling load was increased to 63.4 kips; which is an increase of nearly 24%. With two layers of LM CFRP strands, the buckling load was increased to 81.3 kips; to which is almost a 59% increase from the un-strengthened specimen. There was also a reduction of the measured steel strain as the number of LM CFRP layers increases. This behavior indicates the effectiveness of the CFRP strands in sharing the applied load with the steel plate.

The string potentiometers placed along the vertical centerline of the specimen measured the lateral deflection of the specimen induced by the applied load. The net lateral deflection was determined by subtracting the average measured deflections at the top and bottom of the specimen from the average measured deflection at the mid-height of the specimen. Figure 4.27 displays the lateral deflections of II-24-(5/16)-LM specimens as the number of LM CFRP layers was increased. The corresponding buckling loads for each of the specimens are also shown on Figure 4.27.

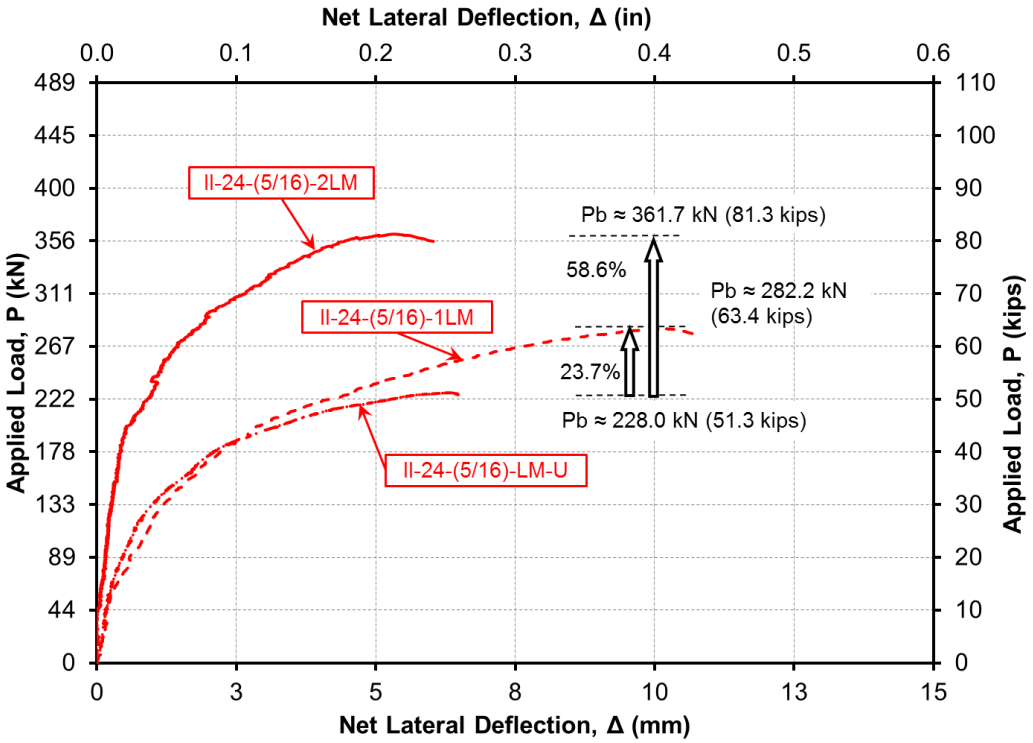

Figure 4.27: Net Lateral Deflection-Load Relationship at Mid-height of II-24-(5/16)-LM Specimens

Figure 4.27 shows that there is a general increase of initial lateral stiffness of the specimens by increasing the number of layers of LM CFRP strands. Moreover, the specimen with two layers of LM CFRP strands exhibits the highest initial lateral stiffness when compared to the un-strengthened specimen and the specimen with one layer of LM CFRP strands.

4.2.2 Specimens: II-24-(5/16)-IM

The specimens in this category were 24 inches tall, 20 inches wide and five-sixteenths inches thick. Thus, the specimens have a slenderness ratio and aspect ratio of 77 and 1.2, respectively. Specimen II-24-(5/16)-IM-U was used as an un-strengthened control specimen. Specimen II-24-(5/16)-1IM was strengthened with one layer of intermediate modulus (IM) small diameter CFRP strands on each face of the specimen. Specimen II-24-(5/16)-2IM was strengthened with two layers of IM small diameter CFRP strands on each face of the specimen.

The measured average strains at the mid-height of the specimens are presented in Figure 4.28 for the compression and tension faces. The buckling load of the un-strengthened specimen, II-24-(5/16)-IM-U, was 52.3 kips. Adding a single layer of IM CFRP strands increased the buckling load to 70.6 kips, which is an increase of 35%. With two layers of IM CFRP strands, the buckling load was 88.1 kips; a 63% increase from the un-strengthened specimen. Similar to the II-24-(5/16)-LM specimens, there is a reduction of the measured steel strain at any given load level as the number of IM CFRP layers was increased.

This behavior indicates the contribution of the CFRP strands in sharing the applied load with the steel plate.

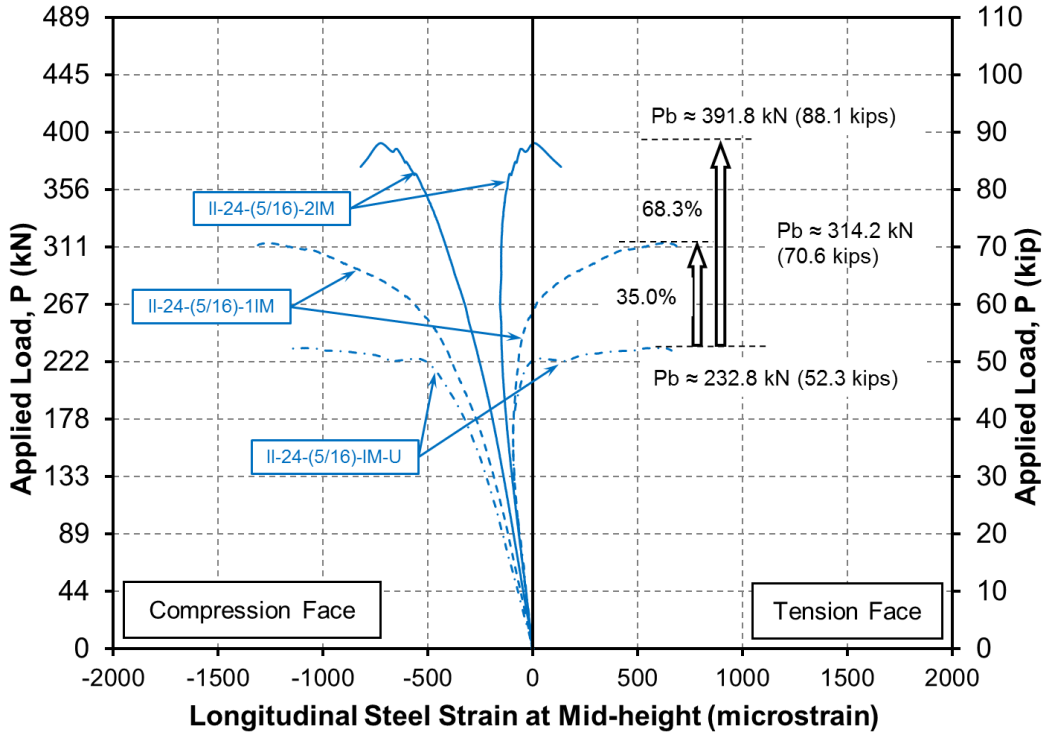

Figure 4.28: Longitudinal Strain-Load Relationship at Mid-height of II-24-(5/16)-IM Specimens

Figure 4.29 shows the lateral deflections of II-24-(5/16)-IM specimens induced by the applied compressive load. The corresponding buckling loads for each of the specimens are indicated on Figure 4.29 as well. It is evident that increasing the number of layers of IM CFRP strands increases the initial lateral stiffness of the specimen. Furthermore, it is clear

that specimen II-24-(5/16)-2IM exhibits the highest initial lateral stiffness of the three tested II-24-(5/16)-IM specimens.

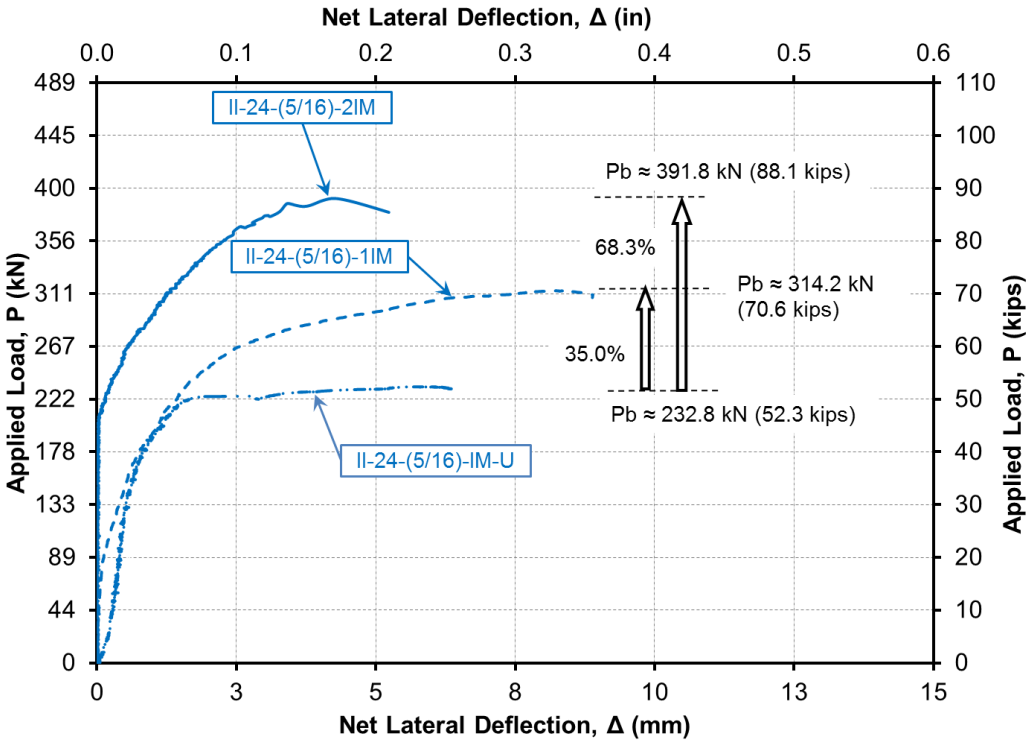

Figure 4.29: Net Lateral Deflection-Load Relationship at Mid-height of II-24-(5/16)-IM Specimens

4.2.3 Specimens: II-24-(5/16)-HM

The specimens in this category are 24 inches tall, 20 inches wide and five-sixteenths inches thick. Thus, the specimens have a slenderness ratio and aspect ratio of 77 and 1.2, respectively. Specimen II-24-(5/16)-HM-U was used as an un-strengthened control specimen. Specimen II-24-(5/16)-1HM was strengthened with one layer of high modulus (HM) small diameter CFRP strands on each face of the specimen. Specimen II-24-(5/16)-2HM was strengthened with two layers of HM small diameter CFRP strands on each face of the specimen. The measured average strains at the mid-height of the specimens are presented in Figure 4.30 for the compression and tension faces.

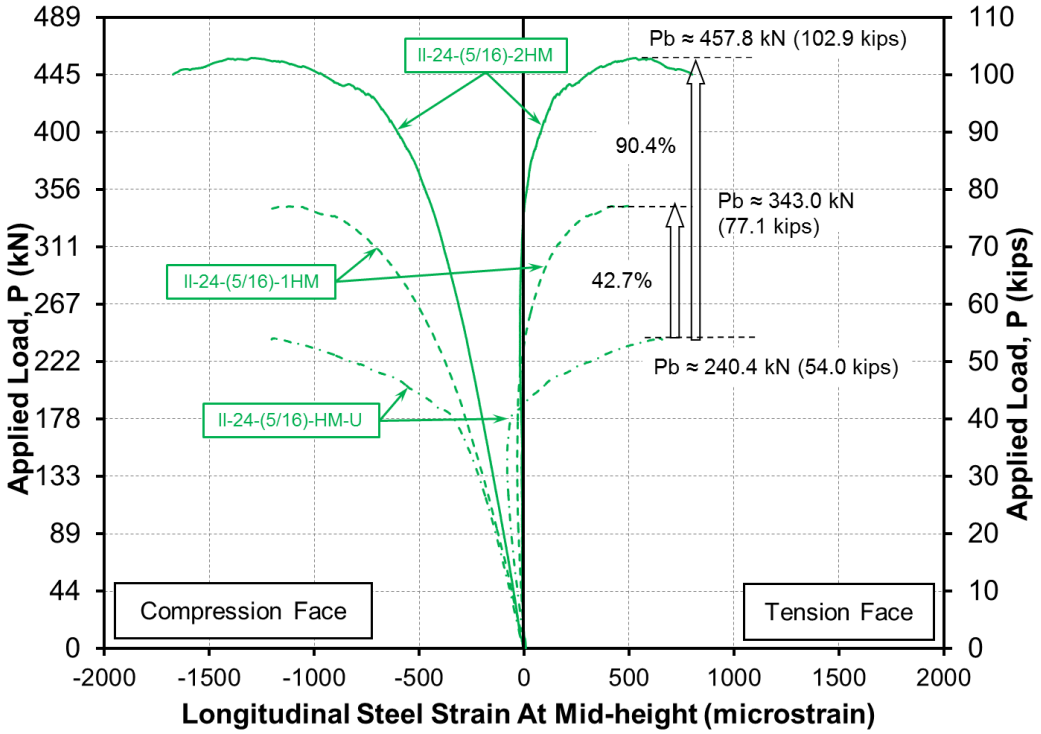

Figure 4.30: Longitudinal Strain-Load Relationship at Mid-height of II-24-(5/16)-HM Specimens

The buckling load of the un-strengthened specimen, II-24-(5/16)-HM-U, was 54.0 kips. Applying a single layer of IM CFRP strands increased the buckling load of the specimen to 77.1 kips, which is an increase of nearly 43%. With two layers of HM CFRP strands, the buckling load was 102.9 kips; a 90% increase in comparison to the un-strengthened specimen. Similar to the II-24-(5/16)-LM and IM specimens, Figure 4.30 displays the contribution of the HM CFRP strands by reducing the measured strain, and thus the level of stress, of the steel at any given load level.

Figure 4.31 displays the lateral deflections of II-24-(5/16)-HM specimens induced by the applied compressive load. The corresponding buckling loads for each of the specimens are indicated on Figure 4.31 as well. Figure 4.31 shows that specimen II-24-(5/16)-2HM exhibits the highest initial lateral stiffness of the three II-24-(5/16)-HM tested specimens.

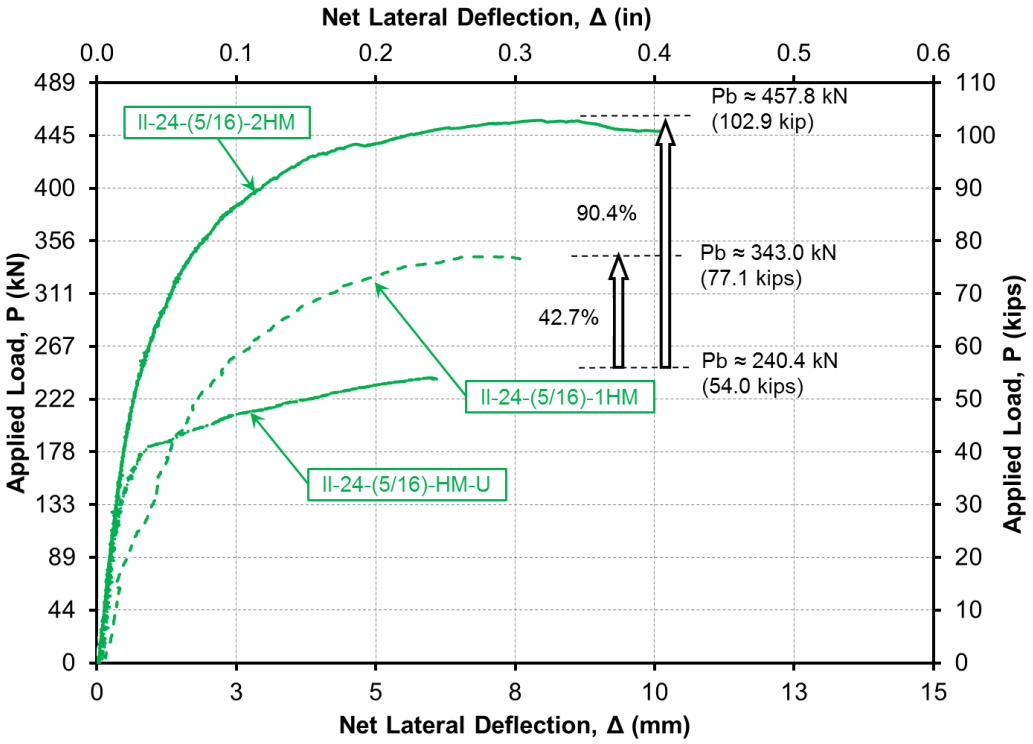

Figure 4.31: Net Lateral Deflection-Load Relationship at Mid-height of II-24-(5/16)-HM Specimens

Figure 4.32 depicts the percent increase in buckling loads for the tested II-24-(5/16) specimens with different CFRP strand types. It is clear that increasing the number of layers of CFRP strands increases the buckling load of a specimen. Furthermore, increasing the

elastic modulus of the CFRP strands proves to be more effective in increasing the buckling load of a specimen.

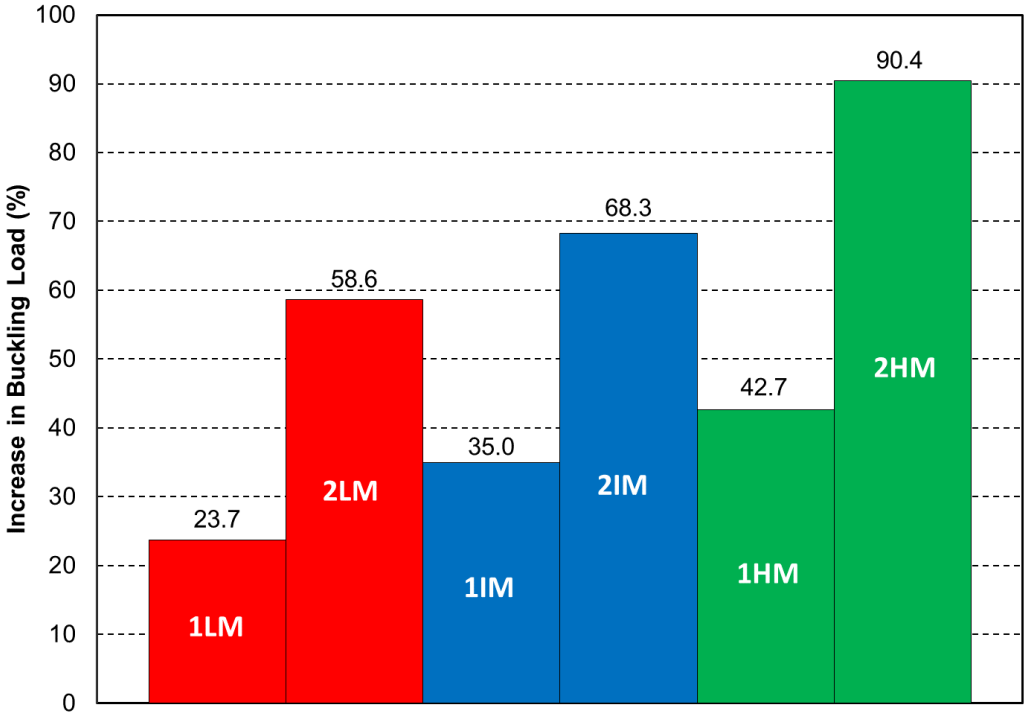

Figure 4.32: Percent Increase in Buckling Loads for II-24-(5/16) Specimens

4.2.4 Specimens: II-48-(5/16)-LM

The specimens in this category were 48 inches tall, 20 inches wide and five-sixteenths inches thick. Thus, the specimens have a slenderness ratio and aspect ratio of 154 and 2.4, respectively. Specimen II-48-(5/16)-LM-U was used as an un-strengthened control specimen. Specimen II-48-(5/16)-1LM was strengthened with one layer of LM small diameter CFRP strands on each face of the specimen. Specimen II-48-(5/16)-2LM was strengthened with two layers of LM small diameter CFRP strands on each face of the specimen.

The average measured strains at the mid-height of the specimens are presented in Figure 4.33 for the compression and tension faces. The strains shown for specimens II-48-(5/16)-LM-U and II-48-(5/16)-1LM are the measured steel strains. The measured average strain values shown for specimen II-48-(5/16)-2LM are at the level of the second layer of CFRP strengthening.

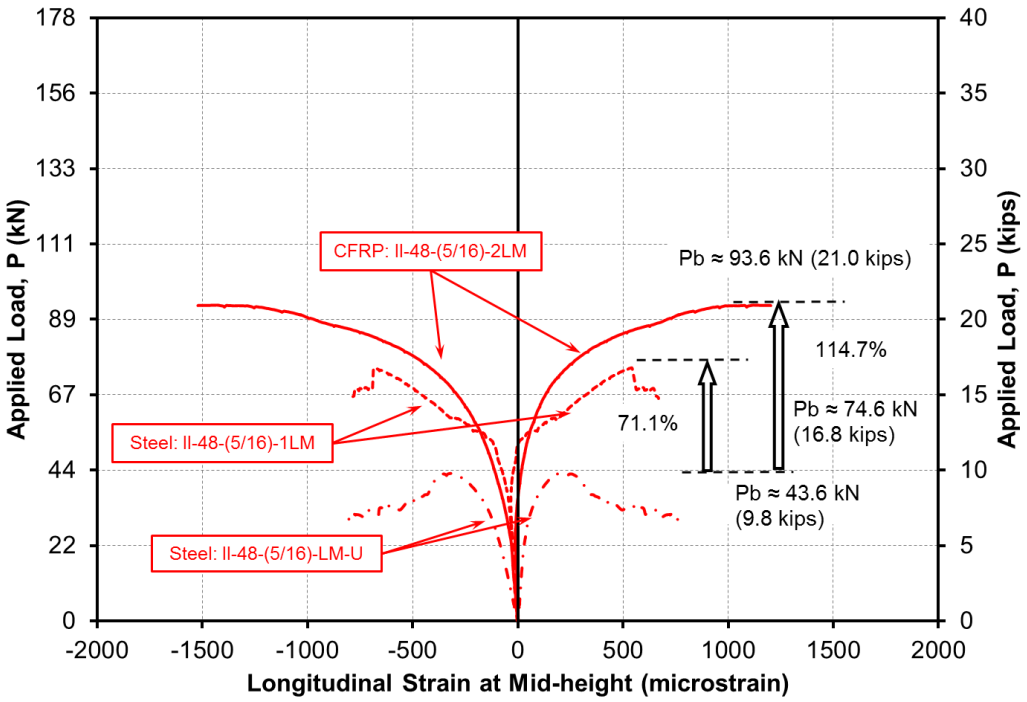

Figure 4.33: Longitudinal Strain-Load Relationship at Mid-height of II-48-(5/16)-LM Specimens

The buckling load of the un-strengthened specimen, II-48-(5/16)-LM-U, was 9.8 kips. The addition of a single layer of LM CFRP strands increased the buckling load to 16.8 kips; which is an increase of over 71%. With two layers of LM CFRP strands, the buckling load was 21.0 kips; nearly a 115% increase from the un-strengthened specimen. It is evident that there is a significant reduction in the measured strain at the level of the steel from the un-strengthened specimen to the strengthened specimen with a single layer of LM CFRP strands. Thus, showing the contribution of the CFRP strengthening system to the load carrying capacity of the specimen.

Figure 4.34 shows the lateral deflections of II-48-(5/16)-LM specimens induced by the applied compressive load. The corresponding buckling loads for each of the specimens are shown on Figure 4.34 as well. Figure 4.34 shows that there is a general increase of initial lateral stiffness of the specimen with an increase in the number of layers of LM CFRP strands. Moreover, specimen II-48-(5/16)-2LM exhibits the highest initial lateral stiffness of the three tested II-48-(5/16)-LM specimens.

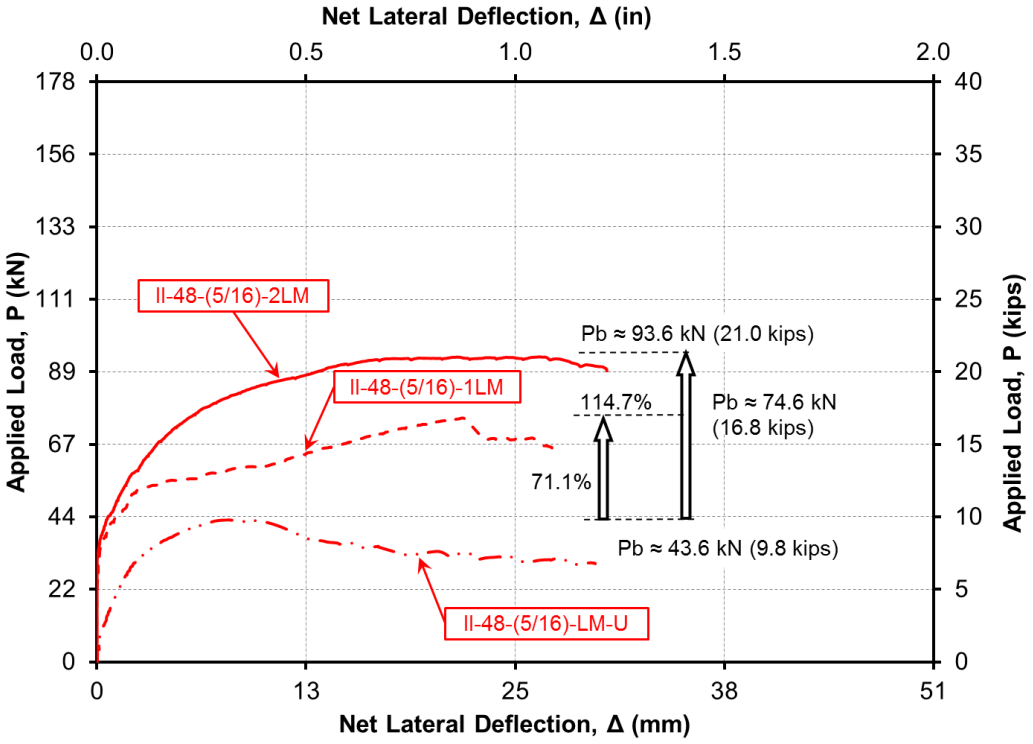

Figure 4.34: Net Lateral Deflection-Load Relationship at Mid-height of II-48-(5/16)-LM Specimens

4.2.5 Specimens: II-48-(5/16)-IM

The specimens in this category were 48 inches tall, 20 inches wide and five-sixteenths inches thick. Thus, the specimens have a slenderness ratio and aspect ratio of 154 and 2.4, respectively. Specimen II-48-(5/16)-IM-U was used as an un-strengthened control specimen. Specimen II-48-(5/16)-1IM was strengthened with one layer of IM small diameter CFRP strands on each face of the specimen. Specimen II-48-(5/16)-2IM was strengthened with two layers of IM small diameter CFRP strands on each face of the specimen.

The measured average strains at the mid-height of the specimens are presented in Figure 4.35 for the compression and tension faces. The strains shown for specimens II-48-(5/16)-IM-U and II-48-(5/16)-1IM are the measured steel strains. The measured average strain values for specimen II-48-(5/16)-2IM are at the level of the second layer of CFRP strengthening.

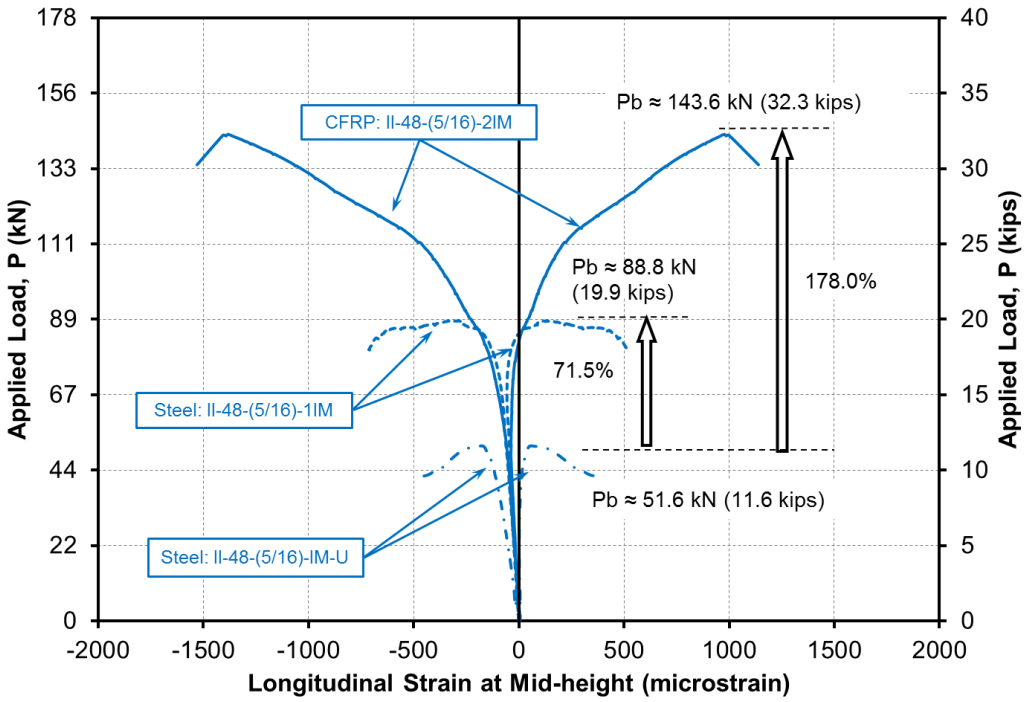

Figure 4.35: Longitudinal Strain-Load Relationship at Mid-height of II-48-(5/16)-IM Specimens

The buckling load of the un-strengthened specimen, II-48-(5/16)-IM-U, was 11.6 kips. The addition of a single layer of IM CFRP strands increased the buckling load to 19.9 kips, which is an increase of nearly 72% in comparison to the un-strengthened specimen. With the addition of a second layer of IM CFRP strands, the buckling load was increased to 32.3 kips; a 178% increase from the un-strengthened specimen. Test results indicate that there is a reduction in the measured strain at the level of the steel from the un-strengthened specimen to the strengthened specimen with a single layer of IM CFRP strands.

Figure 4.36 shows the lateral deflections of II-48-(5/16)-IM specimens induced by the applied compressive load. The corresponding buckling loads for each of the specimens are shown on Figure 4.36 as well.

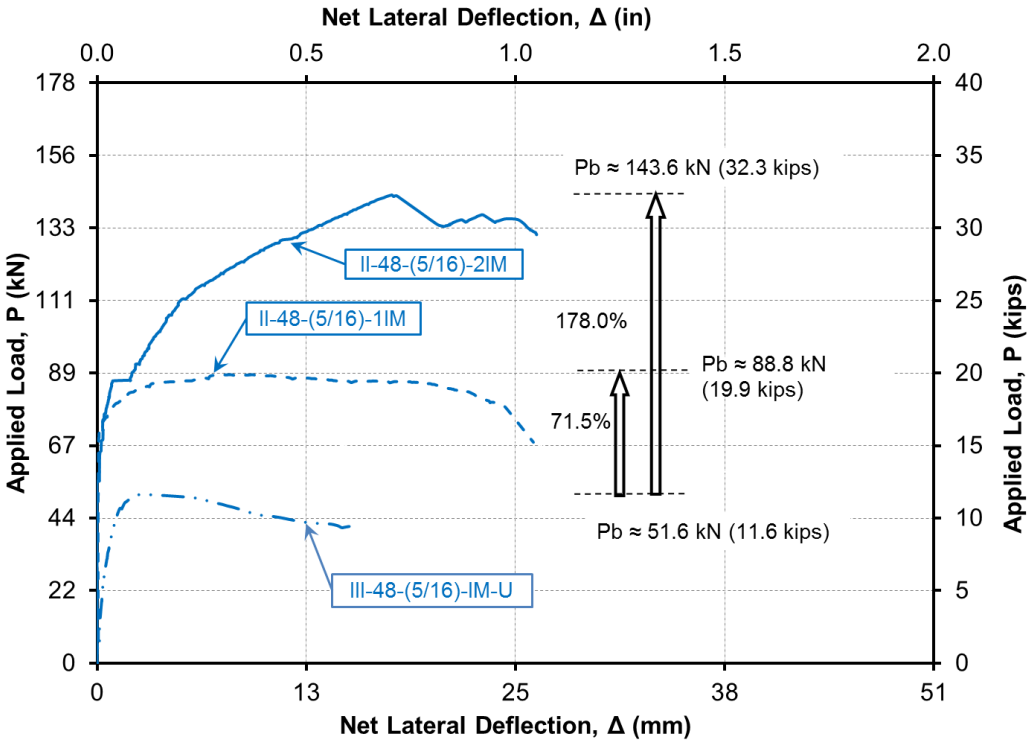

Figure 4.36: Net Lateral Deflection-Load Relationship at Mid-height of II-48-(5/16)-IM Specimens

Figure 4.36 shows a general increase of initial lateral stiffness of the specimen with an increase in the number of layers of IM CFRP strands. Specimen II-48-(5/16)-2IM also exhibits the highest initial lateral stiffness of the three tested specimens.

4.2.6 Specimens: II-48-(5/16)-HM

The specimens in this category are 48 inches tall, 20 inches wide and five-sixteenths inches thick. Thus, the specimens have a slenderness ratio and aspect ratio of 154 and 2.4, respectively. Specimen II-48-(5/16)-HM-U was used as an un-strengthened control specimen. Specimen II-48-(5/16)-1HM was strengthened with one layer of HM small diameter CFRP strands on each face of the specimen. Specimen II-48-(5/16)-2HM was strengthened with two layers of HM small diameter CFRP strands on each face of the specimen.

The measured average strains at the mid-height of the specimens are presented in Figure 4.37 for the compression and tension faces. The strains shown for specimens II-48-(5/16)-HM-U and II-48-(5/16)-1HM are the measured steel strains. The measured average strain values for specimen II-48-(5/16)-2HM are at the level of the second layer of CFRP strengthening.

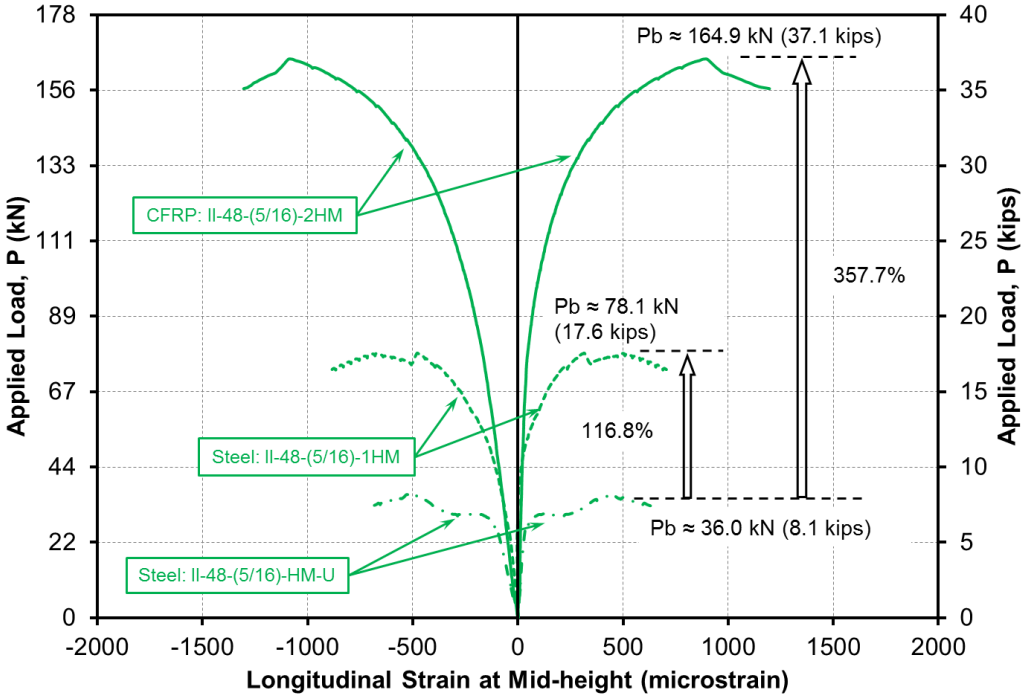

Figure 4.37: Longitudinal Strain-Load Relationship at Mid-height of II-48-(5/16)-HM Specimens

The buckling load of the un-strengthened specimen, II-48-(5/16)-HM-U, was 8.1 kips. Adding one layer of HM CFRP strands increased the buckling load to 17.6 kips, which is an increase of nearly 117%. The addition of a second layer of HM CFRP strands increased the buckling load to 164.9 kips. This buckling load is nearly 360% higher than the un-strengthened specimen. Figure 4.37 shows that there is a reduction in the measured steel strain from the un-strengthened specimen to the strengthened specimen with a single layer of HM CFRP strands. This clearly shows the effectiveness of the CFRP strengthening system in carrying the applied load in conjunction with the steel plate.

Figure 4.38 shows the lateral deflections of II-48-(5/16)-HM specimens as the number of layers of HM CFRP increases. The corresponding buckling loads for each of the specimens are also shown on Figure 4.38.

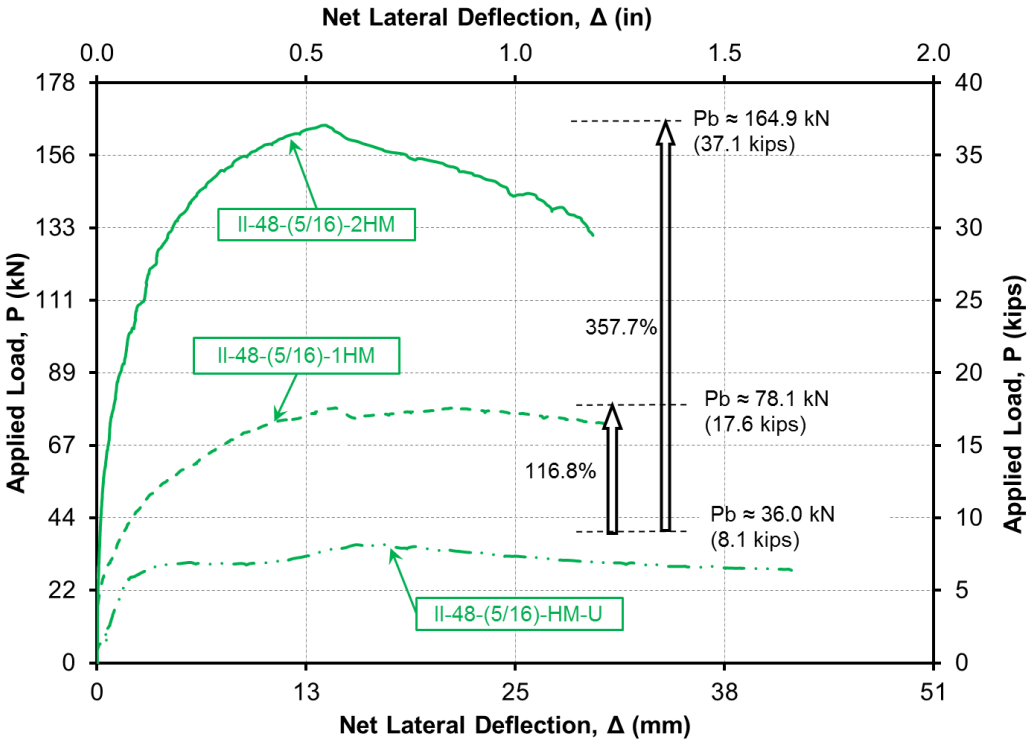

Figure 4.38: Net Lateral Deflection-Load Relationship at Mid-height of II-48-(5/16)-HM Specimens

Figure 4.38 shows that the initial lateral stiffness of the specimen increases along with increasing number of layers of HM CFRP strands. Specimen II-48-(5/16)-2HM also exhibits the highest initial lateral stiffness of the three tested II-48-(5/16)-HM specimens.

Figure 4.39 shows the percent increase in buckling loads for the tested II-48-(5/16) specimens with varying types of CFRP strands. The figure shows that increasing the number of layers of CFRP strands increases the buckling load of a specimen. Furthermore, increasing the elastic modulus of the CFRP strands proves to be more effective in increasing the buckling load of a specimen.

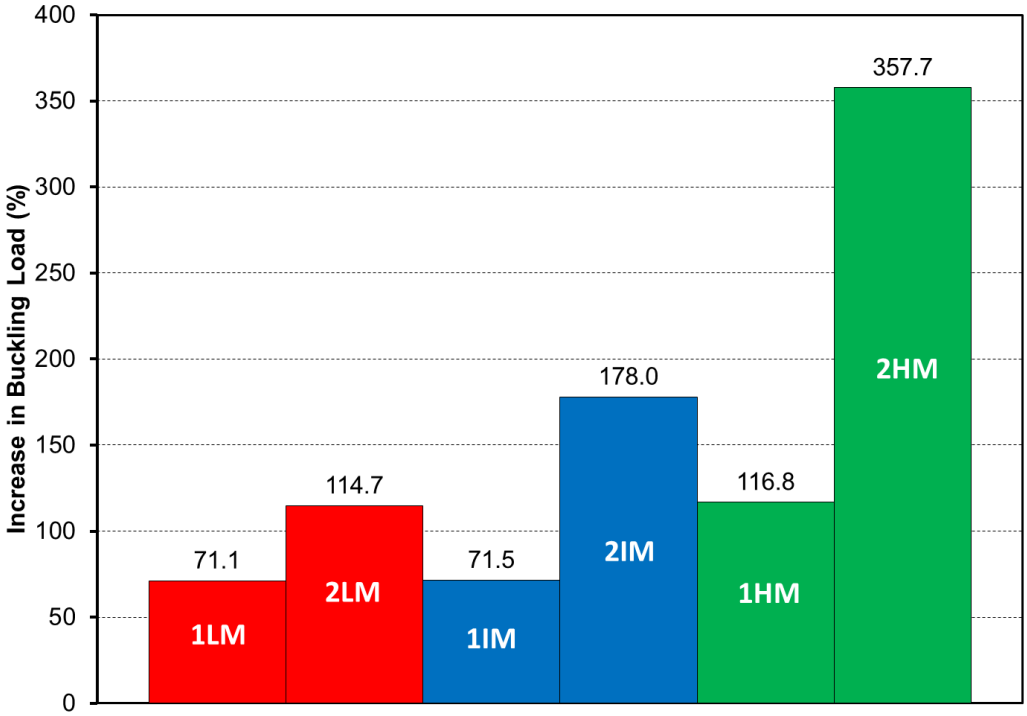

Figure 4.39: Percent Increase in Buckling Loads for II-48-(5/16) Specimens

4.2.7 Research Findings of Phase II

Several observations were made from the measured behavior of the specimens test in Phase II. Test results indicated that the CFRP strengthening systems became more effective as the slenderness ratio of the steel plate increased. Furthermore, the addition of the CFRP strengthening systems increased the initial lateral stiffness of the specimens. The test results also showed that by increasing the number of layers of CFRP strands on both sides of the specimen, the buckling load also increased, proportionally.

Test results from Phase II indicated that as the elastic modulus of the small diameter CFRP strands increased, the effectiveness of the strengthening system increased as well. Furthermore, it was observed that HM small diameter CFRP strands were the most effective in increasing the buckling capacity in comparison to LM and IM CFRP strands.

It should be noted that no signs of debonding were observed on the compression or tension faces of the specimens, similar to the behavior exhibited in Phase I of the experimental program.

4.3 Comparison with Theoretical Buckling Loads

In order to determine whether or not the measured buckling loads of the strengthened specimens are within an acceptable range of values, and can be predicted, theoretical buckling loads were calculated using fundamental principles. The test specimens that are being investigated are restrained only at the top and bottom, where the load is applied. There are no restraints on the unloaded edges, therefore using plate buckling equations would not be applicable in this situation. Furthermore, the majority of the test specimens are very slender in nature and experienced elastic buckling. Therefore, the Euler buckling equation was used as the comparison baseline. The Euler buckling equation is given in Equation 4.1.

$$\boldsymbol{P_b = \frac{\pi^2 EI}{(KL)^2}} \qquad \text{Equation 4.1}$$

Where:

P_b = Euler buckling load

E = Elastic Modulus of the Material

I = Moment of Inertia

K = Effective Length Factor

L = Height of the specimen

Due to the pinned boundary conditions, the effective length factor of K is assumed to be equal to one for the analysis. Since the steel and the CFRP strengthening system have different material properties, the cross-section needed to be transformed into a homogenous material. The CFRP strengthening system was transformed into an equivalent layer of steel using a modular ratio, n. The modular ratio was defined as the ratio between the elastic modulus of the CFRP strengthening system and the elastic modulus of the steel. Thus, this theoretically transforms the strengthened specimen into an equivalent steel cross-section.

Equation 4.2 predicts the buckling capacity of the strengthened specimens using the transformed cross-section properties.

$$\boldsymbol{P_{bc} = \frac{\pi^2 E I_T}{(KL)^2}} \qquad \text{Equation 4.2}$$

Where:

P_{bc} = Euler buckling load of the composite section

E = Elastic Modulus of the steel

I_T = Moment of Inertia of the transformed cross- section

The cross section shown in Figure 4.40 was utilized to calculate the section properties of the strengthened specimens.

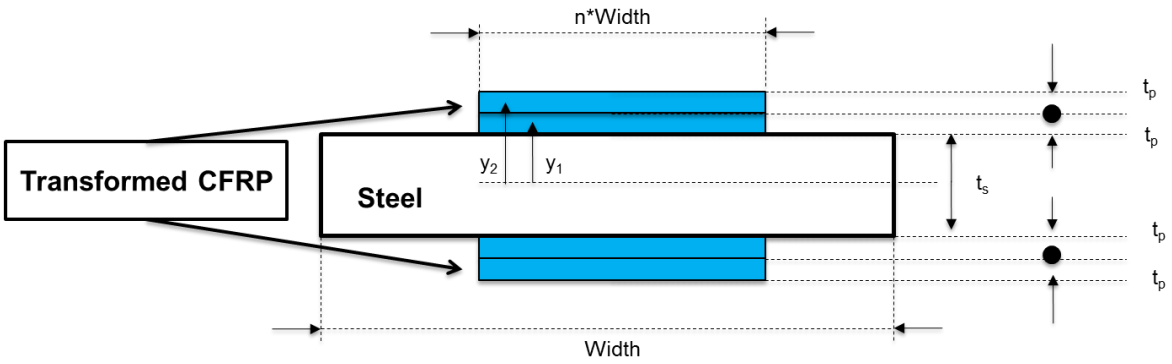

Figure 4.40: Strengthened Cross Section

The thickness of the CFRP strengthening system, t_p, was assumed to be one-eighth inches thick per layer for the purposes of the analysis. By using Equation 4.2, theoretical buckling loads were calculated for all of the strengthened test specimens in the experimental program. The calculated theoretical buckling loads were then compared to those measured in the experimental program. In order to match the experimental buckling loads to the theoretical buckling loads, the effective length factor, K, was determined for each specimen tested. Figure 4.41 presents the measured effective length factors for all of the specimens tested in the experimental program.

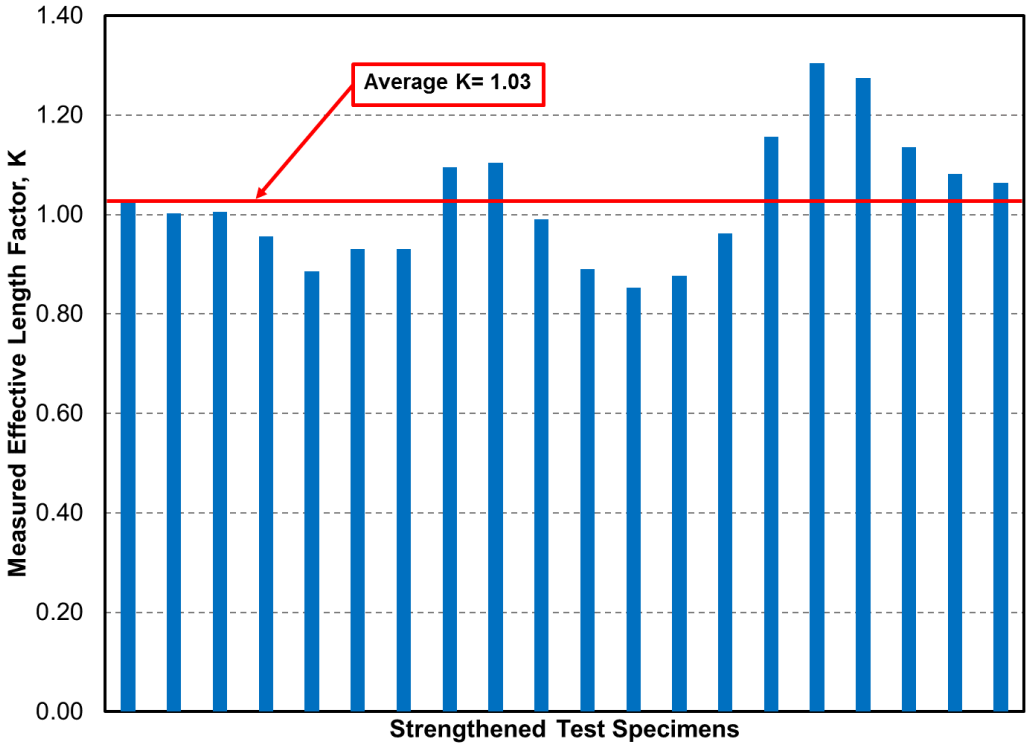

Figure 4.41: Test Specimen K Values

Figure 4.41 shows that the average measured effective length factor, K, was equal to 1.03. This value is very close to the assumed value of one. The measured average value being higher than one can be attributed to the displacement and rotation occurring at the end of the specimens, and possible effect of the friction forces between the sleeve and the pin. For an ideal pin-pin connection, i.e.: K = 1.0, there is zero deflection at the end of the specimen, and it must be able to freely rotate at the end of the specimen. The support conditions experienced in the experimental program vary from an ideal condition. The center of rotation of the specimens is at the center of their sleeves, as shown in Figure 4.42. Thus, this makes the effective length of the specimen longer than the height of the specimen. The

deflections measured at the top of each specimen in the experimental program caused by the rotation of each sleeve confirms this behavior. Moreover, the presence of friction in the experimental test setup was minimized by taking proper procedural steps. For example, chrome painting the high strength steel pins and applying grease to the surfaces of the steel pins and inside of the steel sleeves prior to testing.

It should be noted that the main objective of the research program is to study the effectiveness of the proposed strengthening system. Since the same boundary conditions were used for testing the strengthened and un-strengthened specimens, the research findings are valid regardless of the boundary conditions used in the experimental program.

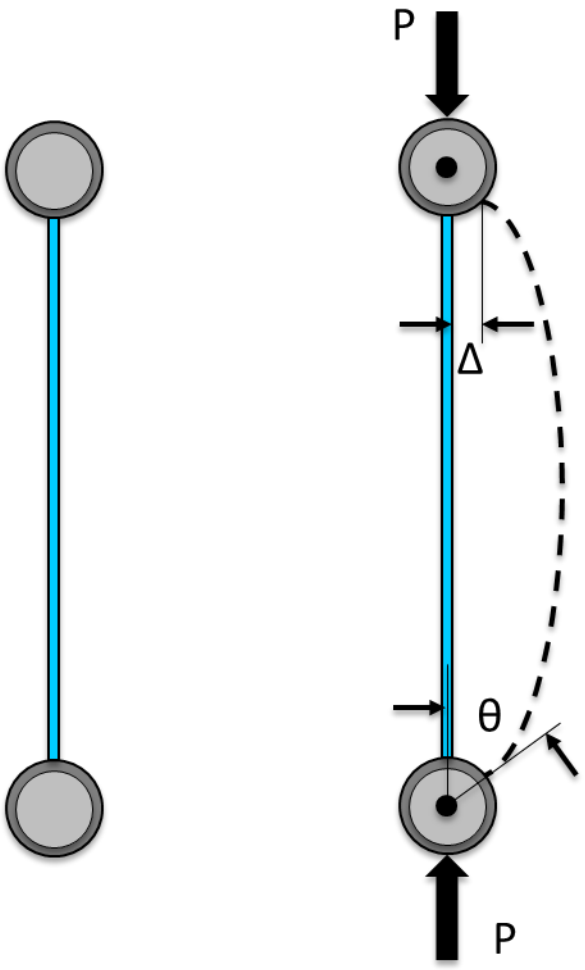

Figure 4.42: Deflection and Rotation of Test Specimen

The results show that the Euler buckling equation using transformed section properties may be used to predict the elastic buckling capacity of a steel plate strengthened with the proposed CFRP system using the appropriate effective length factor, K.

CHAPTER 5 : Summary and Conclusions

This chapter provides a summary of a research program investigating the use of small diameter CFRP strands to increase the buckling capacity of steel web plates. The investigation focused on the effects of slenderness and aspect ratios of steel plates on the effectiveness of the small diameter CFRP strands. The research also provided knowledge regarding the effectiveness of CFRP strands with varying elastic modulus values for this application. Test results from the experimental program were used to provide clear insight to determine whether the small diameter strands being investigated are suitable for compression and shear strengthening applications.

5.1 Summary

This research investigated the potential use of CFRP strengthening and repair of steel bridge girders. Its lightweight, high-strength mechanical properties make it a very attractive alternative in comparison to steel. Furthermore, its resistance to corrosion make its implementation even more desirable. A two phase experimental program was completed to investigate the application of small diameter CFRP strands to steel web plates subjected to uniaxial compression forces. The first phase of the experimental program focused on the effects that the geometry of a specimen had on the effectiveness of the CFRP strengthening system. Various slenderness and aspect ratios were investigated in order to determine these effects. In this phase, strengthened specimens were strengthened with HM small diameter CFRP strands.

The second phase of the experimental program focused on the effects that varying elastic modulus values of small diameter CFRP strands had on the buckling behavior of strengthened specimens. In this phase, two slenderness and aspect ratios were investigated. Furthermore, three different CFRP strand types were investigated in order to determine which strand type would be the most effective in increasing the buckling capacity of a specimen. Mechanical properties for the steel and CFRP materials used in both phases of the experimental program were verified through testing.

5.2 Conclusions

Several conclusions were made from the measured behavior in the specimens tested in the experimental program. The conclusions are summarized as follows:

- Small diameter CFRP strands have proven to be an effective strengthening system.
- The proposed strengthening system has excellent bond characteristics in compression and in tension, including large lateral deflection behavior.
- The polyurea putty did not have any obvious contributions to the bond characteristics between the steel and the CFRP strengthening system.
- The typical failure of the test specimens in the experimental program was elastic buckling. The majority of the test specimens buckled at a strain values much smaller than their yield strain values, with the exception of one specimen.
- The initial imperfections for each steel plate were very apparent when comparing

various specimens and had a significant effect on the behavior.

- The CFRP strengthening system is more effective for higher slenderness ratios.
- The initial lateral stiffness of a specimen increases with the use of the CFRP strengthening system.
- The increase in buckling capacity is proportional to the increase in the number of layers (i.e.: increase in reinforcement ratio) of the CFRP strengthening system.
- High modulus CFRP small diameter strands provide a more effective strengthening system in comparison to intermediate modulus and low modulus CFRP small diameter strands.
- The elastic buckling capacity of steel plates strengthened with the proposed CFRP system may be predicted by using the Euler buckling equation using the transformed section properties and applying the appropriate effective length factor.

Based on the conclusions drawn from the research program it is clear that the use of high modulus small diameter CFRP strands are extremely effective in increasing the compression resistance of a steel member. Thus, it has excellent potential to increase the overall shear strength of steel girders.

5.3 Future Work

The next experimental program plans to focus on subjecting steel plates strengthened with the proposed CFRP system to pure shear forces in order to determine their direct behavior in this application. The next experimental program is expected to consider the effectiveness of the proposed CFRP strengthening system by exploring the following parameters: slenderness ratio, aspect ratio, CFRP strand types, CFRP reinforcement ratio, and the orientation of CFRP strands.

REFERENCES

Aguilera, & Fam. (2013). Bonded FRP Plates for Strengthening Rectangular Hollow Steel Section T-Joints Against Web Buckling Induced by Transverse Compression. *Journal of Composites for Construction*, 421-432.

Bambach, & Elchalakani. (2007). Plastic Mechanism Analysis of Steel SHS Strengthened with CFRP under Large Axial Deformation. *Thin-Walled Structures*, 159-170.

Bhetwal, & Yamada. (2012). Effects of CFRP Reinfrocements onf the Buckling Behavior of Thin-Walled Steel Cylinders Under Compression. *International Journal of Structural Stability and Dynamics*, 131-151.

Dawood. (2008). *Bond Charactersistics and Environmental Durability of CFRP Materials for Strengthening Steel Bridges and Structures.* Raleigh: NCSU.

Haedir, & Zhao. (2011). Design of Short CFRP-Reinforced Steel Tubular Columns. *Journal of Constructional Steel Research*, 497-509.

Harries, Peck, & Abraham. (2009). Enhancing Stability of Strucutral Steel Sections using FRP. *Thin-Walled Structures*, 1092-1101.

Hidekuma, Kobayashi, Okuyama, Miyashita, & Nagai. (2012). *Experimental Study on Debonding Behavior of CFRP for Axial Tensile Reinforced Steel Plate by CFRP Strand Sheets.*

Holloway, & Cadei. (2002). Progress in the Technique of Upgrading Metallic Structures with Advanced Polymer Composites. *Progress in Structural Engineering and Materials*, 131-148.

Jiao, & Zhao. (2004). Simulation of CFRP Strengthend Butt-Welded Very High Strength (VHS) Circular Steel Tubes in Tension. *Thin-Walled Structures*, 963-978.

Kabir, & Nazari. (2011). Enhancing Ultimate Compressive Strength of Notch Embedded Steel Cylinders Using Overwrap CFRP Patch. *Applied Composite Materials*, 723-738.

Linghoff, A.-E. K. (2009). Performance of Steel Beams Strengthened With CFRP Laminate-Part 1: Laboratory Tests. *Elsevier*, 509-515.

Naramshiri, Jumaat, & Sulong. (2010). Shear Strengthening of Steel I-Beams by using CFRP Strips. *Academic Journals*, 2155-2168.

Patnaik, Bauer, & Srivatsan. (2008). The Extrinsic Influence of Carbon Fibre Reinforced Plastic Laminates to Strengthen Steel Structures. *Sadhana*, 261-272.

Schnerch, D. R. (2006). *Bond Behavior of CFRP Strengthened Steel Structures.*

Shaat, & Fam. (2006). Axial Loading Tests on Short and Long Hollow Structural Steel Columns Retrofitted Using Carbon Fibre Reinforced Polymers. *Canadian Journal of Civil Engineering*, 458-470.

Shaat, & Fam. (2009). Slender Steel Columns Strengthened Using High-Modulus CFRP Plates for Buckling Control. *Journal of Composites for Construction*, 2-12.

Tabrizi, S. F. (2013). *Strengthening of Steel Structures with Carbon Fiber Reinforced Polymer (CFRP).* Raleigh: NCSU.

Wu, Zhao, Duan, & Al-Mahaidi. (2012). Bond Characteristics Between Ultra-High Modulus CFRP Laminates and Steel. *Thin-Walled Structures*, 147-157.

Xia, & Teng. (2005). Behaviour of FRP-To-Steel Bonded Joints. *International Symposium on Bond Behaviour of FRP in Structures* (pp. 411-418). Hong Kong: IIFC.

Zhao, & Al-Mahaidi. (2009). Web Buckling of Lighsteel Beams Strengthened with CFRP Subjected to End-Bearing Forces. *Thin-Walled Structures*, 1029-1036.

Zhao, Fernando, & Al-Mahaidi. (2006). CFRP Strengthened RHS sujected to Transverse End Bearing Force. *Engineering Structures*, 1555-1565.

APPENDICES

APPENDIX A: Longitudinal Strain-Load Relationships

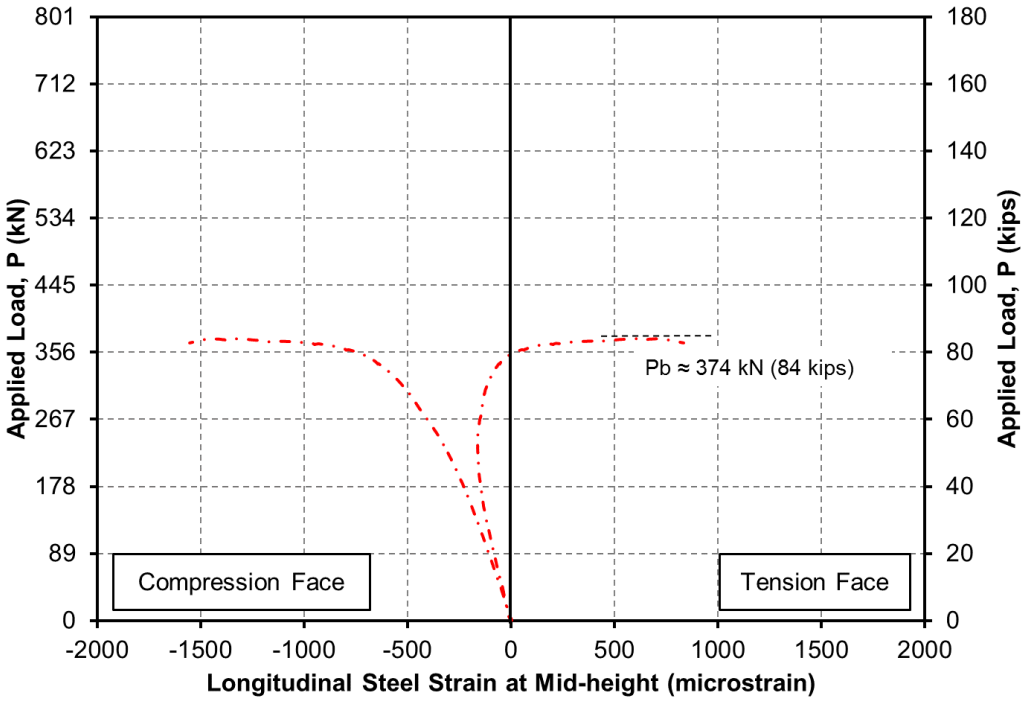

Figure A.1: Longitudinal Strain-Load Relationship at Mid-height of Specimen I-24-(3/8)-U

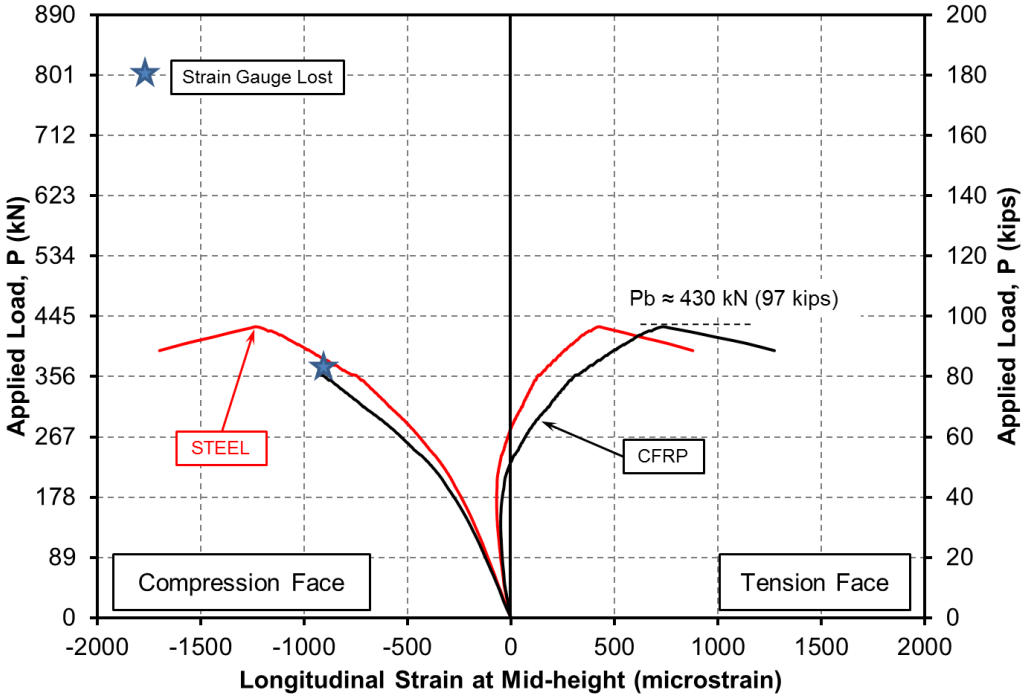

Figure A.2: Longitudinal Strain-Load Relationship at Mid-height of Specimen I-24-(3/8)-S-P

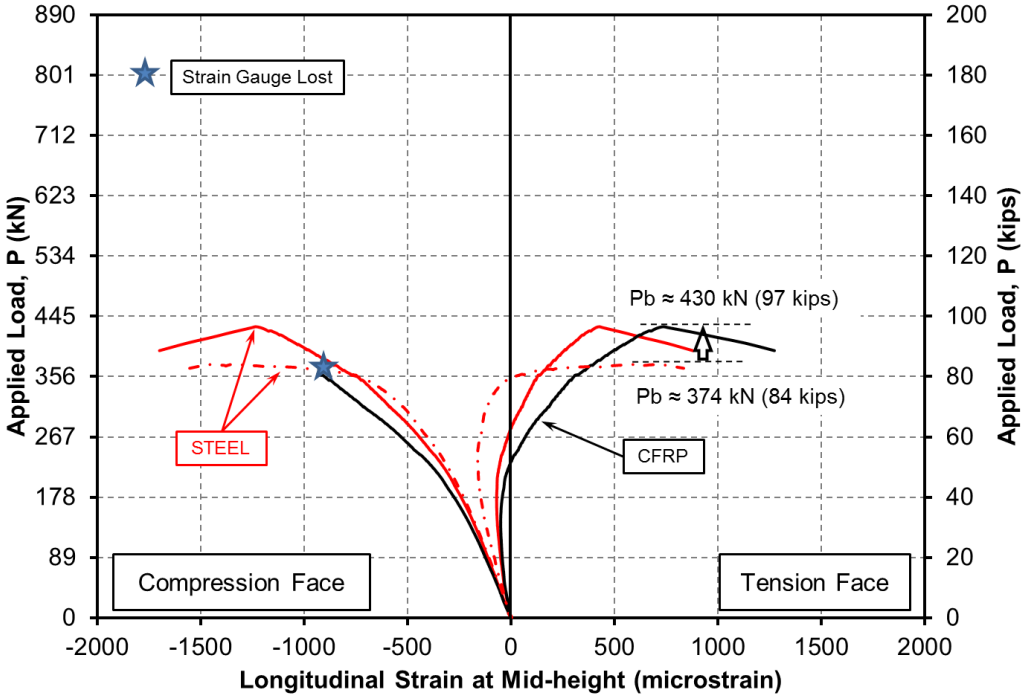

Figure A.3: Longitudinal Strain-Load Relationship Comparison of I-24-(3/8) Specimens

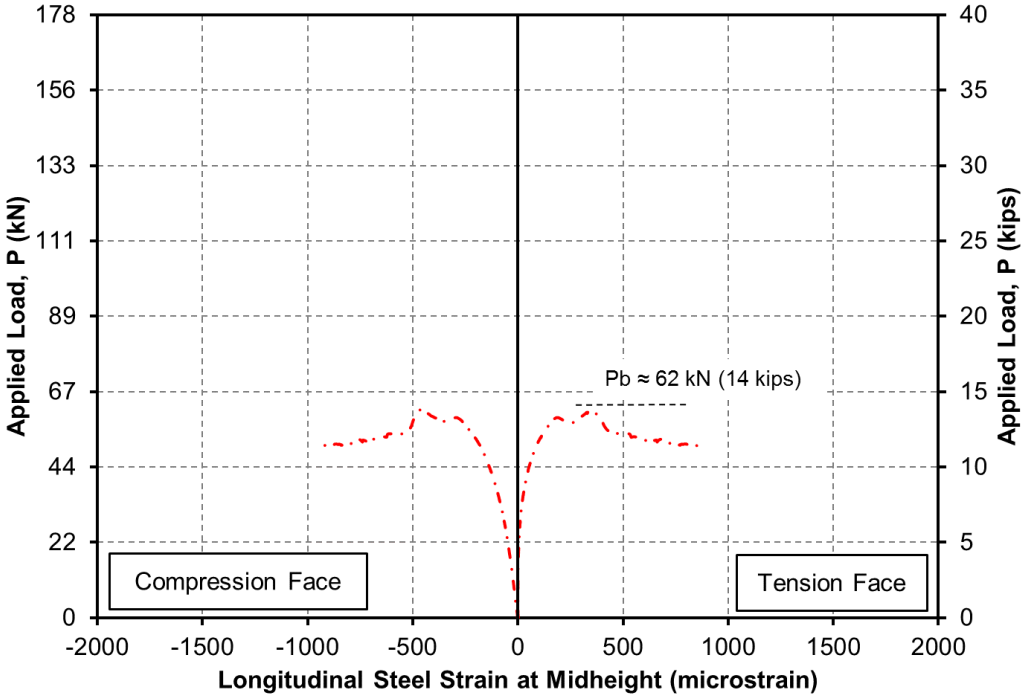

Figure A.4: Longitudinal Strain-Load Relationship at Mid-height of Specimen I-48-(3/8)-U

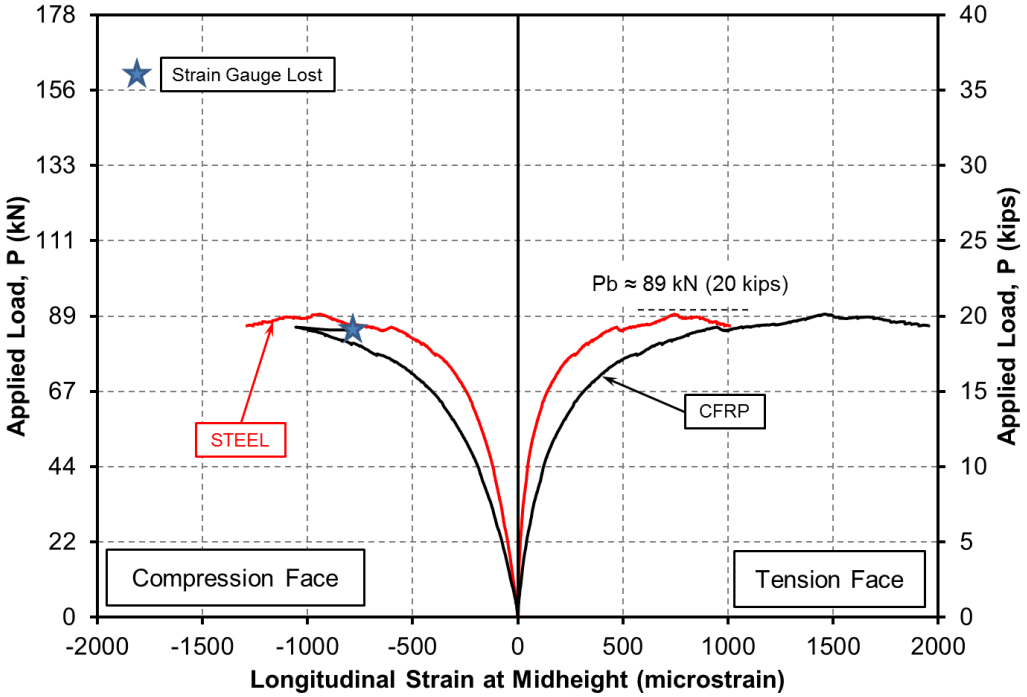

Figure A.5: Longitudinal Strain-Load Relationship at Mid-height of Specimen I-48-(3/8)-S-P

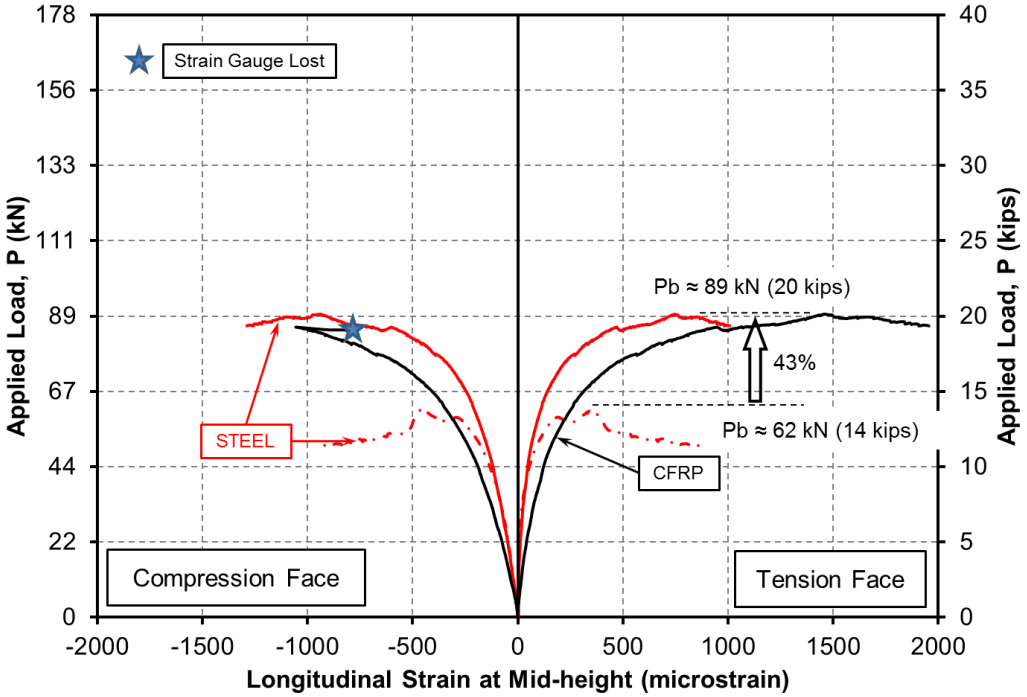

Figure A.6: Longitudinal Strain-Load Relationship Comparison of I-48-(3/8) Specimens

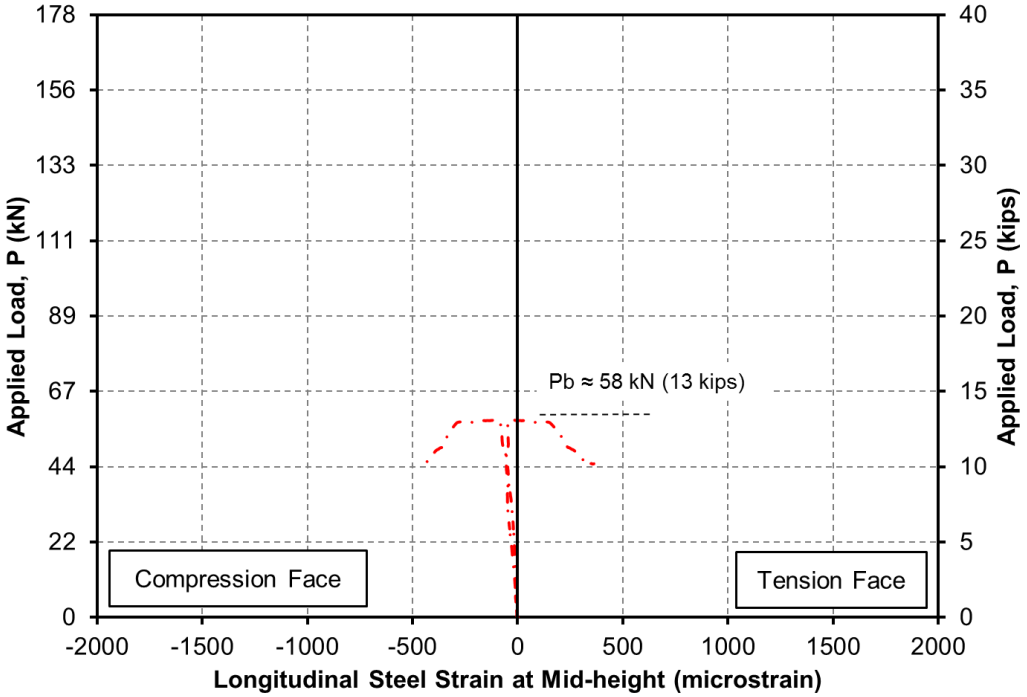

Figure A.7: Longitudinal Strain-Load Relationship at Mid-height of Specimen I-48-(5/16)-U

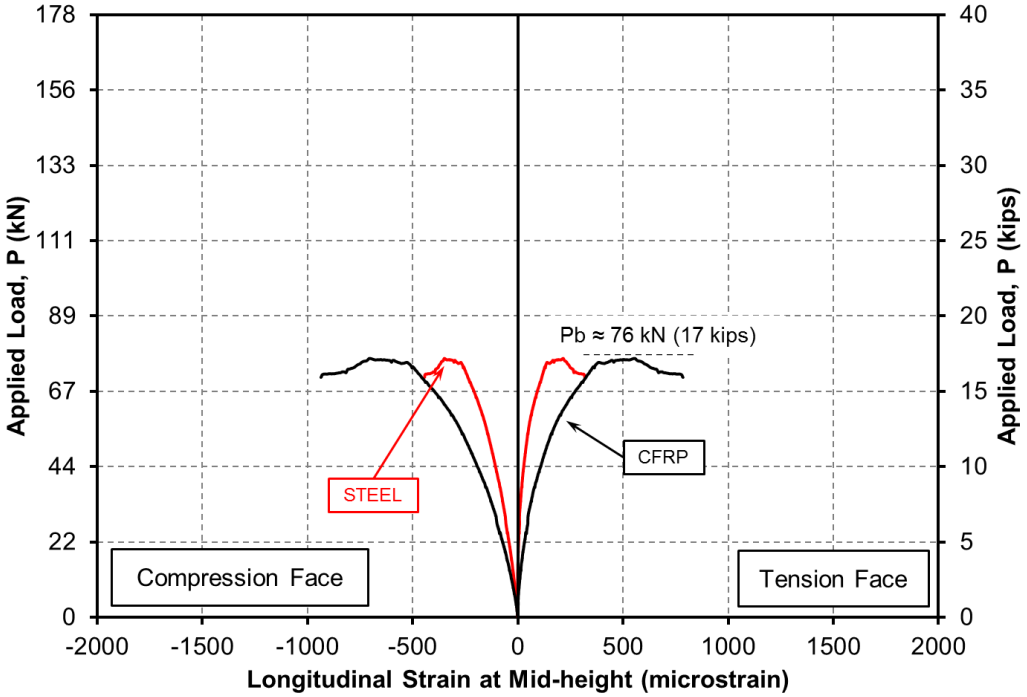

Figure A.8: Longitudinal Strain-Load Relationship at Mid-height of Specimen I-48-(5/16)-S-P

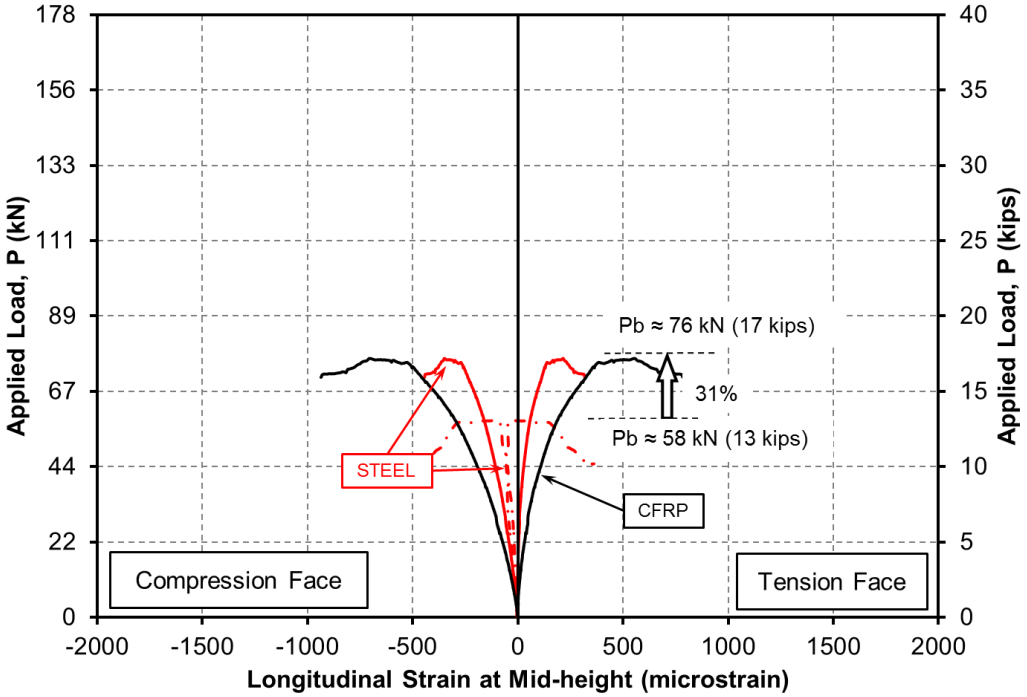

Figure A.9: Longitudinal Strain-Load Relationship Comparison of I-48-(5/16) Specimens

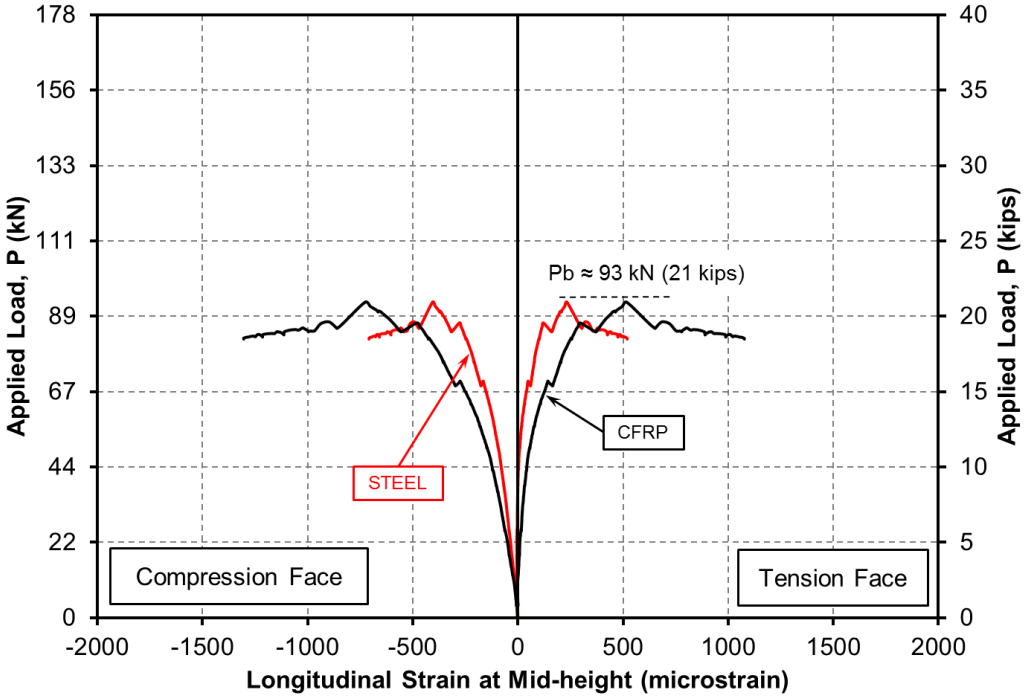

Figure A.10: Longitudinal Strain-Load Relationship at Mid-height of Specimen I-48-(5/16)-S

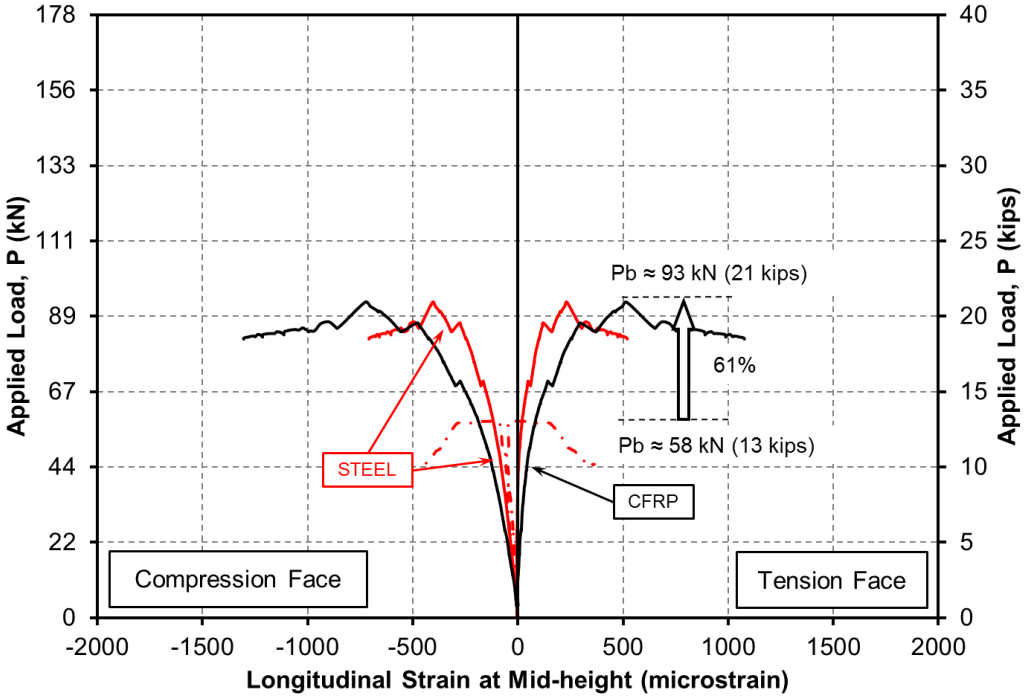

Figure A.11: Longitudinal Strain-Load Relationship Comparison of I-48-(5/16) Specimens without Putty

APPENDIX B: Net Lateral Deflection-Load Relationships

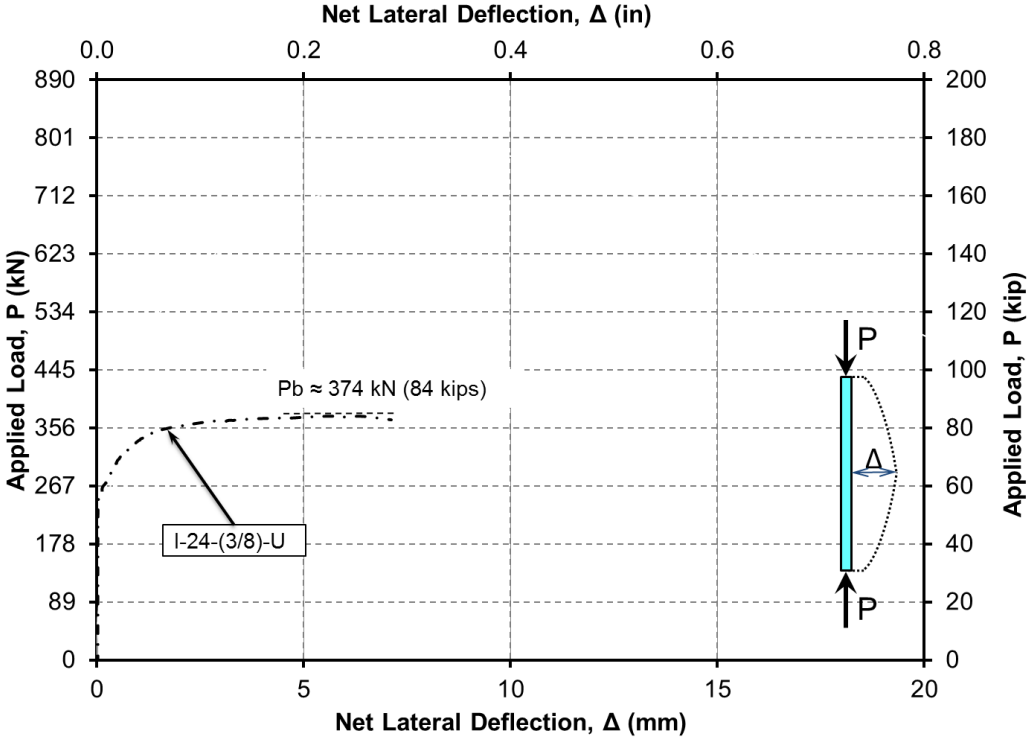

Figure B.11: Net Lateral Deflection-Load Relationship at Mid-height of Specimen I-24-(3/8)-U

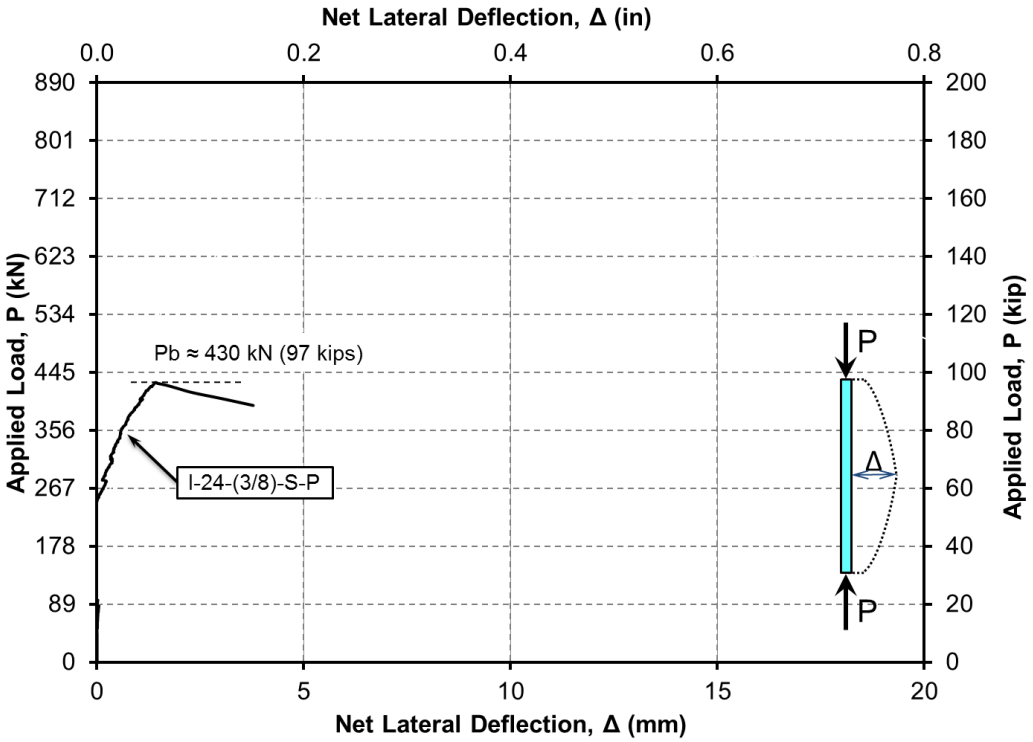

Figure B.22: Net Lateral Deflection-Load Relationship at Mid-height of Specimen I-24-(3/8)-S-P

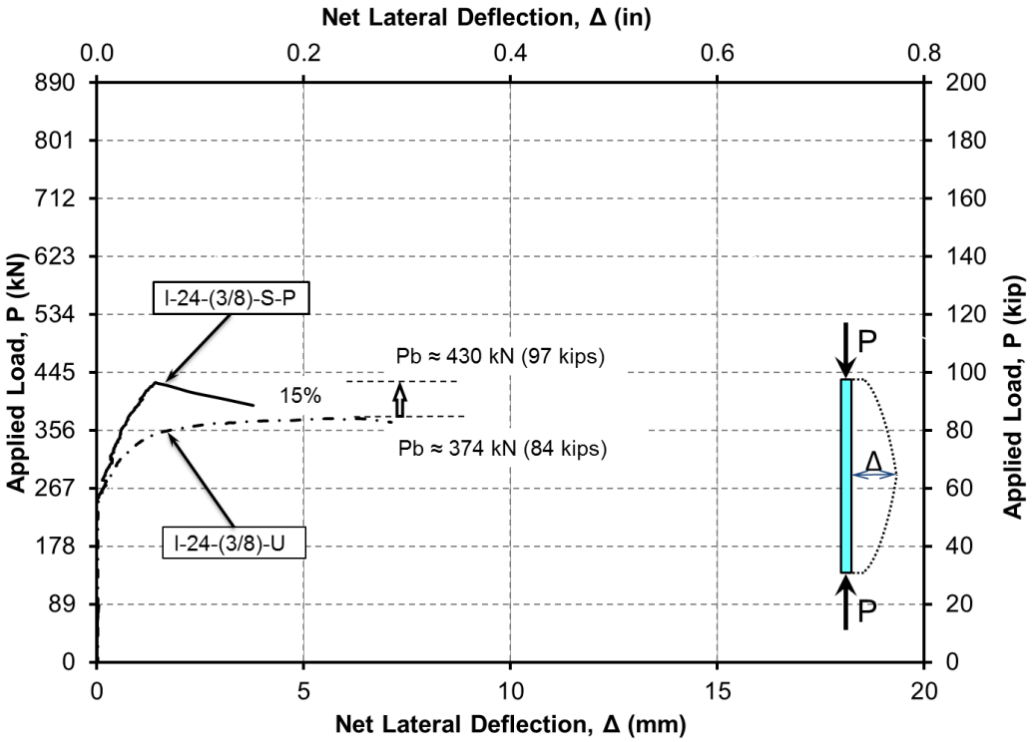

Figure B.33: Net Lateral Deflection-Load Relationship Comparison of I-24-(3/8) Specimens

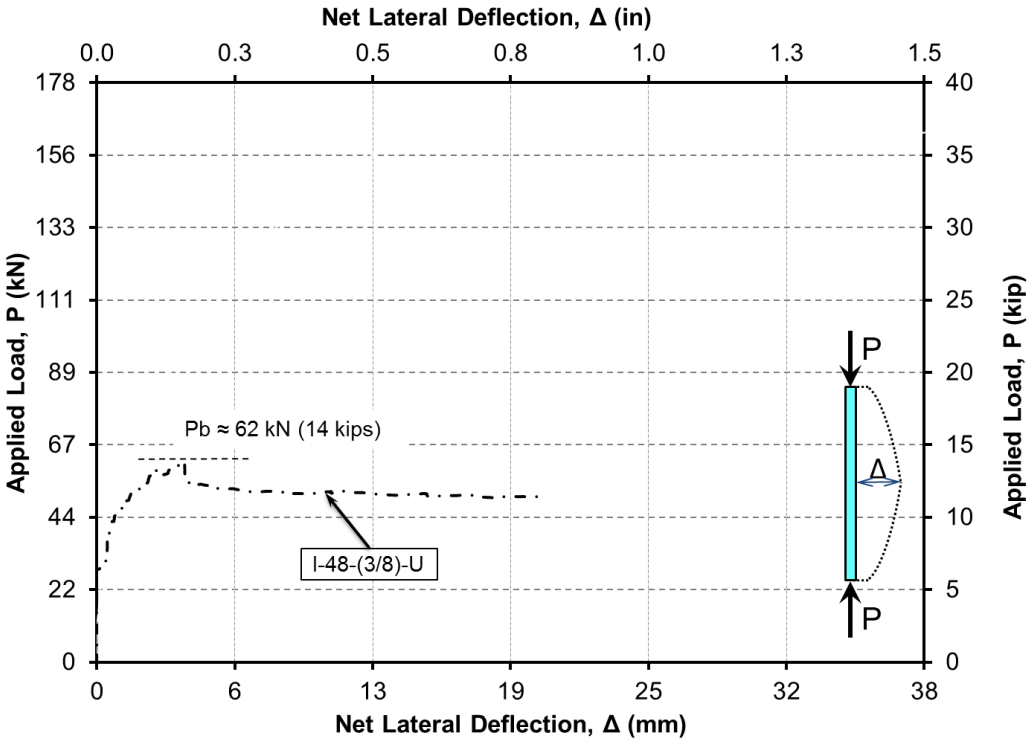

Figure B.44: Net Lateral Deflection-Load Relationship at Mid-height of Specimen I-48-(3/8)-U

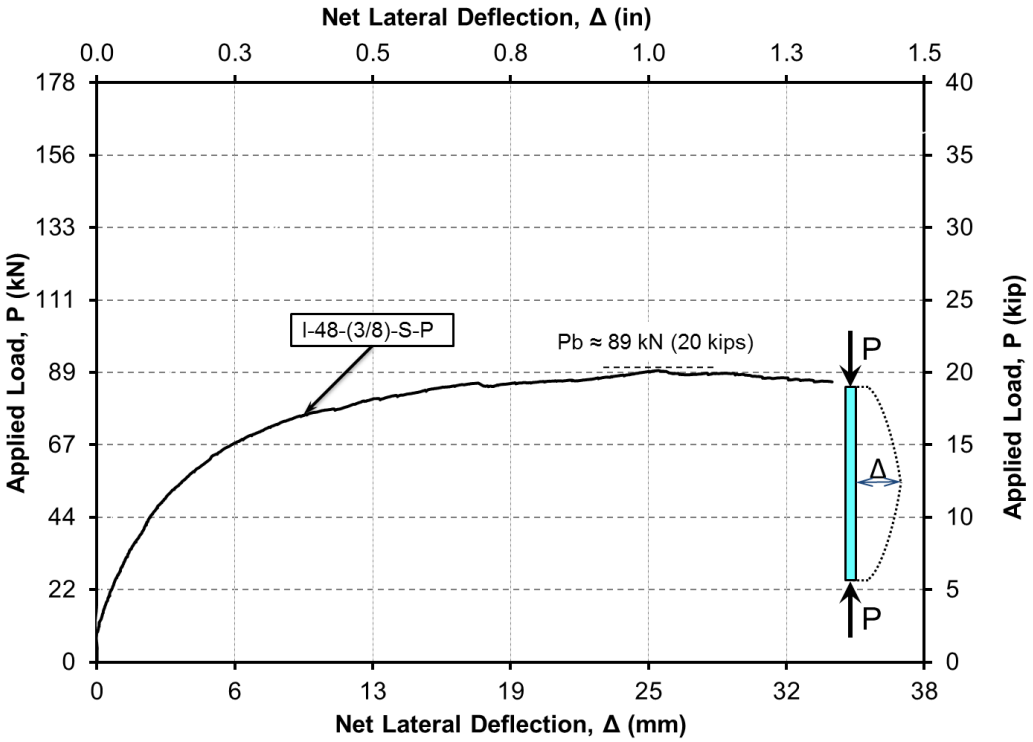

Figure B.55: Net Lateral Deflection-Load Relationship at Mid-height of Specimen I-48-(3/8)-S-P

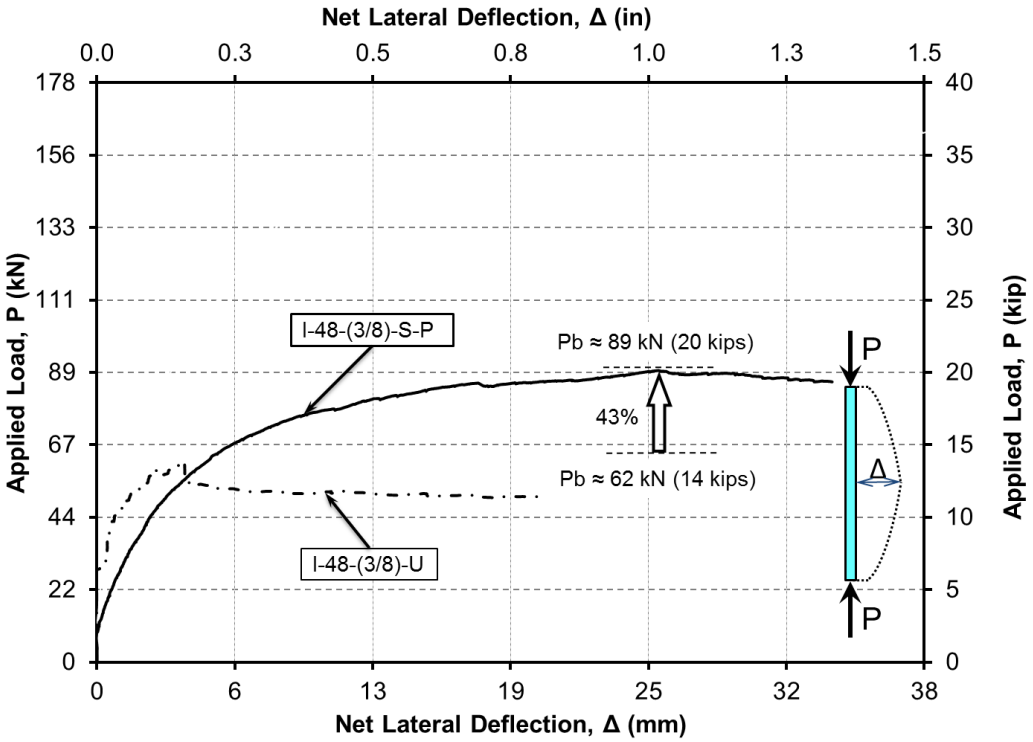

Figure B.66: Net Lateral Deflection-Load Relationship Comparison of I-48-(3/8) Specimens

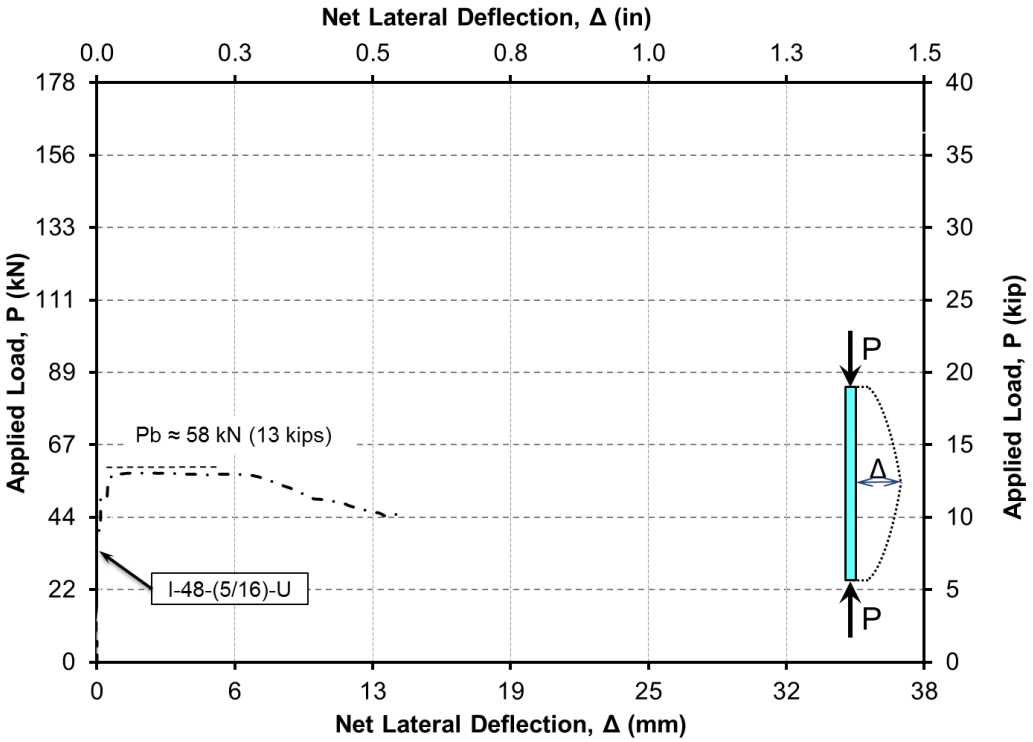

Figure B.77: Net Lateral Deflection-Load Relationship at Mid-height of Specimen I-48-(5/16)-U

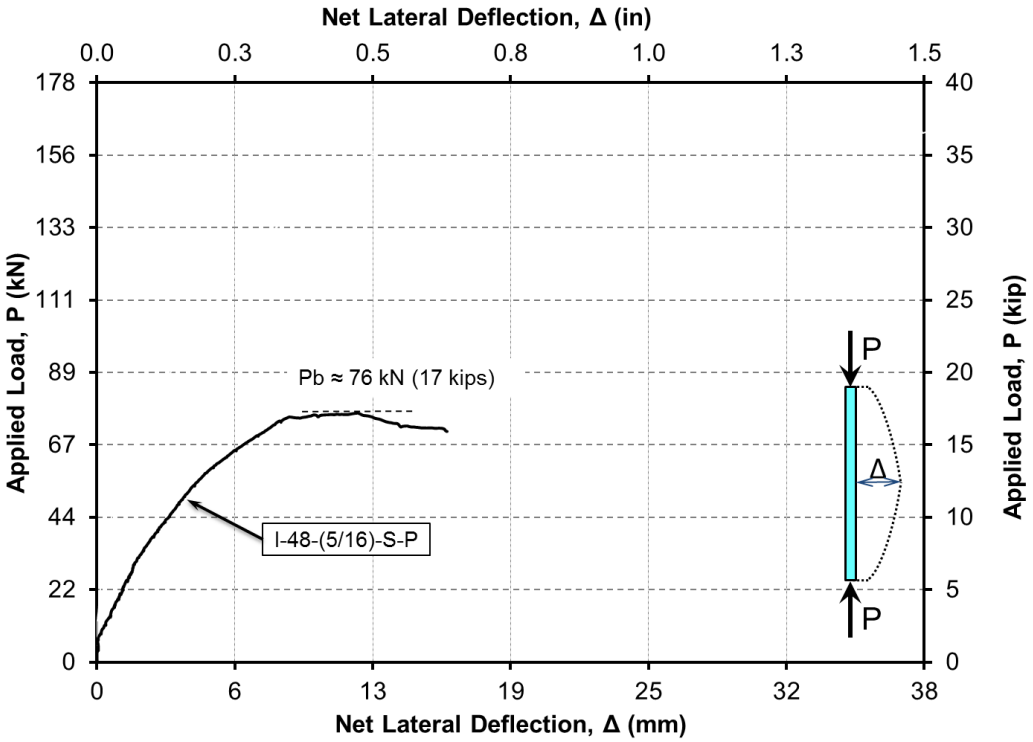

Figure B.88: Net Lateral Deflection-Load Relationship at Mid-height of Specimen I-48-(5/16)-S-P

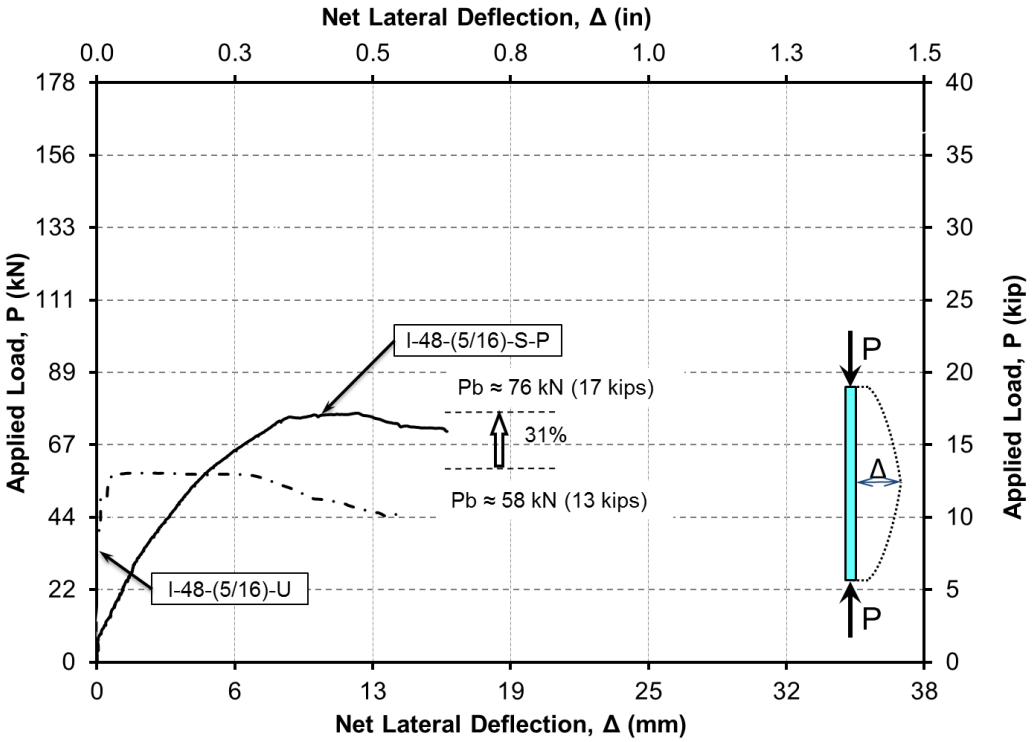

Figure B.99: Net Lateral Deflection-Load Relationship Comparison of I-48-(5/16) Specimens

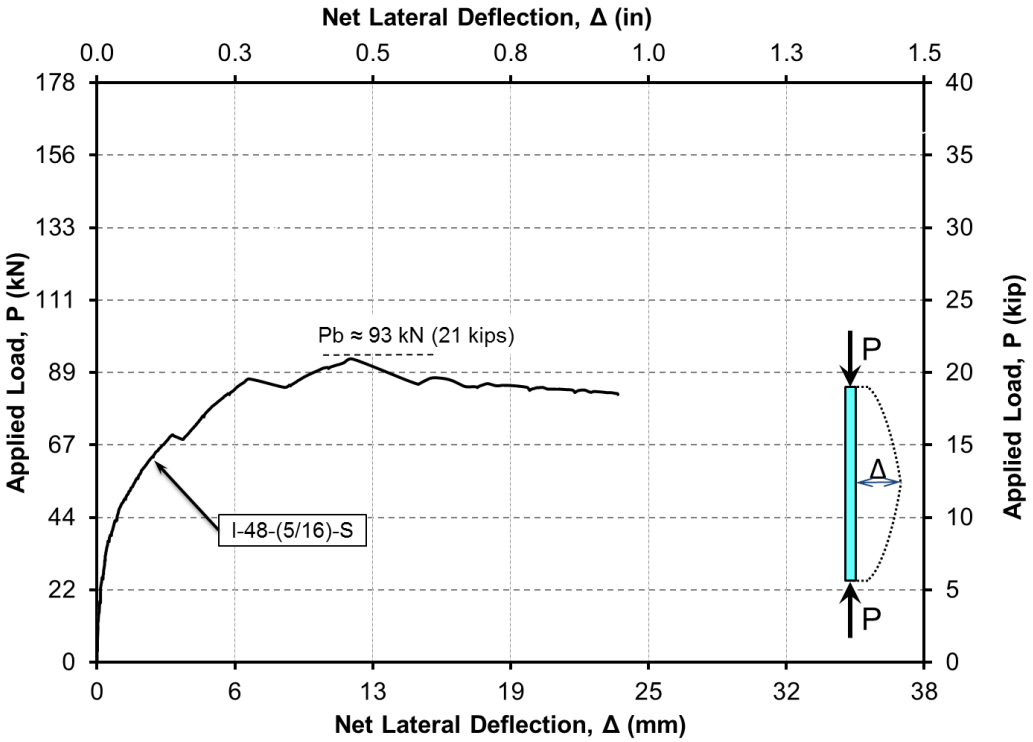

Figure B.1010: Net Lateral Deflection-Load Relationship at Mid-height of Specimen I-48-(5/16)-S

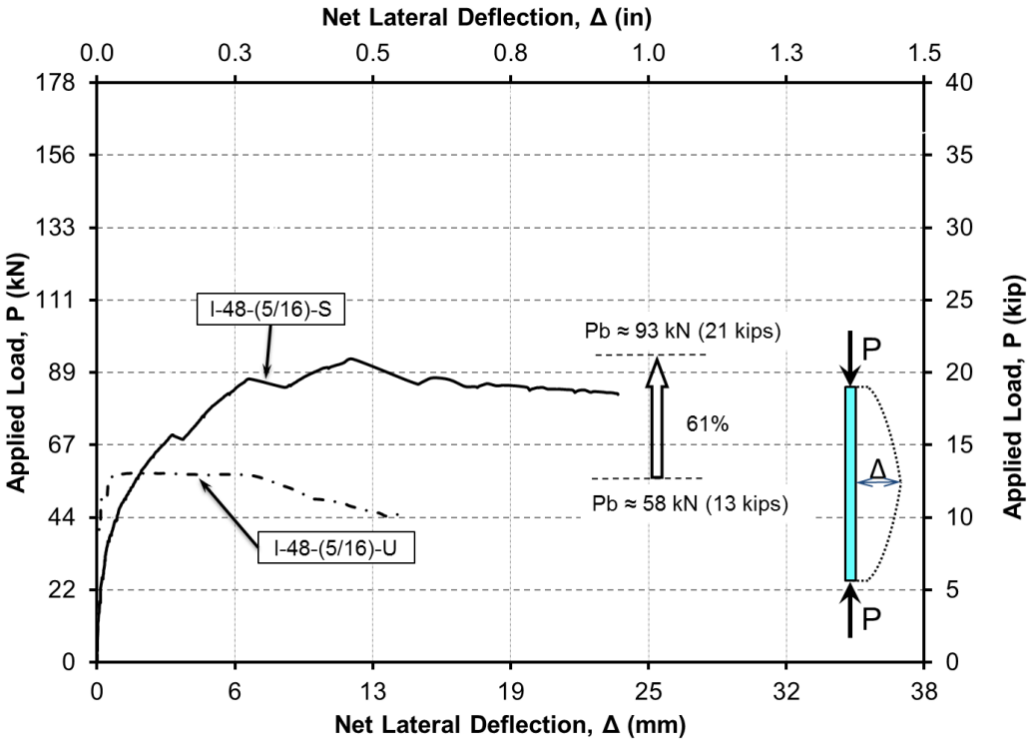

Figure B.1111: Net Lateral Deflection-Load Relationship Comparison of I-48-(5/16) Specimens without Putty